Homogenisation of Linear Electromagnetic Materials: Theoretical and Numerical Studies

Tom G. Mackay

A thesis submitted to the Faculty of Computing Science,
Mathematics & Statistics, University of Glasgow,
for the degree of Doctor of Philosophy

Department of Mathematics
University of Glasgow
September 2001

ProQuest LLC.
789 East Eisenhower Parkway
P.O. Box 1346
Ann Arbor, MI 48106 – 1346

Abstract

The calculation of the electromagnetic response of random composite materials is a matter not only of long–standing scientific interest, but also of increasing technological significance. Provided electromagnetic wavelengths are sufficiently long as compared with the length scales of inhomogeneities, composites may be considered as effectively homogeneous and their constitutive properties estimated by means of homogenisation formalisms. The work of this thesis concerns two aspects of homogenisation theory for linear electromagnetic materials.

Firstly, the well–established Maxwell Garnett and Bruggeman homogenisation formalisms, along with the recently–developed incremental and differential Maxwell Garnett formalisms, are applied to investigate the constitutive properties of complex composite materials. Two classes of structures are considered: (i) Through a detailed parametric study of a chiroplasma composite, a structure more general than that of the Faraday chiral mediums is revealed; this generalised structure arises when the component phases possess non–spherical topology. (ii) Biaxial composite structures are found to develop whenever the component phases present two noncollinear distinguished axes. Distinguished axes of the component phases arising from both electromagnetic and topological origins are considered for nondissipative dielectric, dissipative dielectric–magnetic and bianisotropic materials. A generalised biaxial structure, for which the principal axes of the real and imaginary parts of the constitutive dyadics do not coincide, is demonstrated. Additionally, orthorhombic biaxial structures are presented which can arise even though the distinguished axes of the component phases are non–orthogonal.

Secondly, the strong–property–fluctuation theory (SPFT) is developed for bianisotropic materials, under the bilocal approximation. The SPFT represents a major advance over traditional approaches to homogenisation, such as provided by the Maxwell Garnett and Bruggeman formalisms, by accommodating a more comprehensive description of the distributional statistics of the component phases. In particular, the SPFT takes account of scattering losses and in its zero–order implementation the SPFT reduces to the Bruggeman homogenisation formalism. Detailed numerical studies are presented which highlight the role of the correlation length, as well as the component phase topology and orientation diversity. Also, the choice of covariance function is demonstrated to exert only a secondary influence as compared with the effects of the correlation length. Finally, through calculating the third–order mass operator approximation, the convergence of the bilocally–approximated SPFT is confirmed for isotropic chiral composites as well as for chiroferrites which are both weakly uniaxial and weakly gyrotropic.

Acknowledgements

The work described in this thesis was carried out under the supervision of Dr. Werner S. Weiglhofer (Department of Mathematics, University of Glasgow). Additionally, the studies detailed in Chapter 4 were conducted in collaboration with Prof. Akhlesh Lakhtakia (Department of Engineering Science and Mechanics, Pennsylvania Sate University). Financial support was provided by *The Carnegie Trust for the Universities of Scotland.*

The author wishes to express his sincere thanks to Dr. Weiglhofer, Prof. Lakhtakia and *The Carnegie Trust for the Universities of Scotland.* The author is also most grateful to the Department of Mathematics, University of Glasgow.

Dedicated to the memory of the late Mrs. A.R. Mackay

Publications and Presentations

The work described herein has to date yielded the following refereed journal articles:

P1. W.S. Weiglhofer and T.G. Mackay, "Numerical studies of the constitutive parameters of a chiroplasma composite medium", *Archiv für Elektronik und Übertragungstechnik (International Journal of Electronics and Communications)* **54**, 259–265 (2000);

P2. T.G. Mackay and W.S. Weiglhofer, "Homogenization of biaxial composite materials: nondissipative dielectric properties", *Electromagnetics* **21**, 15–26 (2001);

P3. T.G. Mackay and W.S. Weiglhofer, "Homogenization of biaxial composite materials: dissipative anisotropic properties", *Journal of Optics A: Pure and Applied Optics* **2**, 426–432 (2000);

P4. T.G. Mackay and W.S. Weiglhofer, "Homogenization of biaxial composite materials: bianisotropic properties", *Journal of Optics A: Pure and Applied Optics* **3**, 45–52 (2001);

P5. T.G. Mackay, A. Lakhtakia and W.S. Weiglhofer, "Strong–property–fluctuation theory for homogenization of bianisotropic composites: formulation", *Physical Review E* **62**, 6052–6064 (2000); erratum **63**, 049901(E) (2001);

P6. T.G. Mackay, A. Lakhtakia and W.S. Weiglhofer, "Ellipsoidal topology, orientation diversity and correlation length in bianisotropic mediums", *Archiv für Elektronik und Übertragungstechnik (International Journal of Electronics and Communications)* **55**, 259–265 (2001);

P7. T.G. Mackay, A. Lakhtakia and W.S. Weiglhofer, "Homogenisation of similarly oriented, metallic ellipsoidal inclusions using the bilocally–approximated strong–property–fluctuation theory", *Optics Communications* **197**, 89–95 (2001);

P8. T.G. Mackay, A. Lakhtakia and W.S. Weiglhofer, "Third–order implementation and convergence of the strong–property–fluctuation theory in electromagnetic homogenisation", *Physical Review E* **64** (2001) (in press);

and the following conference papers:

C1. T.G. Mackay and W.S. Weiglhofer, "Numerical homogenization studies of biaxial bianisotropic composite materials", *Proceedings of Bianisotropics 2000, 8th International Conference on Electromagnetics of Complex Media*, A.M. Barbosa and A.L. Topa, editors, Lisbon, Portugal, 237–240 (2000);

C2. T.G. Mackay, A. Lakhtakia and W.S. Weiglhofer, "Strong–property–fluctuation theory for homogenization of bianisotropic composites", *Proceedings of Bianisotropics 2000, 8th International Conference on Electromagnetics of Complex Media*, A.M. Barbosa and A.L. Topa, editors, Lisbon, Portugal, 31–34 (2000);

C3. T.G. Mackay, A. Lakhtakia and W.S. Weiglhofer, "Homogenization of bianisotropic composites via strong–property–fluctuation theory", *Proceedings of the URSI International Symposium on Electromagnetic Theory*, Victoria, Canada, 377–379 (2001);

C4. T.G. Mackay, A. Lakhtakia and W.S. Weiglhofer, "The strong–property–fluctuation theory applied to the homogenisation of linear bianisotropic composites", *Proceedings of the SPIE International Symposium on Optical Science and Technology: Complex Mediums II*, A. Lakhtakia, W.S. Weiglhofer and I.J. Hodgkinson, editors, San Diego, USA, 243–255 (2001).

List of Symbols and Abbreviations

$\underline{r}$	position vector (3–vector)
ω	angular frequency
t	time
f_ℓ	volume fraction of phase ℓ
L	correlation length
Γ	covariance function
ϵ_0	free–space permittivity
μ_0	free–space permeability
$\underline{D}$	dielectric displacement (3–vector)
$\underline{E}$	electric field (3–vector)
$\underline{H}$	magnetic field (3–vector)
$\underline{B}$	magnetic induction (3–vector)
$\underline{\mathbf{F}}$	electric–magnetic field vector (6–vector)
$\underline{\mathbf{C}}$	dielectric displacement–magnetic induction vector (6–vector)
$\underline{\underline{\epsilon}}$	permittivity constitutive dyadic (3×3 dyadic)
$\underline{\underline{\mu}}$	permeability constitutive dyadic (3×3 dyadic)
$\underline{\underline{\xi}}$	magnetoelectric constitutive dyadic (3×3 dyadic)
$\underline{\underline{\zeta}}$	magnetoelectric constitutive dyadic (3×3 dyadic)
$\underline{\underline{\mathbf{K}}}$	constitutive dyadic (6×6 dyadic)
$\underline{\underline{\mathbf{G}}}$	dyadic Green function (6×6 dyadic)
$\underline{\underline{\mathbf{D}}}$	depolarisation dyadic (6×6 dyadic)
$\underline{\underline{U}}$	shape dyadic (3×3 dyadic)
$\underline{\underline{\mathbf{I}}}$	identity dyadic (6×6 dyadic)
$\underline{\underline{I}}$	identity dyadic (3×3 dyadic)
HCM	homogenised composite material
MG	Maxwell Garnett
Br	Bruggeman
IMG	incremental Maxwell Garnett
DMG	differential Maxwell Garnett
SPFT	strong–property–fluctuation theory
BCM	bianisotropic comparison medium

Contents

Chapter 1

Introduction

1.1 Overview and notation

The work of this thesis concerns the linear electromagnetic properties of random composite mediums in the long–wavelength regime. That is, we consider the case where electromagnetic wavelengths are sufficiently long compared with the length scales of inhomogeneities that the composite may be assumed to be effectively homogeneous. Estimation of the constitutive properties of such a homogenised composite material (HCM)—by means of so–called *homogenisation formalisms* [1]–[3]—is a matter of considerable scientific and technological importance, with applications across a diverse range of disciplines. For example, homogenisation formalisms may be utilised in the design and characterisation of novel materials [4, 5], in microwave remote sensing measurements [6], as well as in the study of atmospheric aerosols and interstellar dust [7].

Two of the most widely–used homogenisation formalisms are the Maxwell Garnett (MG) formalism [1] and the Bruggeman (Br) formalism [5]. The basic MG formalism applies only to low concentrations of particulate inclusions randomly embedded in a host medium. However, the restriction to dilute composites is overcome in the recently–developed incremental Maxwell Garnett (IMG) [8] and differential Maxwell Garnett (DMG) [9] homogenisation formalisms. In Section 1.3, a brief outline of the MG, Br, IMG and DMG formalisms is provided; detailed descriptions are available in the research literature [1, 9, 10].

In Chapter 2, the MG, Br, IMG and DMG homogenisation formalisms are all utilised in a comprehensive numerical study of a chiroplasma [11]. When the particulate constituents have spherical topology, the resulting HCM structure is found to belong to the class of *Faraday chiral mediums* [12]; whereas more general HCM structures are revealed when the constituents are based on ellipsoidal topology.

Biaxial HCM structures are investigated in Chapter 3. Specifically, we focus on scenarios where the constituent phases are themselves non–biaxial but collectively they present two noncollinear distinguished axes; these axes can have either an electromag-

netic or topological origin. The relationship between the biaxial HCM structure and the geometry, orientation and composition of the component mediums is explored for the nondissipative dielectric case [13]. Extending these studies to include the effects of dissipation in dielectric–magnetic materials, a generalised biaxial HCM structure is revealed for which the principal axes of real and imaginary parts of the permittivity and permeability constitutive dyadics do not coincide [14]. Furthermore, in the bianisotropic regime, yet more general HCM structures arise; in particular, complex symmetries are found in the constitutive dyadics which would not be anticipated from a familiarity with the dielectric or dielectric–magnetic case [15].

A significant limitation of most homogenisation approaches—as exemplified by the MG, Br, IMG and DMG formalisms—arises from their simplistic treatments of the distributional statistics of the constituent phases. A notable exception is the *strong–property–fluctuation theory* (SPFT) which, in principle, can accommodate spatial correlation functions of arbitrarily high order. In the SPFT, statistical cumulants of the spatial distribution of the component material phases are used perturbatively to refine an initial ansatz on the nature of the HCM. The bilocally–approximated SPFT for bianisotropic HCMs is developed in Chapter 4 [16]. Under the bilocal approximation, a covariance function and its associated correlation length are used to characterise the distributional statistics of the component material phases. Detailed numerical calculations which consider the influence of ellipsoidal topology, orientation diversity and correlation length are also presented [17]. The influence of the covariance function is explored through a study concerning the homogenisation of ellipsoidal metallic inclusions with a non–conducting host medium [18]. Finally, by calculating higher–order terms, the convergence of the bilocally–approximated SPFT is demonstrated for isotropic chiral HCMs, as well as for chiroferrite composites which are both weakly uniaxial and weakly gyrotropic [19].

A discussion of results and suggestions for further studies are provided in Chapter 5.

The following notation is adopted: 6–vectors (3–vectors) are in bold (normal) face and underlined, whereas 6×6 (3×3) dyadics are in bold (normal) face and underlined twice. The adjoint, determinant, inverse, trace, transpose and ℓj^{th} entry of a dyadic $\underline{\underline{\mathbf{Q}}}$ are represented by $\text{adj}\,(\underline{\underline{\mathbf{Q}}})$, $\det \underline{\underline{\mathbf{Q}}}$, $\underline{\underline{\mathbf{Q}}}^{-1}$, $\text{tr}\,\underline{\underline{\mathbf{Q}}}$, $\underline{\underline{\mathbf{Q}}}^{T}$ and $[\,\underline{\underline{\mathbf{Q}}}\,]_{\ell j}$, respectively. For dyadics and vectors, the dot product denotes contraction of indices. The unit vector corresponding to a vector $\underline{n}$ is signified by $\hat{\underline{n}}$, and the triad of Cartesian unit vectors by $(\,\underline{u}_x,\, \underline{u}_y,\, \underline{u}_z\,)$. The ensemble average of a quantity N is written as $\langle\, N \,\rangle$. The 6×6 (3×3) identity dyadic is denoted by $\underline{\underline{\mathbf{I}}}$ $(\underline{\underline{I}})$. The permittivity and permeability of free space (i.e., vacuum) are given as ϵ_0 and μ_0, respectively. A list of the most commonly used symbols and abbreviations is provided on page v.

1.2 Fundamentals of electromagnetics in complex mediums

Theoretical descriptions of the macroscopic electromagnetic properties of materials are founded on the Maxwell equations, which may be stated in the time domain as [20]

$$\nabla \times \tilde{\underline{H}}(\underline{r},t) - \frac{\partial}{\partial t}\tilde{\underline{D}}(\underline{r},t) = \tilde{\underline{J}}_e(\underline{r},t), \tag{1.1}$$

$$\nabla \times \tilde{\underline{E}}(\underline{r},t) + \frac{\partial}{\partial t}\tilde{\underline{B}}(\underline{r},t) = -\tilde{\underline{J}}_m(\underline{r},t), \tag{1.2}$$

$$\nabla \cdot \tilde{\underline{D}}(\underline{r},t) = \tilde{\rho}_e(\underline{r},t), \tag{1.3}$$

$$\nabla \cdot \tilde{\underline{B}}(\underline{r},t) = \tilde{\rho}_m(\underline{r},t). \tag{1.4}$$

In (1.1)–(1.4), $\tilde{\underline{D}}(\underline{r},t)$, $\tilde{\underline{E}}(\underline{r},t)$, $\tilde{\underline{B}}(\underline{r},t)$ and $\tilde{\underline{H}}(\underline{r},t)$ represent the dielectric displacement, electric field, magnetic induction and magnetic field, respectively, while the electric (magnetic) current and charge densities are represented by $\tilde{\underline{J}}_e(\underline{r},t)$ ($\tilde{\underline{J}}_m(\underline{r},t)$) and $\tilde{\rho}_e(\underline{r},t)$ ($\tilde{\rho}_m(\underline{r},t)$), respectively. The divergence relations (1.3) and (1.4) do not contribute to the analyses of this thesis, since they are a consequence of the curl relations (1.1) and (1.2), combined with the following continuity equations for the source terms

$$\nabla \cdot \tilde{\underline{J}}_{e,m}(\underline{r},t) + \frac{\partial}{\partial t}\tilde{\rho}_{e,m}(\underline{r},t) = 0. \tag{1.5}$$

Equations (1.1) and (1.2) present two vector differential equations in four unknown vector fields. In order to specify unique solutions, further equations are required. These are provided by the *constitutive relations*. For our present purposes, we restrict our attention to the most general linear constitutive relations for spatially–local materials; i.e. [21, 22],

$$\tilde{\underline{D}}(\underline{r},t) = \int_{-\infty}^{t} \left[\tilde{\underline{\underline{\epsilon}}}(\underline{r},t-t') \cdot \tilde{\underline{E}}(\underline{r},t') + \tilde{\underline{\underline{\xi}}}(\underline{r},t-t') \cdot \tilde{\underline{H}}(\underline{r},t') \right] dt', \tag{1.6}$$

$$\tilde{\underline{B}}(\underline{r},t) = \int_{-\infty}^{t} \left[\tilde{\underline{\underline{\zeta}}}(\underline{r},t-t') \cdot \tilde{\underline{E}}(\underline{r},t') + \tilde{\underline{\underline{\mu}}}(\underline{r},t-t') \cdot \tilde{\underline{H}}(\underline{r},t') \right] dt', \tag{1.7}$$

where $\tilde{\underline{\underline{\epsilon}}}(\underline{r},t)$, $\tilde{\underline{\underline{\xi}}}(\underline{r},t)$, $\tilde{\underline{\underline{\zeta}}}(\underline{r},t)$ and $\tilde{\underline{\underline{\mu}}}(\underline{r},t)$ are the time–domain constitutive dyadics. Materials described by the constitutive relations (1.6) and (1.7) are called *bianisotropic*.

It is mathematically convenient to introduce the frequency–domain constitutive dyadics $\underline{\underline{\epsilon}}(\underline{r},\omega)$, $\underline{\underline{\xi}}(\underline{r},\omega)$, $\underline{\underline{\zeta}}(\underline{r},\omega)$ and $\underline{\underline{\mu}}(\underline{r},\omega)$, defined through the Fourier transformations

$$\tilde{\underline{\underline{\gamma}}}(\underline{r},t) = \frac{1}{2\pi}\int_{-\infty}^{\infty} \underline{\underline{\gamma}}(\underline{r},\omega)\, \exp(-i\omega t)\, d\omega, \qquad (\gamma = \epsilon, \xi, \zeta, \mu), \tag{1.8}$$

along with the field phasors $\underline{D}(\underline{r},\omega)$, $\underline{E}(\underline{r},\omega)$, $\underline{B}(\underline{r},\omega)$ and $\underline{H}(\underline{r},\omega)$, defined similarly via

$$\tilde{\underline{T}}(\underline{r},t) = \frac{1}{2\pi}\int_{-\infty}^{\infty} \underline{T}(\underline{r},\omega)\, \exp(-i\omega t)\, d\omega, \qquad (T = D, B, E, H). \tag{1.9}$$

Thus, the constitutive relations (1.6) and (1.7) are expressed in the frequency domain as

$$\underline{D}(\underline{r},\omega) = \underline{\underline{\epsilon}}(\underline{r},\omega)\cdot\underline{E}(\underline{r},\omega)+\underline{\underline{\xi}}(\underline{r},\omega)\cdot\underline{H}(\underline{r},\omega)\,, \tag{1.10}$$

$$\underline{B}(\underline{r},\omega) = \underline{\underline{\zeta}}(\underline{r},\omega)\cdot\underline{E}(\underline{r},\omega)+\underline{\underline{\mu}}(\underline{r},\omega)\cdot\underline{H}(\underline{r},\omega)\,. \tag{1.11}$$

Furthermore, the frequency–domain Maxwell curl equations (1.1) and (1.2) are given by

$$\nabla\times\underline{H}(\underline{r},\omega)+i\omega\underline{D}(\underline{r},\omega) = \underline{J}_e(\underline{r},\omega), \tag{1.12}$$

$$\nabla\times\underline{E}(\underline{r},\omega)-i\omega\underline{B}(\underline{r},\omega) = -\underline{J}_m(\underline{r},\omega), \tag{1.13}$$

wherein the source terms $\underline{J}_{e,m}(\underline{r},\omega)$ are the Fourier transforms of $\tilde{\underline{J}}_{e,m}(\underline{r},t)$, defined as in (1.9).

A self–consistent system of differential equations arises through substituting the constitutive relations (1.10) and (1.11) into the Maxwell curl equations (1.12) and (1.13); i.e., we have

$$\left[\,\underline{\underline{\mathbf{L}}}(\nabla)+i\omega\underline{\underline{\mathbf{K}}}(\underline{r},\omega)\,\right]\cdot\underline{\mathbf{F}}(\underline{r},\omega)=\underline{\mathbf{Q}}(\underline{r},\omega), \tag{1.14}$$

where, in 6–vector/dyadic notation [23], the linear differential operator $\underline{\underline{\mathbf{L}}}(\nabla)$ and constitutive dyadic $\underline{\underline{\mathbf{K}}}(\underline{r},\omega)$ have the representations

$$\underline{\underline{\mathbf{L}}}(\nabla)=\left[\begin{array}{cc}\underline{\underline{0}} & \nabla\times\underline{\underline{I}}\\ -\nabla\times\underline{\underline{I}} & \underline{\underline{0}}\end{array}\right],\qquad \underline{\underline{\mathbf{K}}}(\underline{r},\omega)=\left[\begin{array}{cc}\underline{\underline{\epsilon}}(\underline{r},\omega) & \underline{\underline{\xi}}(\underline{r},\omega),\\ \underline{\underline{\zeta}}(\underline{r},\omega) & \underline{\underline{\mu}}(\underline{r},\omega)\end{array}\right], \tag{1.15}$$

while the electromagnetic field vector $\underline{\mathbf{F}}(\underline{r},\omega)$ and source vector $\underline{\mathbf{Q}}(\underline{r},\omega)$ are defined as

$$\underline{\mathbf{F}}(\underline{r},\omega)=\left[\begin{array}{c}\underline{E}(\underline{r},\omega)\\ \underline{H}(\underline{r},\omega)\end{array}\right],\qquad \underline{\mathbf{Q}}(\underline{r},\omega)=\left[\begin{array}{c}\underline{J}_e(\underline{r},\omega)\\ \underline{J}_m(\underline{r},\omega)\end{array}\right]. \tag{1.16}$$

Since (1.14) is a linear vector equation, its solution may be expressed in terms of the dyadic Green function $\underline{\underline{\mathbf{G}}}(\underline{r},\underline{r}',\omega)$ as

$$\underline{\mathbf{F}}(\underline{r},\omega)=\int_{V'}\underline{\underline{\mathbf{G}}}(\underline{r},\underline{r}',\omega)\cdot\underline{\mathbf{Q}}(\underline{r}',\omega)\,d^3\underline{r}', \tag{1.17}$$

where field and source points are represented by $\underline{r}$ and $\underline{r}'$, respectively, and all source points are contained within the integration volume V'. The dyadic Green function $\underline{\underline{\mathbf{G}}}(\underline{r},\underline{r}',\omega)$ itself arises as the solution to the differential equation

$$\left[\,\underline{\underline{\mathbf{L}}}(\nabla)+i\omega\underline{\underline{\mathbf{K}}}(\underline{r},\omega)\,\right]\cdot\underline{\underline{\mathbf{G}}}(\underline{r},\underline{r}',\omega)=\delta(\underline{r}-\underline{r}')\,\underline{\underline{\mathbf{I}}}\,, \tag{1.18}$$

in which the role of the source term (cf. equation (1.14)) is provided by the product of the Dirac delta function $\delta(\underline{r}-\underline{r}')$ and the 6×6 identity dyadic $\underline{\underline{\mathbf{I}}}$. Parenthetically, we remark that explicit representations of dyadic Green functions are available only for certain highly symmetric mediums, such as isotropic and uniaxial mediums [24].

The bianisotropic constitutive relations (1.10) and (1.11), specified in terms of the four 3×3 constitutive dyadics $\underline{\underline{\epsilon}}(\underline{r},\omega)$, $\underline{\underline{\xi}}(\underline{r},\omega)$, $\underline{\underline{\zeta}}(\underline{r},\omega)$ and $\underline{\underline{\mu}}(\underline{r},\omega)$, characterise the most general class of linear materials. In general, the constitutive dyadics are complex–valued and therefore 36 complex–valued parameters are involved in the description of bianisotropy. However, all linear materials are required to satisfy the Post constraint [25]–[27]

$$\mathrm{tr}\left[\left(\underline{\underline{\mu}}(\underline{r},\omega) \right)^{-1} \cdot \left(\underline{\underline{\zeta}}(\underline{r},\omega) + \underline{\underline{\xi}}(\underline{r},\omega) \right) \right] = 0\,; \tag{1.19}$$

hence, only 35 independent complex–valued parameters are needed to characterise a bianisotropic medium. A comprehensive list of the many subclasses which are contained within the bianisotropic class of materials has recently been compiled by Weiglhofer [22]. Of particular relevance to the studies described in this thesis are the distinctions between homogeneous and nonhomogeneous mediums and between dissipative and nondissipative mediums: A homogeneous medium is characterised by constitutive dyadics which are independent of the spatial coordinate $\underline{r}$. The constitutive dyadics of a nondissipative medium are required to fulfill the following conditions [28]

$$\underline{\underline{\epsilon}}(\underline{r},\omega) = \underline{\underline{\epsilon}}^{+}(\underline{r},\omega), \qquad \underline{\underline{\xi}}(\underline{r},\omega) = \underline{\underline{\zeta}}^{+}(\underline{r},\omega), \qquad \underline{\underline{\mu}}(\underline{r},\omega) = \underline{\underline{\mu}}^{+}(\underline{r},\omega), \tag{1.20}$$

where $^{+}$ indicates the hermitian conjugate.

Henceforth, we shall be dealing exclusively with frequency–domain electromagnetic field vectors and constitutive dyadics. For convenience, we adopt the usual practice of suppressing the ω dependency in our notation.

1.3 Homogenisation formalisms

We present in this section the general homogenisation framework and the specific MG, Br, IMG and DMG homogenisation formalisms which are utilised in the proceeding chapters.

1.3.1 Generalities

Throughout this thesis we concentrate exclusively on two–phase random composite mediums. The component phases are designated as a and b. All space is partitioned into the disjoint regions V_a and V_b which contain the phases a and b, respectively. The composite structure may be envisaged as arising from a random mixture of phase a particulate inclusions in a phase b host medium. The volume fraction of phase a is given by f_a, while that of phase b by $f_b = 1 - f_a$.

The component phases themselves are taken to be homogeneous; i.e., constitutive dyadics are assumed to be independent of the spatial coordinate $\underline{r}$. We consider the most general linear case where the component phases are characterised by bianisotropic

constitutive relations, given in the frequency domain as

$$\underline{\mathbf{C}}(\underline{r}) = \underline{\underline{\mathbf{K}}}_\ell \cdot \underline{\mathbf{F}}(\underline{r}), \qquad \underline{r} \in V_\ell, \qquad (\ell = a, b), \tag{1.21}$$

wherein the 6–vector electromagnetic fields

$$\underline{\mathbf{C}}(\underline{r}) = \left[\begin{array}{c} \underline{D}(\underline{r}) \\ \underline{B}(\underline{r}) \end{array} \right] \qquad \text{and} \qquad \underline{\mathbf{F}}(\underline{r}) = \left[\begin{array}{c} \underline{E}(\underline{r}) \\ \underline{H}(\underline{r}) \end{array} \right], \tag{1.22}$$

are specified in terms of the complex–valued dielectric displacement $\underline{D}$, electric field $\underline{E}$, magnetic field $\underline{H}$ and magnetic induction $\underline{B}$ phasors introduced in Section 1.2; while the complex–valued 6×6 constitutive dyadic

$$\underline{\underline{\mathbf{K}}}_\ell = \left[\begin{array}{cc} \underline{\underline{\epsilon}}_\ell & \underline{\underline{\xi}}_\ell \\ \underline{\underline{\zeta}}_\ell & \underline{\underline{\mu}}_\ell \end{array} \right], \tag{1.23}$$

comprises the 3×3 permittivity and permeability dyadics $\underline{\underline{\epsilon}}_\ell$ and $\underline{\underline{\mu}}_\ell$, respectively, as well as the magnetoelectric constitutive dyadics $\underline{\underline{\xi}}_\ell$ and $\underline{\underline{\zeta}}_\ell$. Furthermore, we assume the inclusions are randomly distributed as similarly oriented, conformal ellipsoids with surfaces parameterised as

$$\underline{R}_e(\theta, \phi) = \eta \underline{\underline{U}} \cdot \hat{\underline{R}}(\theta, \phi), \tag{1.24}$$

where $\hat{\underline{R}}(\theta, \phi)$ is the radial unit vector depending on the spherical polar coordinates θ and ϕ, $\underline{\underline{U}}$ is a real–valued symmetric *shape* dyadic, and η is a linear measure.

A mathematical construct of key importance in homogenisation formalisms is the singularity of the free–space dyadic Green function, i.e., the *depolarisation dyadic* $\underline{\underline{\mathbf{D}}}$. The depolarisation dyadic associated with a $\underline{\underline{U}}$–shaped exclusion volume in a bianisotropic medium with constitutive dyadics $\underline{\underline{\epsilon}}$, $\underline{\underline{\xi}}$, $\underline{\underline{\zeta}}$ and $\underline{\underline{\mu}}$, is given as [29]

$$\underline{\underline{\mathbf{D}}} = \left[\begin{array}{cc} \underline{\underline{D}}_{ee} & \underline{\underline{D}}_{em} \\ \underline{\underline{D}}_{me} & \underline{\underline{D}}_{mm} \end{array} \right], \tag{1.25}$$

where

$$\underline{\underline{D}}_{\lambda\lambda'} = \underline{\underline{U}}^{-1} \cdot \underline{\underline{D}}'_{\lambda\lambda'} \cdot (\underline{\underline{U}}^{-1})^T, \qquad (\lambda, \lambda' = e, m), \tag{1.26}$$

and

$$\underline{\underline{D}}'_{\lambda\lambda'} = \frac{1}{4\pi i\omega} \int_{\phi_q=0}^{2\pi} \int_{\theta_q=0}^{\pi} \frac{(\hat{\underline{q}} \cdot \underline{\underline{\tau}}_{\lambda\lambda'} \cdot \hat{\underline{q}})\, \hat{\underline{q}}\, \hat{\underline{q}} \quad \sin\theta_q \, d\theta_q \, d\phi_q}{(\hat{\underline{q}} \cdot \underline{\underline{\epsilon}}' \cdot \hat{\underline{q}})(\hat{\underline{q}} \cdot \underline{\underline{\mu}}' \cdot \hat{\underline{q}}) - (\hat{\underline{q}} \cdot \underline{\underline{\xi}}' \cdot \hat{\underline{q}})(\hat{\underline{q}} \cdot \underline{\underline{\zeta}}' \cdot \hat{\underline{q}})}, \tag{1.27}$$

with

$$\begin{gathered} \underline{\underline{\epsilon}}' = (\underline{\underline{U}}^{-1})^T \cdot \underline{\underline{\epsilon}} \cdot \underline{\underline{U}}^{-1}, \quad \underline{\underline{\xi}}' = (\underline{\underline{U}}^{-1})^T \cdot \underline{\underline{\xi}} \cdot \underline{\underline{U}}^{-1}, \quad \underline{\underline{\zeta}}' = (\underline{\underline{U}}^{-1})^T \cdot \underline{\underline{\zeta}} \cdot \underline{\underline{U}}^{-1}, \\ \underline{\underline{\mu}}' = (\underline{\underline{U}}^{-1})^T \cdot \underline{\underline{\mu}} \cdot \underline{\underline{U}}^{-1}, \quad \underline{\underline{\tau}}_{ee} = \underline{\underline{\mu}}', \quad \underline{\underline{\tau}}_{em} = -\underline{\underline{\xi}}', \quad \underline{\underline{\tau}}_{me} = -\underline{\underline{\zeta}}', \quad \underline{\underline{\tau}}_{mm} = \underline{\underline{\epsilon}}'. \end{gathered} \tag{1.28}$$

Parenthetically, we note that depolarisation dyadics associated with cylindrical exclusion volumes in anisotropic mediums have also been developed recently [30]. These may be used to develop homogenisation formalisms pertaining to composites consisting of needle– or disk–shaped inclusions; however, this matter will not be considered here.

1.3.2 Maxwell Garnett formalism

The MG homogenisation formalism has been extensively applied, despite being restricted to dilute composites [1]. In the general case of a bianisotropic composite, in which the inclusion and host phases are characterised by the constitutive dyadics $\underline{\underline{K}}_a$ and $\underline{\underline{K}}_b$, respectively, and the ellipsoidal inclusion geometry is specified by the shape dyadic $\underline{\underline{U}}$, we have [31]

$$\underline{\underline{\mathbf{K}}}_{MG} = \underline{\underline{\mathbf{K}}}_b + f_a\, \underline{\underline{\boldsymbol{\alpha}}}^{a/b} \cdot \left(\underline{\underline{\mathbf{I}}} - i\omega f_a\, \underline{\underline{\mathbf{D}}}^{I/b} \cdot \underline{\underline{\boldsymbol{\alpha}}}^{a/b} \right)^{-1}, \tag{1.29}$$

as the MG estimate of the constitutive dyadic of the HCM. The term

$$\underline{\underline{\boldsymbol{\alpha}}}^{a/b} = \left(\underline{\underline{\mathbf{K}}}_a - \underline{\underline{\mathbf{K}}}_b \right) \cdot \left[\underline{\underline{\mathbf{I}}} + i\omega \underline{\underline{\mathbf{D}}}^{U/b} \cdot \left(\underline{\underline{\mathbf{K}}}_a - \underline{\underline{\mathbf{K}}}_b \right) \right]^{-1}, \tag{1.30}$$

in (1.29) is a generalised polarisability dyadic, and $\underline{\underline{\mathbf{D}}}^{U/b}$ ($\underline{\underline{\mathbf{D}}}^{I/b}$) is the depolarisation dyadic associated with an exclusion volume specified by the shape dyadic $\underline{\underline{U}}$ ($\underline{\underline{I}}$), in the phase b host medium.

1.3.3 Bruggeman formalism

The Br homogenisation formalism has the advantage over the MG formalism in that it applies for all volume fractions $f_a \in (0,1)$ [5]. A characteristic feature of the Br formalism is that the inclusion phase and host phase are treated symmetrically. Consequently, when dealing with the Br formalism both the inclusion and host phases may be assumed to have particulate topologies and the distinction between the "inclusion" and "host" phases is rather artificial (although, for convenience, we will continue to refer to phases a and b as the inclusion and host phases, respectively).

For bianisotropic composites, arising from particulate component phases a and b of ellipsoidal topology characterised by the shape dyadics $\underline{\underline{U}}^a$ and $\underline{\underline{U}}^b$, respectively, the Br estimate of the HCM constitutive dyadic $\underline{\underline{\mathbf{K}}}_{Br}$ is obtained by solving the nonlinear equation

$$f_a\, \underline{\underline{\boldsymbol{\alpha}}}^{a/Br} + f_b\, \underline{\underline{\boldsymbol{\alpha}}}^{b/Br} = \underline{\underline{\mathbf{0}}}. \tag{1.31}$$

The generalised polarisabilities in (1.31) are

$$\underline{\underline{\boldsymbol{\alpha}}}^{a/Br} = \left(\underline{\underline{\mathbf{K}}}_a - \underline{\underline{\mathbf{K}}}_{Br} \right) \cdot \left[\underline{\underline{\mathbf{I}}} + i\omega \underline{\underline{\mathbf{D}}}^{U^a/Br} \cdot \left(\underline{\underline{\mathbf{K}}}_a - \underline{\underline{\mathbf{K}}}_{Br} \right) \right]^{-1}, \tag{1.32}$$

$$\underline{\underline{\boldsymbol{\alpha}}}^{b/Br} = \left(\underline{\underline{\mathbf{K}}}_b - \underline{\underline{\mathbf{K}}}_{Br} \right) \cdot \left[\underline{\underline{\mathbf{I}}} + i\omega \underline{\underline{\mathbf{D}}}^{U^b/Br} \cdot \left(\underline{\underline{\mathbf{K}}}_b - \underline{\underline{\mathbf{K}}}_{Br} \right) \right]^{-1}, \tag{1.33}$$

and $\underline{\underline{\mathbf{D}}}^{U^a/Br}$ ($\underline{\underline{\mathbf{D}}}^{U^b/Br}$) is the depolarisation dyadic of a $\underline{\underline{U}}_a$–shaped ($\underline{\underline{U}}_b$–shaped) exclusion volume in the HCM with constitutive dyadic $\underline{\underline{\mathbf{K}}}_{Br}$.

The usual method of dealing with (1.31) is to apply the simple Jacobi technique [32], by which an iterative solution is developed as

$$\underline{\underline{\mathbf{K}}}_{Br}[n] = \mathcal{T}(\underline{\underline{\mathbf{K}}}_{Br}[n-1]), \qquad (n = 1, 2, \ldots), \tag{1.34}$$

with the initial value $\underline{\underline{\mathbf{K}}}_{Br}[0] = \underline{\underline{\mathbf{K}}}_{MG}$ and the operator $\mathcal{T}$ defined as

$$\begin{aligned}\mathcal{T}(\underline{\underline{\mathbf{K}}}_{Br}) \;=\; & \left\{ f_a \underline{\underline{\mathbf{K}}}_a \cdot \left[\underline{\underline{\mathbf{I}}} + i\omega \underline{\underline{\mathbf{D}}}^{U^a/Br} \cdot \left(\underline{\underline{\mathbf{K}}}_a - \underline{\underline{\mathbf{K}}}_{Br} \right) \right]^{-1} + \right. \\ & \left. f_b \underline{\underline{\mathbf{K}}}_b \cdot \left[\underline{\underline{\mathbf{I}}} + i\omega \underline{\underline{\mathbf{D}}}^{U^b/Br} \cdot \left(\underline{\underline{\mathbf{K}}}_b - \underline{\underline{\mathbf{K}}}_{Br} \right) \right]^{-1} \right\} \\ & \cdot \left\{ f_a \left[\underline{\underline{\mathbf{I}}} + i\omega \underline{\underline{\mathbf{D}}}^{U^a/Br} \cdot \left(\underline{\underline{\mathbf{K}}}_a - \underline{\underline{\mathbf{K}}}_{Br} \right) \right]^{-1} + \right. \\ & \left. f_b \left[\underline{\underline{\mathbf{I}}} + i\omega \underline{\underline{\mathbf{D}}}^{U^b/Br} \cdot \left(\underline{\underline{\mathbf{K}}}_b - \underline{\underline{\mathbf{K}}}_{Br} \right) \right]^{-1} \right\}^{-1}. \end{aligned} \tag{1.35}$$

1.3.4 Incremental and differential Maxwell Garnett formalisms

The IMG homogenisation formalism is a recent refinement of the MG formalism in which the HCM is built incrementally, by adding the inclusion phase not all at once but in a fixed number (N) of stages [8, 9]. After each increment, the composite is homogenised using the MG formalism. Thereby, the IMG formalism cures one of the major limitations of the MG formalism, namely the restriction of its applicability to modest proportions of inclusion density. We have the iteraction scheme

$$\underline{\underline{\mathbf{K}}}[n+1] = \underline{\underline{\mathbf{K}}}[n] + \delta\, \underline{\underline{\boldsymbol{\alpha}}}^{a/n} \cdot \left(\underline{\underline{\mathbf{I}}} - i\omega\delta\, \underline{\underline{\mathbf{D}}}^{I/n} \cdot \underline{\underline{\boldsymbol{\alpha}}}^{a/n} \right)^{-1}, \qquad (n = 0, 1, \ldots, N-1), \tag{1.36}$$

where we set $\delta = 1 - f_b^{1/N}$ and $\underline{\underline{\mathbf{K}}}[0] = \underline{\underline{\mathbf{K}}}_b$. In (1.36), $\underline{\underline{\boldsymbol{\alpha}}}^{a/n}$ is the polarisability dyadic of a $\underline{U}$–shaped inclusion relative to a medium with constitutive dyadic $\underline{\underline{\mathbf{K}}}[n]$, i.e.,

$$\underline{\underline{\boldsymbol{\alpha}}}^{a/n} = \left(\underline{\underline{\mathbf{K}}}_a - \underline{\underline{\mathbf{K}}}[n] \right) \cdot \left[\underline{\underline{\mathbf{I}}} + i\omega \underline{\underline{\mathbf{D}}}^{U/n} \cdot \left(\underline{\underline{\mathbf{K}}}_a - \underline{\underline{\mathbf{K}}}[n] \right) \right]^{-1}, \tag{1.37}$$

while $\underline{\underline{\mathbf{D}}}^{I/n}$ ($\underline{\underline{\mathbf{D}}}^{U/n}$) is the depolarisation dyadic of a spherical ($\underline{U}$–shaped) exclusion region in the medium with constitutive dyadic $\underline{\underline{\mathbf{K}}}[n]$. The IMG estimate of the HCM constitutive dyadic

$$\underline{\underline{\mathbf{K}}}_{IMG} = \underline{\underline{\mathbf{K}}}[N], \tag{1.38}$$

follows after N iterations. All numerical IMG results presented in this thesis were computed for $N = 5$ iterations.

The DMG homogenisation formalism arises from the IMG formalism in the limit $N \to \infty$. That is, the DMG estimate of the HCM constitutive dyadic $\underline{\underline{\mathbf{K}}}_{DMG}$ is given via the ordinary differential equation

$$\frac{\partial}{\partial \upsilon} \underline{\underline{\mathbf{K}}}(\upsilon) = \frac{1}{1-\upsilon}\, \underline{\underline{\boldsymbol{\alpha}}}^{a/\upsilon}, \tag{1.39}$$

with initial value $\underline{\underline{\mathbf{K}}}(0) = \underline{\underline{\mathbf{K}}}_b$. In (1.39), υ is a continuous variable representing the inclusion volume fraction and $\underline{\underline{\boldsymbol{\alpha}}}^{a/\upsilon}$ is the polarisability dyadic of a $\underline{U}$–shaped inclusion relative to a medium with constitutive dyadic $\underline{\underline{\mathbf{K}}}(\upsilon)$. The particular solution of (1.39) for which $\upsilon = f_a$ is the DMG estimate; i.e.,

$$\underline{\underline{\mathbf{K}}}_{DMG} = \underline{\underline{\mathbf{K}}}(f_a). \tag{1.40}$$

1.3.5 Comparison of homogenisation formalisms

Extensive numerical calculations have revealed that the IMG and DMG estimates of HCM constitutive parameters are bounded by the corresponding MG and Br estimates and that the IMG values rapidly converge to the DMG values as $N \to \infty$ [9]–[11].

Significant differences between the MG, Br, IMG and DMG estimates of HCM constitutive parameters arise when there is strong electromagnetic contrast between the component phases. In such cases the most appropriate choice of homogenisation formalism depends on the composite microstructure and numerical considerations: For a low concentration of ellipsoidal inclusions embedded in a simply connected host medium, the basic MG formalism is suitable; at higher inclusion concentrations the MG is invalid and the IMG/DMG formalisms are preferable to the Br as their implementation involves simpler and more robust algorithms. Where the topologies of the inclusion and host phases are both envisaged as ellipsoidal, and particularly where the composite is expected to show a percolation threshold, the Br formalism is the most appropriate.

Chapter 2

A Homogenised Chiroplasma Composite

2.1 Introduction

Chiroplasmas, along with chiroferrites, are examples of mediums which belong to the general class of *Faraday chiral mediums*. This classification term was introduced in 1992 by Engheta *et al.* [12] in an attempt to describe a material combining *natural optical activity* — as exhibited by isotropic chiral mediums [33] — with *Faraday rotation* displayed by gyrotropic mediums [28]. Chiroplasmas and chiroferrites were theoretically conceived as composite mediums [12] comprising, respectively, chiral objects either immersed in a magnetically–biased plasma or embedded in a magnetically–biased ferrite. The frequency–domain constitutive relations of Faraday chiral mediums were rigorously developed more recently [34].

In this chapter a detailed numerical investigation of the constitutive parameters of a chiroplasma is presented [11]. In particular, the relationship between the structure of the HCM's constitutive dyadics and the constitutive parameters and topology of the constituent mediums is explored. It will be demonstrated that the incorporation non–spherical component phase topology leads to a generalisation of the HCM structure, beyond the concept of Faraday chiral mediums. This study complements and extends previous numerical studies relating to chiroferrites [35, 9].

2.2 Homogenisation preliminaries

We consider a chiroplasma HCM arising from two component phases: Component phase a is taken to be an isotropic chiral medium with

$$\underline{D} = \epsilon_0 \epsilon^c \, \underline{E} + i \, (\epsilon_0 \mu_0)^{1/2} \, \xi^c \, \underline{H} \,, \tag{2.1}$$

$$\underline{B} = - \, i \, (\epsilon_0 \mu_0)^{1/2} \, \xi^c \, \underline{E} + \mu_0 \mu^c \, \underline{H} \,, \tag{2.2}$$

as its constitutive relations [33], where ϵ^c, μ^c and ξ^c are the relative permittivity, relative permeability and the chirality parameter, respectively. A magnetically–biased (cold) plasma described by the constitutive relations [28, 36]

$$\underline{D} = \epsilon_0 \left[\epsilon^p \underline{\underline{I}} - i\epsilon_g^p \underline{u}_z \times \underline{\underline{I}} + (\epsilon_u^p - \epsilon^p) \underline{u}_z \underline{u}_z \right] \cdot \underline{E}, \tag{2.3}$$

$$\underline{B} = \mu_0 \mu^p \underline{H}, \tag{2.4}$$

where ϵ^p, ϵ_g^p, ϵ_u^p are relative permittivity scalars and μ^p is the relative permeability scalar of the plasma, is selected as component phase b. The cartesian unit vector $\underline{u}_z$ is parallel to the quasi–magnetostatic biasing field of the plasma.

Only component phases based on spherical topology are considered in Section 2.3, while the influence of non–spherical inclusions is explored in Section 2.4. The MG, Br, IMG and DMG homogenisation formalisms are all utilised to estimate the 3×3 constitutive dyadics of the HCM chiroplasma ($\underline{\underline{\epsilon}}_{HCM}$, $\underline{\underline{\xi}}_{HCM}$, $\underline{\underline{\zeta}}_{HCM}$ and $\underline{\underline{\mu}}_{HCM}$), which are related in the general bianisotropic constitutive relations

$$\underline{D} = \underline{\underline{\epsilon}}_{HCM} \cdot \underline{E} + \underline{\underline{\xi}}_{HCM} \cdot \underline{H}, \tag{2.5}$$

$$\underline{B} = \underline{\underline{\zeta}}_{HCM} \cdot \underline{E} + \underline{\underline{\mu}}_{HCM} \cdot \underline{H}. \tag{2.6}$$

2.3 Numerical homogenisation studies

2.3.1 Constitutive structure of a chiroplasma

Where the component phases are endowed with spherical topology, all four homogenisation formalisms (MG, Br, IMG and DMG) result in a HCM with the 3×3 constitutive dyadics

$$\underline{\underline{\epsilon}}_{HCM} = \epsilon_0 \left[\epsilon^{HCM} \underline{\underline{I}} - i\epsilon_g^{HCM} \underline{u}_z \times \underline{\underline{I}} + \left(\epsilon_u^{HCM} - \epsilon^{HCM} \right) \underline{u}_z \underline{u}_z \right], \tag{2.7}$$

$$\underline{\underline{\xi}}_{HCM} = i \left(\epsilon_0 \mu_0 \right)^{1/2} \left[\xi^{HCM} \underline{\underline{I}} - i\xi_g^{HCM} \underline{u}_z \times \underline{\underline{I}} + \left(\xi_u^{HCM} - \xi^{HCM} \right) \underline{u}_z \underline{u}_z \right], \tag{2.8}$$

$$\underline{\underline{\zeta}}_{HCM} = -i \left(\epsilon_0 \mu_0 \right)^{1/2} \left[\xi^{HCM} \underline{\underline{I}} - i\xi_g^{HCM} \underline{u}_z \times \underline{\underline{I}} + \left(\xi_u^{HCM} - \xi^{HCM} \right) \underline{u}_z \underline{u}_z \right], \tag{2.9}$$

$$\underline{\underline{\mu}}_{HCM} = \mu_0 \left[\mu^{HCM} \underline{\underline{I}} - i\mu_g^{HCM} \underline{u}_z \times \underline{\underline{I}} + \left(\mu_u^{HCM} - \mu^{HCM} \right) \underline{u}_z \underline{u}_z \right]. \tag{2.10}$$

Thus, the HCM combines gyrotropic anisotropy (through the dyadics $\underline{\underline{\epsilon}}_{HCM}$ and $\underline{\underline{\mu}}_{HCM}$) with gyrotropic–like bianisotropy (through $\underline{\underline{\xi}}_{HCM}$ and $\underline{\underline{\zeta}}_{HCM}$) [37, 22]. Furthermore, it is clear that the chiroplasma HCM inherits the nonreciprocal nature of the constituent plasma, despite the fact that the magnetoelectric properties of the HCM are attributable to the chiral constitutive medium which is reciprocal. A similar finding was reported for the chiroferrite composite medium [35]. In view of the developments in Section 2.4, it should be emphasised, however, that the special form of (2.7)–(2.10) applies strictly only if the constituent mediums are visualised as having a particulate spherical topology.

We begin our detailed numerical investigations by considering component mediums which are intrinsically nondissipative. For the plasma we choose $\epsilon^p = 3$, $\epsilon_u^p = 1$,

$\epsilon_g^p = 1.5$ and $\mu^p = 4$, whereas the permittivity and permeability of the chiral medium are given by $\epsilon^c = 5$ and $\mu^c = 1.5$, respectively. Figure 2.1(a) shows the behaviour of the three non–zero elements of $\underline{\underline{\xi}}_{HCM}$ for a composite with the volumetric proportion of the chiral medium selected as $f_a = 0.3$ while the chirality parameter ξ^c is varied from -2 to $+2$. Figure 2.1(b) assumes the same parameters but for the difference that ξ^c is now assigned a fixed value of 1.5 and the variation is with respect to the volumetric proportion f_a of the chiral constituent in the HCM. Consequently, $f_a = 0$ corresponds to a HCM which is purely the plasma medium, whereas $f_a = 1$ is an HCM that is identical to the chiral medium.

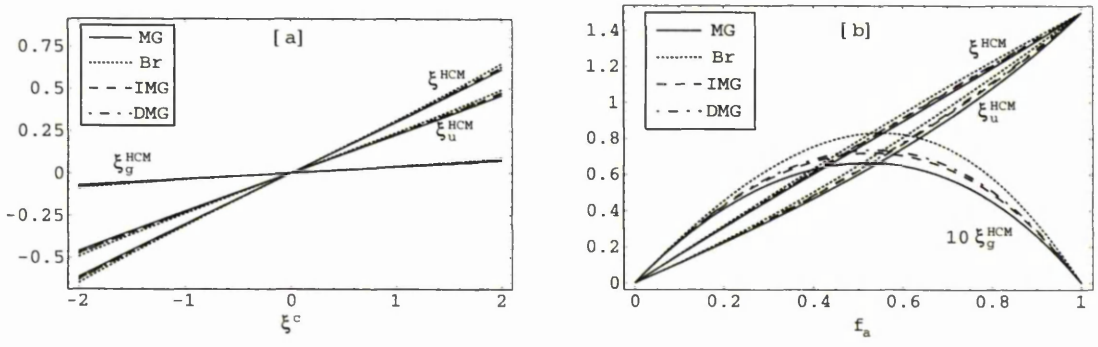

Figure 2.1: Estimates of constitutive parameters of a composite medium comprising a plasma: $\epsilon^p = 3$, $\epsilon_u^p = 1$, $\epsilon_g^p = 1.5$, $\mu^p = 4$ and an isotropic chiral medium: $\epsilon^c = 5$, $\mu^c = 1.5$. Plotted are ξ^{HCM}, ξ_u^{HCM}, ξ_g^{HCM} (a) as functions of ξ^c for $f_a = 0.3$ and (b) as functions of f_a for $\xi^c = 1.5$.

The diagrams show clearly that the magnetoelectric dyadics of the HCM have acquired a gyrotropic structure due to the interaction between the (dielectric) gyrotropy of the plasma and the isotropic magnetoelectric property of the chiral medium. Figure 2.1(a) shows that the HCM magnetoelectric scalar parameters are linearly proportional to the chirality parameter and vanish, as expected, for the value $\xi^c = 0$, while Figure 2.1(b) reveals that the maximum effect of anisotropy is reached for a volumetric proportion $f_a \approx 0.5$. We note that the graphs in Figure 2.1(b) are also consistent with those of Figure 7 of [10] in which a chiroplasma was briefly considered as part of a review of recent developments in the homogenisation of linear bianisotropic composite materials.

Figures for the estimates of the constitutive parameters of $\underline{\underline{\epsilon}}_{HCM}$ and $\underline{\underline{\mu}}_{HCM}$ are not reproduced because (i) they show only little variation with respect to ξ^c and (ii) as functions of f_a they show approximately linear behaviour between their respective values that are required at $f_a = 0$ and $f_a = 1$. The graphs in Figure 2.1 also reveal a close agreement between all four homogenisation formalisms: MG, IMG, DMG and Br. Indeed, for all computations carried out in the present study a high degree of consistency was found between the four formalisms; for clarity, only results from the Br and DMG formalisms are displayed in subsequent graphs.

2.3.2 Influence of dissipation

We consider the influence of dissipation from two perspectives. Firstly, we take a nondissipative plasma described by $\epsilon^p = 3$, $\epsilon_u^p = 1$, $\epsilon_g^p = 1.5$ and $\mu^p = 4$ mixed with a dissipative chiral medium given by $\epsilon^c = 5(1 + i\delta)$, $\xi^c = 1.5(1 + i\delta)$ and $\mu^c = 1.5(1 + i\delta)$. The corresponding real and imaginary components of the magnetoelectric HCM constitutive parameters are plotted in Figure 2.2(a) and Figure 2.2(b), respectively, as δ varies in the range $0 \leq \delta \leq 1$ with $f_a = 0.3$; and the imaginary components of ξ^{HCM}, ξ_u^{HCM}, ξ_g^{HCM} are plotted as functions of f_a for $\delta = 0.5$ in Figure 2.2(c). As might be anticipated, the imaginary components of the magnetoelectric HCM constitutive parameters are more strongly dependent on δ than are the real components, and they increase approximately linearly as both δ and the volumetric proportion of dissipative chiral medium increase. The HCM constitutive parameters not displayed in Figure 2.2 behave in a similar manner to those which are.

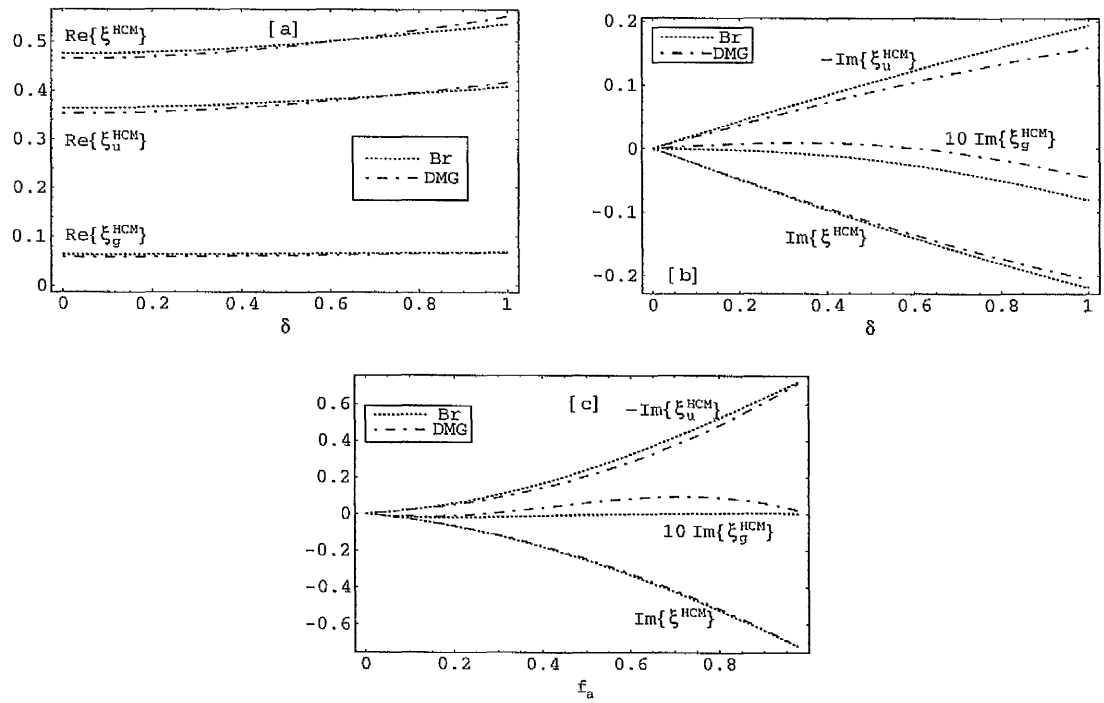

Figure 2.2: Estimates of constitutive parameters of a HCM comprising a nondissipative plasma: $\epsilon^p = 3$, $\epsilon_u^p = 1$, $\epsilon_g^p = 1.5$, $\mu^p = 4$; and a dissipative chiral medium: $\epsilon^c = 5(1+i\delta)$, $\xi^c = 1.5(1+i\delta)$, $\mu^c = 1.5(1+i\delta)$. Plotted are the (a) real and (b) imaginary components of ξ^{HCM}, ξ_u^{HCM}, ξ_g^{HCM} as functions of δ for $f_a = 0.3$; and (c) imaginary components of ξ^{HCM}, ξ_u^{HCM}, ξ_g^{HCM} as functions of f_a for $\delta = 0.5$.

Secondly, when the influence of dissipation is viewed from the alternative perspective in which a nondissipative chiral medium ($\epsilon^c = 5$, $\xi^c = 1.5$, $\mu^c = 1.5$) is mixed with a dissipative plasma ($\epsilon^p = 3(1 + i\delta)$, $\epsilon_u^p = 1 + i\delta$, $\epsilon_g^p = 1.5(1 + i\delta)$, $\mu^p = 4(1 + i\delta)$), an analogous picture to the first emerges. The corresponding imaginary components of the magnetoelectric HCM constitutive parameters are plotted as functions of δ for

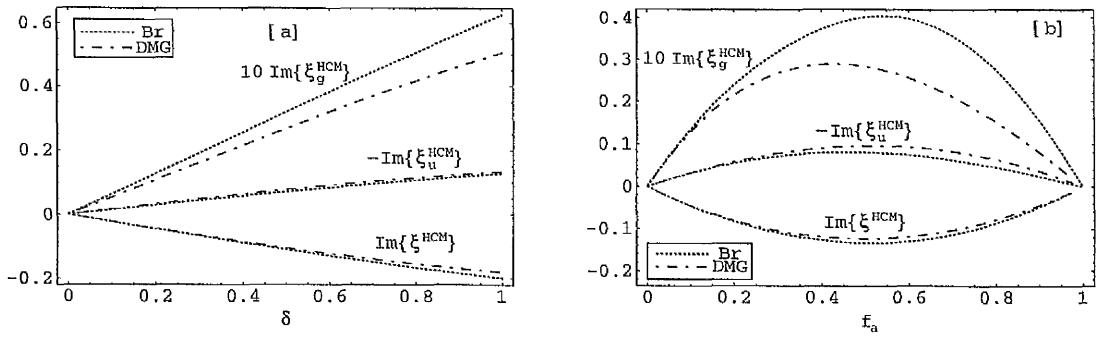

Figure 2.3: Estimates of constitutive parameters of a HCM comprising a dissipative plasma: $\epsilon^p = 3(1+i\delta)$, $\epsilon_u^p = 1+i\delta$, $\epsilon_g^p = 1.5(1+i\delta)$, $\mu^p = 4(1+i\delta)$; and a nondissipative chiral medium: $\epsilon^c = 5$, $\xi^c = 1.5$, $\mu^c = 1.5$. Plotted are the imaginary components of ξ^{HCM}, ξ_u^{HCM}, ξ_g^{HCM} as functions of (a) δ for $f_a = 0.3$ and of (b) f_a for $\delta = 0.5$.

$f_a = 0.3$, and of f_a for $\delta = 0.5$ in Figures 2.3(a) and 2.3(b), respectively. As above, the imaginary components of ϵ^{HCM}, ϵ_u^{HCM}, ϵ_g^{HCM}, as well as the imaginary components of all other HCM constitutive parameters not displayed in Figure 2.3, increase in magnitude approximately linearly as δ increases. The real components of the HCM constitutive parameters for the nondissipative chiral medium/dissipative plasma case are practically indistinguishable from those for the dissipative chiral medium/nondissipative plasma case.

2.3.3 Gyrotropy parameter

We next turn our attention to the way in which the plasma parameter ϵ_g^p endows the HCM with its gyrotropic nature. We choose constituent medium parameters: $\epsilon^p = 3$, $\epsilon_u^p = 1$ and $\mu^p = 4$; $\epsilon^c = 5$, $\xi^c = 1.5$ and $\mu^c = 1.5$. The computed values for the scalar parameters of the dyadics $\underline{\underline{\epsilon}}_{HCM}$ and $\underline{\underline{\xi}}_{HCM}$ are plotted as functions of ϵ_g^p for $f_a = 0.3$ in Figures 2.4(a) and 2.4(b), respectively. Clearly, the gyrotropic nature of the HCM is absent for $\epsilon_g^p = 0$; as ϵ_g^p increases, the degree of gyrotropy of the HCM (as reflected by ϵ_g^{HCM} and ξ_g^{HCM}) increases in an approximately linear fashion, while the diagonal terms of $\underline{\underline{\epsilon}}_{HCM}$ and $\underline{\underline{\xi}}_{HCM}$ remain approximately unchanged. The corresponding parameters of $\underline{\underline{\mu}}_{HCM}$ behave similarly. The increase in ϵ_g^{HCM} relative to ϵ^{HCM} as compared with the increase in ϵ_g^p relative to ϵ^p is displayed in Figure 2.4(c) for $f_a = 0.25, 0.5$ and 0.75. The relative magnitude of ϵ_g^{HCM} is approximately linearly proportional to the relative magnitude of ϵ_g^p and the dependency decreases as the volumetric fraction of the non–gyrotropic constituent medium increases.

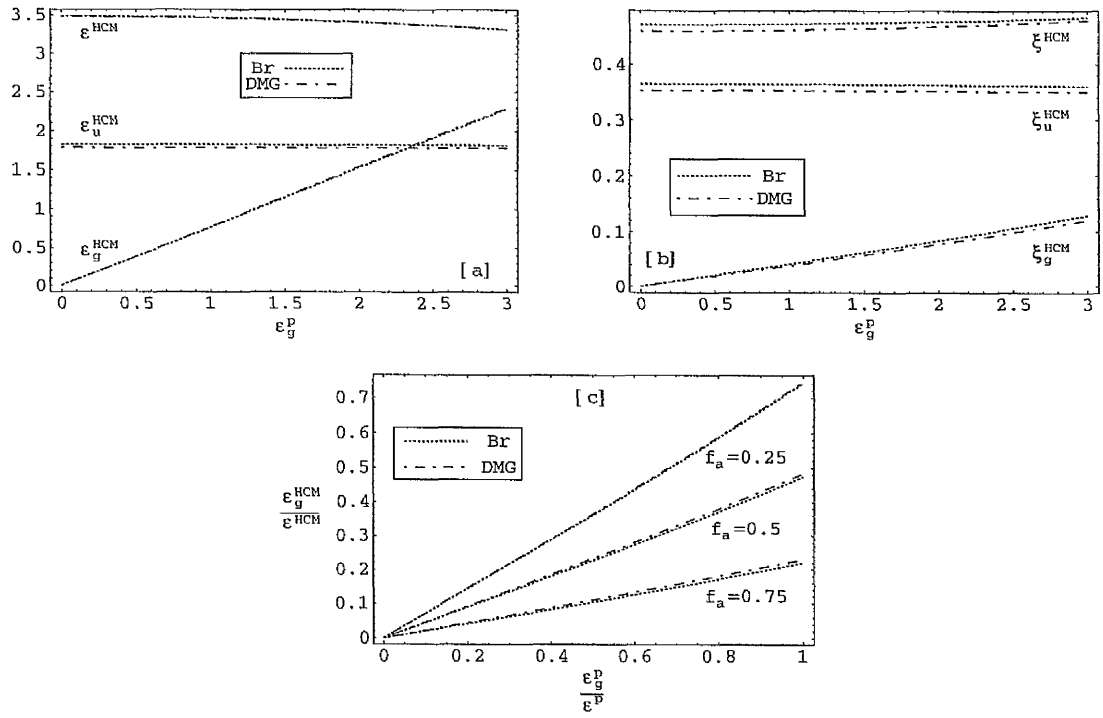

Figure 2.4: Estimates of constitutive parameters of a composite medium comprising plasma and isotropic chiral mediums: $\epsilon^p = 3$, $\epsilon_u^p = 1$, $\mu^p = 4$; $\epsilon^c = 5$, $\xi^c = 1.5$, $\mu^c = 1.5$. Plotted are (a) ϵ^{HCM}, ϵ_u^{HCM}, ϵ_g^{HCM}, and (b) ξ^{HCM}, ξ_u^{HCM}, ξ_g^{HCM} as functions of ϵ_g^p for $f_a = 0.3$. The relative magnitude of HCM gyrotropic scalar ϵ_g^{HCM} is plotted against the equivalent plasma medium quantity in (c) for $f_a = 0.25, 0.5, 0.75$.

2.4 Beyond Faraday chiral mediums

In Section 2.3, spherical chiral inclusions were assumed for all calculations. We now investigate the influence of non–spherical inclusion shapes on the HCM properties. With the same basic constituent parameters as before (i.e. $\epsilon^p = 3$, $\epsilon_g^p = 1.5$, $\epsilon_u^p = 1$, $\mu^p = 4$; $\epsilon^c = 5$, $\xi^c = 1.5$, $\mu^c = 1.5$), we now consider the case where the inclusion phase a consists of *spheroidal* particles characterised by the shape dyadic

$$\underline{\underline{U}}^{ABA} = \begin{pmatrix} A & 0 & 0 \\ 0 & B & 0 \\ 0 & 0 & A \end{pmatrix}. \tag{2.11}$$

(In the case of the Br formalism, as previously, a spherical geometry is assumed for the host plasma medium). We find that the HCM constitutive dyadics are no longer

of the form specified by (2.7)–(2.10), rather they are of the more general form:

$$\underline{\underline{\epsilon}}_{HCM} = \epsilon_0 \begin{pmatrix} \epsilon_{11}^{HCM} & \epsilon_{12}^{HCM} & 0 \\ -\epsilon_{12}^{HCM} & \epsilon_{22}^{HCM} & 0 \\ 0 & 0 & \epsilon_{33}^{HCM} \end{pmatrix}, \tag{2.12}$$

$$\underline{\underline{\xi}}_{HCM} = i(\epsilon_0\mu_0)^{1/2} \begin{pmatrix} \xi_{11}^{HCM} & \xi_{12}^{HCM} & 0 \\ \xi_{21}^{HCM} & \xi_{22}^{HCM} & 0 \\ 0 & 0 & \xi_{33}^{HCM} \end{pmatrix}, \tag{2.13}$$

$$\underline{\underline{\zeta}}_{HCM} = i(\epsilon_0\mu_0)^{1/2} \begin{pmatrix} -\xi_{11}^{HCM} & \xi_{21}^{HCM} & 0 \\ \xi_{12}^{HCM} & -\xi_{22}^{HCM} & 0 \\ 0 & 0 & -\xi_{33}^{HCM} \end{pmatrix}, \tag{2.14}$$

$$\underline{\underline{\mu}}_{HCM} = \mu_0 \begin{pmatrix} \mu_{11}^{HCM} & \mu_{12}^{HCM} & 0 \\ -\mu_{12}^{HCM} & \mu_{22}^{HCM} & 0 \\ 0 & 0 & \mu_{33}^{HCM} \end{pmatrix}. \tag{2.15}$$

The scalar parameters computed for the dyadics $\underline{\underline{\epsilon}}_{HCM}$, $\underline{\underline{\xi}}_{HCM}$ and $\underline{\underline{\mu}}_{HCM}$ are plotted as functions of B/A for $f_a = 0.3$ in Figures 2.5(a)–(c), respectively, and as functions of f_a for $B/A = 2.5$ in Figures 2.6(a)–(c), respectively. At the point $B/A = 1$ the spheroidal shape becomes spherical and the HCM constitutive dyadics revert to the

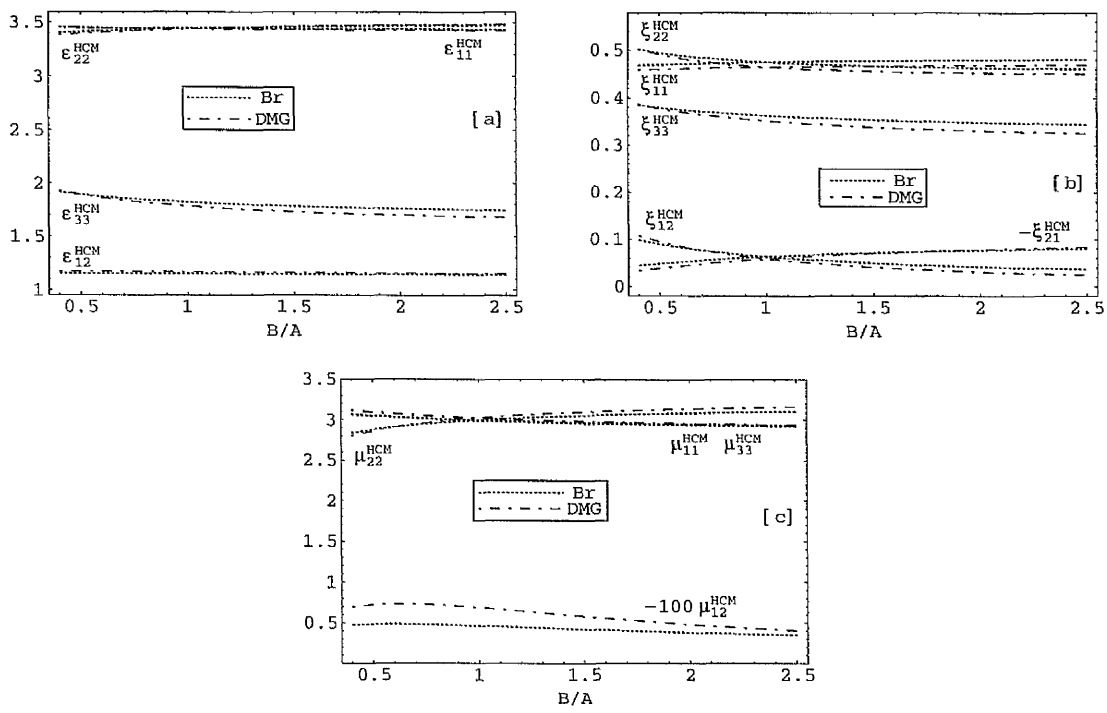

Figure 2.5: Estimates of constitutive parameters of a composite medium comprising plasma and isotropic chiral mediums: $\epsilon^p = 3$, $\epsilon_g^p = 1.5$, $\epsilon_u^p = 1$, $\mu^p = 4$; $\epsilon^c = 5$, $\xi^c = 1.5$, $\mu^c = 1.5$; with spheroidal inclusions described by shape dyadic $\underline{\underline{U}}^{ABA}$. Plotted are (a) ϵ_{11}^{HCM}, ϵ_{22}^{HCM}, ϵ_{33}^{HCM}, ϵ_{12}^{HCM}; (b) ξ_{11}^{HCM}, ξ_{22}^{HCM}, ξ_{33}^{HCM}, ξ_{12}^{HCM}, ξ_{21}^{HCM}; (c) μ_{11}^{HCM}, μ_{22}^{HCM}, μ_{33}^{HCM}, μ_{12}^{HCM} as functions of B/A for $f_a = 0.3$.

form given in (2.7)–(2.10), as is apparent from Figure 2.5. However, as B/A deviates from unity so the HCM becomes more unlike that specified by the dyadics (2.7)–(2.10). This deviation from (2.7)–(2.10) is most marked for intermediate volumetric proportions of chiral inclusion medium and diminishes as f_a tends to unity or zero.

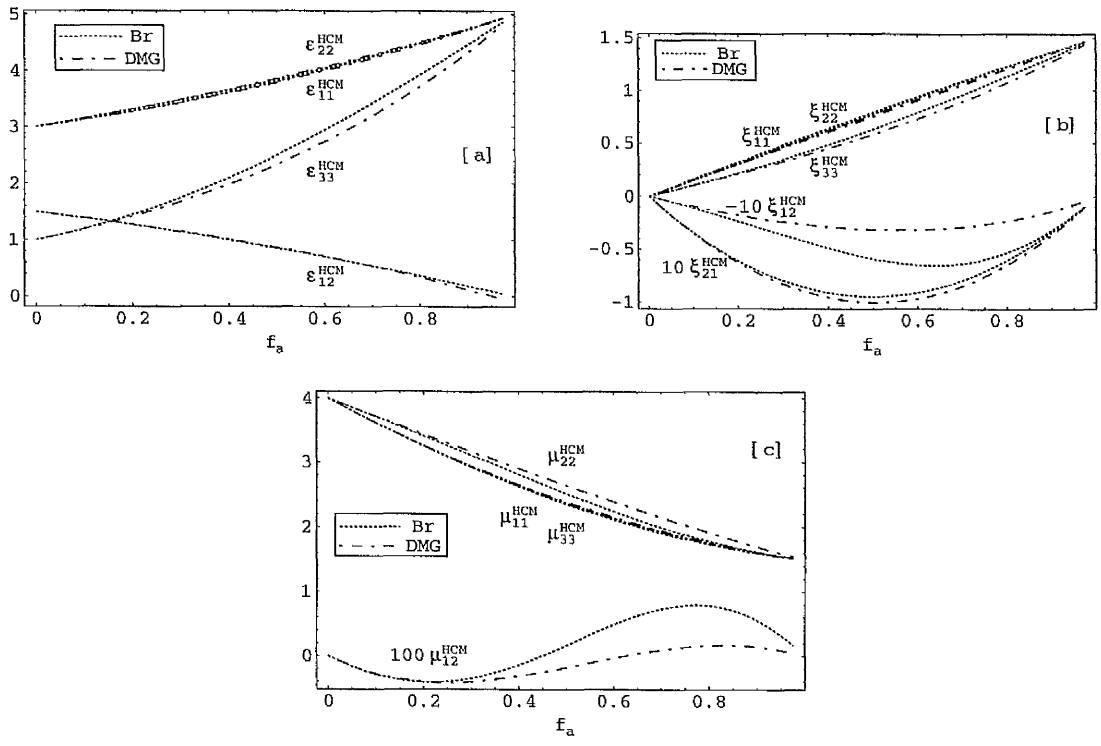

Figure 2.6: As for Figure 2.5 but with constitutive parameters plotted as functions of f_a for $B/A = 2.5$.

If the above calculations are repeated using the shape dyadic

$$\underline{\underline{U}}^{AAB} = \begin{pmatrix} A & 0 & 0 \\ 0 & A & 0 \\ 0 & 0 & B \end{pmatrix}, \tag{2.16}$$

then the HCM constitutive dyadics retain the form of (2.7)–(2.10). The crucial difference between the two shape dyadics being that for $\underline{\underline{U}}^{AAB}$ the distinguished spheroidal axis is aligned along the direction of the quasi–magnetostatic biasing field of the plasma whereas for $\underline{\underline{U}}^{ABA}$ it is perpendicular to the biasing field.

It is also clear that an even richer constitutive structure than expressed through (2.12)–(2.15) will arise for the HCM if none of the principal axes of the spheroidal inclusions coincides with the direction $\underline{u}_z$ any more. The consequence of non–zero entries in the 13, 23, 31 and 32 slots of $\underline{\underline{U}}^{ABA}$ and $\underline{\underline{U}}^{AAB}$ in (2.11) and (2.16), respectively, will lead to general dyadics in (2.12)–(2.15). While such possibilities provide many interesting scenarios, these will not be pursued here.

2.5 Concluding remarks

A detailed numerical study of a chiroplasma composite arising from the homogenisation of a magnetically–biased plasma and an isotropic chiral medium has been presented. Where the component phases are based on spherical topology, the HCM falls into the category of Faraday chiral mediums; more general HCM structures develop in the case where the inclusion phase is based on non–spherical topology.

We note that both the Faraday chiral medium structure (2.7)–(2.10) and the more general HCM structure (2.12)–(2.15) are consistent with the Post constraint (1.19) [25]–[27].

The studies of the chiroplasma presented here complement investigations on chiroferrites in which the plasma is replaced by a magnetically–biased ferrite. Both chiroplasmas and chiroferrites provide promising conceptualisations of novel composites for use in a variety of microwave technologies. Homogenisation studies as reported here are important stepping stones (i) to a better understanding of how the constitutive properties of HCMs depend on constitutive properties and topology of the constituent mediums, and (ii) towards the evaluation of the performance of different homogenisation formalisms themselves.

Chapter 3

Biaxiality in Homogenised Composite Mediums

3.1 Introduction

The notion of biaxiality is well–established in classical optics and crystallography, providing as it does the classification for orthorhombic, monoclinic and triclinic structures [38, 39]. Recent theoretical studies of electromagnetic biaxiality have focussed on Green functions[1] [40]–[42], depolarisation dyadics [43, 30] and wave propagation [44]–[48]. This chapter pertains to the conceptualisation of biaxial composite mediums through the process of homogenisation. We consider in detail the relationship between biaxiality and the geometry, orientation and composition of the component mediums, and explore symmetries in the constitutive dyadics of the biaxial HCMs. Specifically, we investigate scenarios where the particulate component phases are themselves non–biaxial but collectively they present two noncollinear distinguished axes. The distinguished axes of the component phases may arise due to their intrinsic electromagnetic properties or from the particulate geometries.

The development of biaxial composites through the homogenisation of assemblies of parallel ellipsoidal inclusions is a familiar concept in the purely dielectric regime: A brief review of early studies is provided by Ward [5]. Of particular historical interest is the analysis of arrays of parallel dielectric ellipsoids by Wiener [49] (reproduced in [1]). In the context of purely dielectric biaxial HCMs deriving from metallic ellipsoidal constituents, Sherwin *et al.* [50] recently investigated the percolation phenomenon. Further background material on composites with ellipsoidal inclusions may be found in [2]. However, a detailed parametric study of the conceptualisation of biaxial HCMs, relating both the intrinsic electromagnetic properties and the topological structure of the constituents to the HCM form, has not been reported previously. Such an investigation is reported in Section 3.3 [13], where we concentrate on relatively simple

[1] Obtaining the infinite–medium dyadic Green function of a biaxial dielectric medium remains an unsolved problem [24].

constituent mediums with a high degree of electromagnetic and particulate symmetry. Thus, we consider only constituent phases which are, individually, either isotropic or uniaxial with respect to permittivity and comprise particles of ellipsoidal, spheroidal or spherical shape.

The studies of Section 3.3 are extended in Section 3.4 in two ways [14]: (i) allowance for dissipative processes is made in the constitutive properties of the component phases; and (ii) fully anisotropic biaxial HCMs are considered by perusing mediums with dielectric and magnetic constitutive properties as constituents in the homogenisation procedure. Thereby, a generalised anisotropic biaxial structure, for which principal axes of real and imaginary parts of the permittivity and permeability constitutive dyadics do not coincide, is developed.

The process of generalisation is completed in Section 3.5 where biaxiality in the case of fully bianisotropic HCMs is considered [15]. A generalised biaxial bianisotropic structure, characterised by 45 real–valued parameters, is presented. Complex symmetries are highlighted in the constitutive dyadics of the HCMs which would not be anticipated from a familiarity of the dielectric or dielectric–magnetic cases described in Sections 3.3 and 3.4, respectively.

In the present investigations the Br homogenisation formalism has been adopted since, unlike the MG, IMG and DMG approaches, it permits the particulate shapes of the constituent mediums a and b to be varied independently. Except where explicitly stated otherwise, an inclusion volume fraction $f_a = 0.3$ was used for all calculations.

3.2 Characterisations of biaxiality

The relative permittivity dyadic of a nondissipative biaxial dielectric medium may be represented by [48] (see also [28, 41])

$$\underline{\underline{\epsilon}}_{bi} = p_\epsilon \, \underline{\underline{I}} + q_\epsilon (\underline{u}_m \underline{u}_n + \underline{u}_n \underline{u}_m) \,, \tag{3.1}$$

where p_ϵ and q_ϵ are dimensionless real–valued permittivity scalars. Also, $\underline{u}_m$ and $\underline{u}_n$ represent two real–valued unit vectors which may be described in terms of spherical polar coordinates as

$$\underline{u}_\kappa = \sin\theta_\kappa \cos\phi_\kappa \, \underline{u}_x + \sin\theta_\kappa \sin\phi_\kappa \, \underline{u}_y + \cos\theta_\kappa \, \underline{u}_z \,, \qquad (\kappa = m, n) \,. \tag{3.2}$$

The advantage of (3.1) over the widely–used diagonal dyadic representation of biaxial permittivity (see, for example, [51])

$$\underline{\underline{\tilde{\epsilon}}}_{bi} = \epsilon_x \underline{u}_x \underline{u}_x + \epsilon_y \underline{u}_y \underline{u}_y + \epsilon_z \underline{u}_z \underline{u}_z \,, \tag{3.3}$$

is that the representation (3.1) affords an immediate crystallographic interpretation: the unit vectors $\underline{u}_m$ and $\underline{u}_n$ give the two privileged directions in which monochromatic plane waves propagate with only one permissible group velocity; i.e., $\underline{u}_m$ and $\underline{u}_n$ lie along the directions of the *optic ray axes* [38, 13].

In the absence of dissipation (i.e., $p_\epsilon, q_\epsilon, \epsilon_x, \epsilon_y, \epsilon_z \in \mathbb{R}$) the equivalence of representations (3.1) and (3.3) may be straightforwardly shown through diagonalisation of (3.1). In geometrical terms, the three possible diagonalisations may be achieved by choosing the coordinate frame such that $\underline{u}_m$ and $\underline{u}_n$ lie in one of the three coordinate planes with the plane axes bisecting $\underline{u}_m$ and $\underline{u}_n$. Therefore, there are three possibilities:

(i) $\underline{u}_m$ and $\underline{u}_n$ lie in the xy plane with $\phi_m = \pi - \phi_n = \phi$

$$\underline{\underline{\epsilon}}_{bi} = (p_\epsilon - 2q_\epsilon \cos^2\phi)\underline{u}_x\underline{u}_x + (p_\epsilon + 2q_\epsilon \sin^2\phi)\underline{u}_y\underline{u}_y + p_\epsilon \underline{u}_z\underline{u}_z\,; \tag{3.4}$$

(ii) $\underline{u}_m$ and $\underline{u}_n$ lie in the yz plane with $\theta_m = \pi - \theta_n = \theta$

$$\underline{\underline{\epsilon}}_{bi} = p_\epsilon \underline{u}_x\underline{u}_x + (p_\epsilon + 2q_\epsilon \sin^2\theta)\underline{u}_y\underline{u}_y + (p_\epsilon - 2q_\epsilon \cos^2\theta)\underline{u}_z\underline{u}_z\,; \tag{3.5}$$

(iii) $\underline{u}_m$ and $\underline{u}_n$ lie in the xz plane with $\theta_m = \pi - \theta_n = \theta$

$$\underline{\underline{\epsilon}}_{bi} = (p_\epsilon + 2q_\epsilon \sin^2\theta)\underline{u}_x\underline{u}_x + p_\epsilon \underline{u}_y\underline{u}_y + (p_\epsilon - 2q_\epsilon \cos^2\theta)\underline{u}_z\underline{u}_z\,. \tag{3.6}$$

A diagonal representation equivalent to (3.1) can thus be established. Note that the nondissipative biaxial permittivity is characterised by three real–valued parameters in both representations: ϵ_x, ϵ_y, ϵ_z in (3.3) and p_ϵ, q_ϵ, ϕ or θ in (3.4)–(3.6), respectively.

The presence of dissipative processes complicates matters. If we consider representations (3.1) and (3.3) with $p_\epsilon, q_\epsilon, \epsilon_x, \epsilon_y, \epsilon_z \in \mathbb{C}$, the diagonal forms (3.4)–(3.6) still hold but — in trying to establish a correspondence between the different representations — solving (3.3) and (3.4)–(3.6) for θ or ϕ leads to $\theta, \phi \in \mathbb{C}$ in general. This would clearly conflict with our physical interpretation of $\underline{u}_m$ and $\underline{u}_n$ as real–valued unit vectors. This problem can be overcome by extending the representation (3.1) to

$$\underline{\underline{\epsilon}}_{bi} = \underline{\underline{\epsilon}}^r_{bi} + i\,\underline{\underline{\epsilon}}^i_{bi}\,, \tag{3.7}$$

with

$$\underline{\underline{\epsilon}}^\chi_{bi} = a^\chi_\epsilon\,\underline{\underline{I}} + b^\chi_\epsilon(\underline{u}^\chi_m\underline{u}^\chi_n + \underline{u}^\chi_n\underline{u}^\chi_m)\,, \qquad (\chi = r, i), \tag{3.8}$$

wherein a^χ_ϵ and b^χ_ϵ are real–valued scalars, and $\underline{u}^\chi_m$ and $\underline{u}^\chi_n$ are real–valued unit vectors that can be represented in the standard form (3.2). If we similarly express the complex form of (3.3) as

$$\underline{\underline{\tilde{\epsilon}}}_{bi} = \underline{\underline{\tilde{\epsilon}}}^r_{bi} + i\underline{\underline{\tilde{\epsilon}}}^i_{bi}\,, \tag{3.9}$$

where $\underline{\underline{\tilde{\epsilon}}}^r_{bi}$ and $\underline{\underline{\tilde{\epsilon}}}^i_{bi}$ are real–valued diagonal dyadics, then, as in the non–dissipative case, we can identify $\underline{\underline{\tilde{\epsilon}}}^r_{bi}$ with a diagonalised form of $\underline{\underline{\epsilon}}^r_{bi}$ (with real–valued $\underline{u}^r_m$ and $\underline{u}^r_n$), and $\underline{\underline{\tilde{\epsilon}}}^i_{bi}$ with a diagonalised form of $\underline{\underline{\epsilon}}^i_{bi}$ (with real–valued $\underline{u}^i_m$ and $\underline{u}^i_n$). As with the complex diagonal form (3.9), the equivalent permittivity representation (3.7) is specified by six real–valued parameters: diagonal forms of $\underline{\underline{\epsilon}}^r_{bi}$ and $\underline{\underline{\epsilon}}^i_{bi}$ are each specified by two real permittivity scalars ($a^r_\epsilon, b^r_\epsilon$ and $a^i_\epsilon, b^i_\epsilon$, respectively) and one real angle (the half–angle between $\underline{u}^r_m$ and $\underline{u}^r_n$ and between $\underline{u}^i_m$ and $\underline{u}^i_n$, respectively). Observe that, depending

on the relative magnitudes of the diagonal terms in (3.9), the process of diagonalising (3.7) may involve choosing $\underline{u}_m^r$ and $\underline{u}_n^r$ to lie on a different coordinate plane from that of $\underline{u}_m^i$ and $\underline{u}_n^i$.

Biaxial dielectric mediums described by permittivity dyadics of the form (3.9) belong to the *orthorhombic* class of crystals [52]. In this class the three basis vectors defining the primitive unit cell of the Bravais lattice are mutually perpendicular. However, there are more general classes of biaxial crystal structure: if only two of the basis vectors are perpendicular then the structure is called *monoclinic*, while for *triclinic* structures there are no pairs of perpendicular basis vectors. In the case of dissipative monoclinic and triclinic biaxial materials the principal axes of the real and imaginary parts of $\underline{\underline{\tilde{\epsilon}}}_{bi}$ do not coincide [7]. Thus, for the most general dissipative biaxial dielectric structure, nine real–valued parameters are required to characterise the material permittivity: three scalars for each of the diagonal forms of $\underline{\underline{\tilde{\epsilon}}}_{bi}^r$ and $\underline{\underline{\tilde{\epsilon}}}_{bi}^i$ and a further three Eulerian angles relating the principal axes of $\underline{\underline{\tilde{\epsilon}}}_{bi}^r$ to those of $\underline{\underline{\tilde{\epsilon}}}_{bi}^i$. For the general case we may write either

$$\underline{\underline{\tilde{\epsilon}}}_{bi}^r = \begin{bmatrix} \epsilon_x^{r1} & 0 & 0 \\ 0 & \epsilon_y^{r1} & 0 \\ 0 & 0 & \epsilon_z^{r1} \end{bmatrix}, \qquad \underline{\underline{\tilde{\epsilon}}}_{bi}^i = \begin{bmatrix} \epsilon_x^{i1} & \alpha_1 & \alpha_2 \\ \alpha_1 & \epsilon_y^{i1} & \alpha_3 \\ \alpha_2 & \alpha_3 & \epsilon_z^{i1} \end{bmatrix}, \tag{3.10}$$

or

$$\underline{\underline{\tilde{\epsilon}}}_{bi}^r = \begin{bmatrix} \epsilon_x^{r2} & \beta_1 & \beta_2 \\ \beta_1 & \epsilon_y^{r2} & \beta_3 \\ \beta_2 & \beta_3 & \epsilon_z^{r2} \end{bmatrix}, \qquad \underline{\underline{\tilde{\epsilon}}}_{bi}^i = \begin{bmatrix} \epsilon_x^{i2} & 0 & 0 \\ 0 & \epsilon_y^{i2} & 0 \\ 0 & 0 & \epsilon_z^{i2} \end{bmatrix}, \tag{3.11}$$

where all dyadic entries in (3.10) and (3.11) are real–valued.

Representations (3.10) and (3.11) are equivalent to representations of the form (3.7) for the case where only one of the pairs $\underline{u}_m^r$ and $\underline{u}_n^r$ or $\underline{u}_m^i$ and $\underline{u}_n^i$ lies in a coordinate plane with plane axes bisecting the unit vector pair, and the other unit vector pair lies in an arbitrary position. For example, selecting $\underline{u}_m^r$ and $\underline{u}_n^r$ to lie in a coordinate plane with plane axes bisecting $\underline{u}_m^r$ and $\underline{u}_n^r$ results in the diagonalisation of $\underline{\underline{\epsilon}}_{bi}^r$, while the arbitrary position of $\underline{u}_m^i$ and $\underline{u}_n^i$ gives rise to a general symmetric form for $\underline{\underline{\epsilon}}_{bi}^i$. In this case $\underline{\underline{\epsilon}}_{bi}$ is specified by nine real parameters: the diagonalised $\underline{\underline{\epsilon}}_{bi}^r$ is defined by two scalar permittivities along with the half angle between $\underline{u}_m^r$ and $\underline{u}_n^r$, and $\underline{\underline{\epsilon}}_{bi}^i$ is specified by two scalar permittivities together with the four angles defining the arbitrary positions of $\underline{u}_m^i$ and $\underline{u}_n^i$ (i.e., $\theta_m^i, \theta_n^i, \phi_m^i$ and ϕ_n^i). Thus we have a representation equivalent to (3.10) and specified by the same number of real parameters. An equivalent procedure may be applied in the case of representation (3.11).

We conclude that (3.7) provides a convenient and physically–insightful characterisation of dissipative biaxial dielectric mediums. The detailed discussion so far was limited to dissipative biaxial dielectric mediums and revolved around the structure of the relative permittivity dyadic $\underline{\underline{\epsilon}}_{bi}$. Later in this chapter, when we consider biaxial anisotropic and bianisotropic mediums, representations analogous to (3.7) shall be adopted for the relative permeability and magnetoelectric constitutive dyadics.

3.3 Nondissipative dielectric properties

We begin our study of biaxial HCMs by considering the simplest case, namely that of nondissipative dielectric materials [13]. Thus, in this section we consider only component phases characterised by real–valued permittivity dyadics $\underline{\underline{\epsilon}}_a$ and $\underline{\underline{\epsilon}}_b$. The exclusion of dissipative effects constitutes an often–used approximation in parametric homogenisation studies. Furthermore, we restrict the electromagnetic material properties of the component phases to be either isotropic or uniaxial. Correspondingly, all host and inclusion mediums considered here, can be characterised by permittivity dyadics of the form

$$\underline{\underline{\epsilon}}_\ell = \epsilon_0 \left[\begin{array}{ccc} \epsilon_\ell^x \cos^2\lambda_\ell + \epsilon_\ell \sin^2\lambda_\ell & (\epsilon_\ell^x - \epsilon_\ell)\sin\lambda_\ell\cos\lambda_\ell & 0 \\ (\epsilon_\ell^x - \epsilon_\ell)\sin\lambda_\ell\cos\lambda_\ell & \epsilon_\ell^x \sin^2\lambda_\ell + \epsilon_\ell\cos^2\lambda_\ell & 0 \\ 0 & 0 & \epsilon_\ell \end{array} \right], \qquad (\ell = a, b), \quad (3.12)$$

where ϵ_ℓ^x and ϵ_ℓ are scalar permittivity parameters. The distinguished permittivity axis lies in the xy plane at an angle λ_ℓ to the x axis. The dyadic (3.12) is of general uniaxial form; letting the distinguished axis coincide with the x axis (i.e., setting $\lambda_\ell = 0$), reduces (3.12) to the more commonly used form $\underline{\underline{\epsilon}}_\ell = \mathrm{diag}\,(\epsilon_\ell^x, \epsilon_\ell, \epsilon_\ell)$. Also, the isotropic limit is achieved for $\epsilon_\ell^x = \epsilon_\ell$. Permeability is simply taken as the vacuum value μ_0.

Throughout Sections 3.3.1–3.3.2 the, in general, ellipsoidal shapes of the particles comprising component phases a and b are characterised by the shape dyadics $\underline{\underline{U}}_a$ and $\underline{\underline{U}}_b$, respectively, given as

$$\underline{\underline{U}}_\ell = \left[\begin{array}{ccc} \alpha_\ell \cos^2\psi_\ell + \beta_\ell \sin^2\psi_\ell & (\alpha_\ell - \beta_\ell)\sin\psi_\ell\cos\psi_\ell & 0 \\ (\alpha_\ell - \beta_\ell)\sin\psi_\ell\cos\psi_\ell & \alpha_\ell \sin^2\psi_\ell + \beta_\ell\cos^2\psi_\ell & 0 \\ 0 & 0 & \gamma_\ell \end{array} \right], \qquad (\ell = a, b), \quad (3.13)$$

where α_ℓ, β_ℓ and γ_ℓ represent the ellipsoid semi–axis lengths. The specialisation $\beta_\ell = \gamma_\ell$ leads to a spheroidal shape and in which case we refer to the semi–axis of length α_ℓ as the *spheroid axis*; whereas $\alpha_\ell = \beta_\ell = \gamma_\ell$ represents spherical constituent mediums. Semi–axes of lengths α_ℓ and β_ℓ lie in the xy plane with the α_ℓ semi–axis at angle ψ_ℓ to the x axis; the γ_ℓ semi–axis is aligned with the z axis.

In Sections 3.3.1 and 3.3.2 we explore two methods of attaining a biaxial HCM in which both the host and inclusion mediums are isotropic dielectric. Directional effects are introduced by choosing non–spherical shapes for the constituent particles. In Section 3.3.3 then we look at a situation where the distinguished axes in the constituent mediums do not arise from the shape of the particles themselves but from their intrinsic uniaxial permittivity. Finally we investigate two mixed cases in Sections 3.3.4 and 3.3.5 where the two distinguished axes have different sources: one electromagnetic and the other topological.

The permittivity dyadics for all HCM structures arising in Sections 3.3.1–3.3.5 have the biaxial form

$$\underline{\underline{\epsilon}}_{HCM} = \epsilon_0 \left[p_\epsilon \underline{\underline{I}} + q_\epsilon (\underline{u}_m \underline{u}_n + \underline{u}_n \underline{u}_m) \right], \qquad (3.14)$$

where p_ϵ, $q_\epsilon \in \mathbb{R}$ and the unit vectors $\underline{u}_m$ and $\underline{u}_n$ are given by (3.2) with $\theta_m = \pi - \theta_n = \theta$ and $\phi_m = \phi_n = \phi$, i.e.,

$$\underline{u}_m = \sin\theta\,\cos\phi\,\underline{u}_x + \sin\theta\,\sin\phi\,\underline{u}_y + \cos\theta\,\underline{u}_z\,, \tag{3.15}$$

$$\underline{u}_n = \sin\theta\,\cos\phi\,\underline{u}_x + \sin\theta\,\sin\phi\,\underline{u}_y - \cos\theta\,\underline{u}_z\,. \tag{3.16}$$

3.3.1 Isotropic ellipsoidal inclusions/isotropic spherical host

We first consider ellipsoidal inclusions in combination with spherical host particles where both host and inclusion mediums are isotropic with respect to permittivity. We choose

$$\begin{aligned} \epsilon_b^x &= \epsilon_b = 1.2\,,\ \lambda_b = 0\,,\ \alpha_b = \beta_b = \gamma_b = 1\,,\ \psi_b = 0\,; \\ \epsilon_a^x &= \epsilon_a = 3.5\,,\ \lambda_a = 0\,,\ \alpha_a = 2\,,\ \beta_a = 1\,,\ \psi_a = 0\,. \end{aligned} \tag{3.17}$$

Values for the dielectric constitutive parameters, i.e., the scalar, relative permittivity constants p_ϵ and q_ϵ in (3.14) of the resulting HCM along with unit vector angles θ and ϕ in (3.15) and (3.16) were computed as the ellipsoid eccentricity increased along the z axis: γ_a ranged from 0.5 to 1. These results are plotted in Figure 3.1(a). With the exception of the polar angle θ, the HCM parameters show very little variation with γ_a, indeed, no variation at all in the case of ϕ; $\theta \to \pi/2$ and the HCM becomes uniaxial as $\gamma_a \to 1$ (i.e., as the ellipsoidal inclusions become spheroidal). In this particular case the dependency on inclusion volume fraction f_a was also investigated: for $\gamma_a = 0.5$, the HCM constitutive parameters were calculated as a function of f_a over the range 0 to 1 and the results displayed in Figure 3.1(b). The scalar ϵ_a shows an almost linear increase with f_a whereas ϵ_b vanishes as f_a tends to 0 and 1, respectively, and reaches it maximum value for $f_a \approx 0.55$. The orientations of $\underline{u}_m$ and $\underline{u}_n$ are little influenced by f_a: as f_a increases, θ increases only slightly and ϕ remains constant.

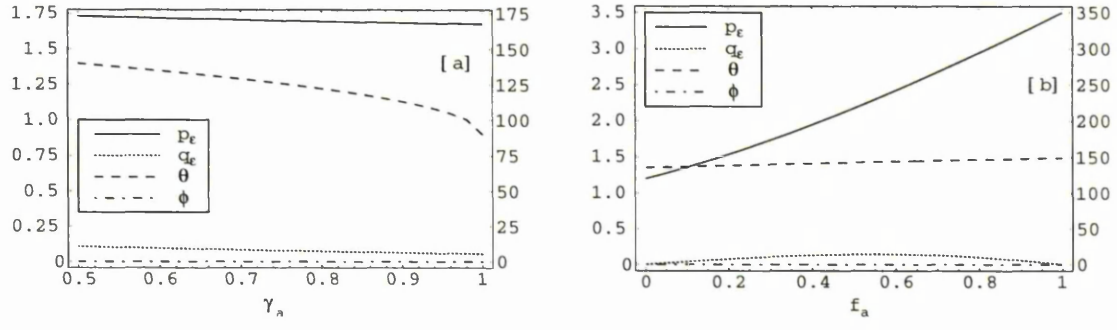

Figure 3.1: Isotropic ellipsoidal inclusions with isotropic spherical host. Relative permittivity scalars p_ϵ and q_ϵ (left scale) and angles θ and ϕ (in degrees, right scale) of the HCM plotted against (a) inclusion ellipsoid semi–axis γ_a and (b) inclusion volume fraction f_a.

3.3.2 Isotropic spheroidal inclusions/isotropic spheroidal host

We now look at the homogenisation of isotropic dielectric mediums where both the host and inclusion phase particles are chosen to be spheroidal. The spheroid axis of the inclusion particles is set at an angle ψ_a in the xy plane to that of the host medium particles. Specifically, the parameters are

$$\begin{aligned} &\epsilon_b^x = \epsilon_b = 1.2\,,\ \lambda_b = 0\,,\ \alpha_b = 2\,,\ \beta_b = \gamma_b = 1\,,\ \psi_b = 0\,; \\ &\epsilon_a^x = \epsilon_a = 3.5\,,\ \lambda_a = 0\,,\ \alpha_a = 2\,,\ \beta_a = \gamma_a = 1\,. \end{aligned} \tag{3.18}$$

Estimates of HCM parameters p_ϵ, q_ϵ, θ and ϕ were computed as ψ_a ranged from 0 to π radians and the results are plotted in Figure 3.2. The plane in which $\underline{u}_m$ and $\underline{u}_n$ lie, as given by ϕ, rotates about the z axis as ψ_a increases, whereas the angle between $\underline{u}_m$ and $\underline{u}_n$, as given by $2(\theta - \pi/2)$, increases to a maximum at $\psi_a = \pi/2$ and falls to 0 as ψ_a tends to 0 and π. At $\psi_a = 0, \pi$, the spheroid axes of the host and inclusion mediums are parallel and anti–parallel, respectively; therefore the constituent mediums together present only one distinguished axis and the resulting HCM is accordingly uniaxial. The scalars p_ϵ and q_ϵ are not greatly influenced by ψ_a.

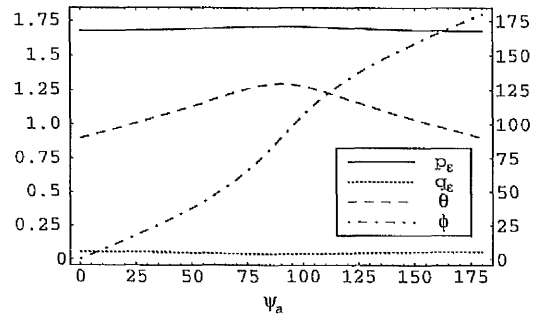

Figure 3.2: Isotropic spheroidal inclusions with isotropic spheroidal host. Relative permittivity scalars p_ϵ and q_ϵ (left scale) and angles θ and ϕ (in degrees, right scale) of the HCM plotted against inclusion spheroid axis angle ψ_a.

3.3.3 Uniaxial spherical inclusions/uniaxial spherical host

We now turn our attention to the case where both host and inclusion phases comprise spherical particles of uniaxial permittivity. The angle λ_a was varied from 0 to π radians and the corresponding parameters of $\underline{\underline{\epsilon}}_{HCM}$, based on the input quantities

$$\begin{aligned} &\epsilon_b^x = 3\,,\ \epsilon_b = 1\,,\ \lambda_b = 0\,,\ \alpha_b = \beta_b = \gamma_b = 1\,,\ \psi_b = 0\,; \\ &\epsilon_a^x = 3\,,\ \epsilon_a = 1\,,\ \alpha_a = \beta_a = \gamma_a = 1\,, \psi_a = 0\,, \end{aligned} \tag{3.19}$$

are displayed in Figure 3.3. The scalar permittivity parameters p_ϵ and q_ϵ are considerably more orientationally dependent than they were in Section 3.3.2. As $\lambda_a \to 0, \pi$, we see that $\theta \to \pi/2$ and the scalars $p_\epsilon \to 1$ and $q_\epsilon \to 1$ and thus the HCM permittivity

dyadic acquires the uniaxial form. Unlike the situation in which the distinguished axes arise from the shape of the constituent particles, the orientation of the plane containing $\underline{u}_m$ and $\underline{u}_n$ does not follow the angle of the distinguished permittivity axis λ_a, rather it oscillates about the x axis.

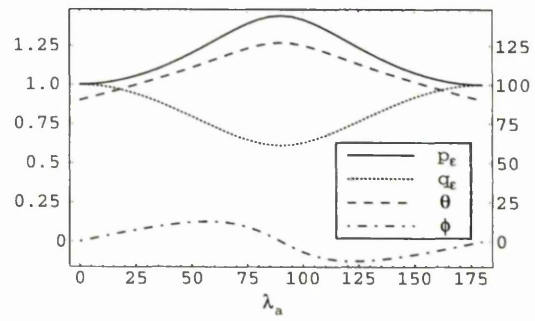

Figure 3.3: As for Figure 3.2 but for uniaxial spherical inclusions with uniaxial spherical host. Constitutive parameters of the HCM plotted against inclusion permittivity axis angle λ_a.

3.3.4 Isotropic spheroidal inclusions/uniaxial spherical host

Here we homogenise spheroidal inclusions with a host medium comprising spherical particles where the inclusion and host phases are taken to be isotropic and uniaxial, respectively, with respect to permittivity:

$$\begin{aligned} &\epsilon_b^x = 3\,,\ \epsilon_b = 1\,,\ \lambda_b = 0\,,\ \alpha_b = \beta_b = \gamma_b = 1\,,\ \psi_b = 0\,; \\ &\epsilon_a^x = \epsilon_a = 3.5\,,\ \lambda_a = 0\,,\ \alpha_a = 2\,,\ \beta_a = \gamma_a = 1\,. \end{aligned} \tag{3.20}$$

As before, the HCM constitutive parameters were computed as a function of the angle ψ_a between the distinguished axes directions in the xy plane; the results are presented in Figure 3.4. All four HCM parameters display a similar pattern of behaviour with respect to orientation angle ψ_a as they did in Figure 3.3; the most notable difference being that the degree of sensitivity on orientation angle is rather less in the present case.

3.3.5 Uniaxial spheroidal inclusions/isotropic spherical host

Finally we consider the alternative mixed case where we have the inclusions solely responsible for directional effects: uniaxial spheroidal inclusions homogenised with an isotropic host medium of spherical particulate topology with chosen values as

$$\begin{aligned} &\epsilon_b^x = \ \epsilon_b = 1.2\,,\ \lambda_b = 0\,,\ \alpha_b = \beta_b = \gamma_b = 1\,,\ \psi_b = 0\,; \\ &\epsilon_a^x = 3\,,\ \epsilon_a = 1\,,\ \lambda_a = 0\,,\ \alpha_a = 2\,,\ \beta_a = \gamma_a = 1\,. \end{aligned} \tag{3.21}$$

In Figure 3.5 the corresponding HCM constitutive parameters are plotted as a function of angle ψ_a, the angle between the two distinguished inclusion axes in the xy plane.

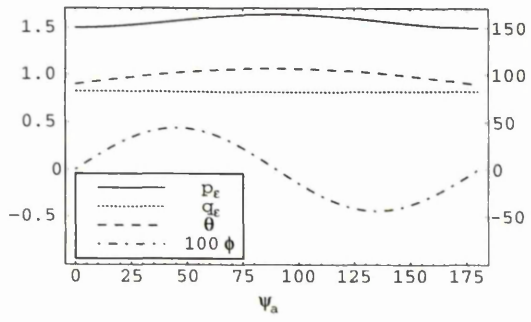

Figure 3.4: As for Figure 3.2 but for isotropic spheroidal inclusions with uniaxial spherical host. Constitutive parameters of the HCM plotted against inclusion spheroid axis angle ψ_a.

As for Section 3.3.4, the plane containing the unit vectors $\underline{u}_m$ and $\underline{u}_n$ does not follow the rotation of the distinguished axes, instead it oscillates about the x axis; however, here it oscillates in the reverse sense. As with all previous results, uniaxiality results when the two distinguished axes in the component mediums become collinear (i.e., for $\psi_a = 0, \pi$).

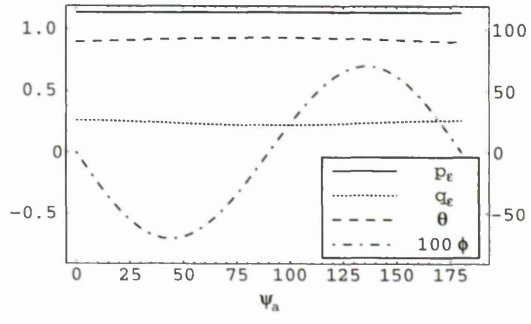

Figure 3.5: As for Figure 3.2 but for uniaxial spheroidal inclusions with isotropic spherical host. Constitutive parameters of the HCM plotted against inclusion spheroid axis angle ψ_a.

3.4 Dissipative anisotropic properties

We now broaden our investigation of biaxial HCMs, firstly by introducing the effects of dissipation in Section 3.4.1, and secondly by considering dielectric–magnetic mediums in Section 3.4.2 [14]. For all calculations presented in Sections 3.4.1 and 3.4.2, the HCM constitutive dyadics are found to have a biaxial form and we adopt the following

generalisation of representation (3.7), (3.8) for their characterisation

$$\underline{\underline{\epsilon}}_{HCM} = \epsilon_0 \left\{ p^r_\epsilon \underline{\underline{I}} + q^r_\epsilon (\underline{u}^r_{m\epsilon}\underline{u}^r_{n\epsilon} + \underline{u}^r_{n\epsilon}\underline{u}^r_{m\epsilon}) + i \left[p^i_\epsilon \underline{\underline{I}} + q^i_\epsilon (\underline{u}^i_{m\epsilon}\underline{u}^i_{n\epsilon} + \underline{u}^i_{n\epsilon}\underline{u}^i_{m\epsilon}) \right] \right\}, \quad (3.22)$$

$$\underline{\underline{\mu}}_{HCM} = \mu_0 \left\{ p^r_\mu \underline{\underline{I}} + q^r_\mu (\underline{u}^r_{m\mu}\underline{u}^r_{n\mu} + \underline{u}^r_{n\mu}\underline{u}^r_{m\mu}) + i \left[p^i_\mu \underline{\underline{I}} + q^i_\mu (\underline{u}^i_{m\mu}\underline{u}^i_{n\mu} + \underline{u}^i_{n\mu}\underline{u}^i_{m\mu}) \right] \right\}, \quad (3.23)$$

where $p^{r,i}_{\epsilon,\mu}$ and $q^{r,i}_{\epsilon,\mu}$ are real–valued scalars and we describe the real–valued unit vectors in terms of spherical polar coordinates

$$\underline{u}^\chi_{\kappa c} = \sin\theta^\chi_{\kappa c}\cos\phi^\chi_{\kappa c}\,\underline{u}_x + \sin\theta^\chi_{\kappa c}\sin\phi^\chi_{\kappa c}\,\underline{u}_y + \cos\theta^\chi_{\kappa c}\,\underline{u}_z\,, \qquad (\chi = r,i;\ \ \kappa = m,n;\ \ c = \epsilon,\mu). \quad (3.24)$$

The biaxiality of the HCM arises from the fact that the constituent mediums collectively possess two noncollinear distinguished axes. These axes originate from either the particulate topologies of the component mediums or from uniaxiality in their electromagnetic constitutive properties. With one exception, in Sections 3.4.1 and 3.4.2 we consider only constituent mediums with distinguished axes lying in the xy plane. As a consequence, our calculations reveal that the HCM unit vector pairs $\underline{u}^\chi_{mc}$ and $\underline{u}^\chi_{nc}$ always lie in planes perpendicular to the xy plane with the xy plane bisecting the angle between $\underline{u}^\chi_{mc}$ and $\underline{u}^\chi_{nc}$. Therefore, we have the following identities

$$\theta^\chi_{mc} = \pi - \theta^\chi_{nc} = \theta^\chi_c, \qquad \phi^\chi_{mc} = \phi^\chi_{nc} = \phi^\chi_c, \qquad (\chi = r,i;\ \ c = \epsilon,\mu). \quad (3.25)$$

The one exception occurs when we consider ellipsoidal inclusions of varying eccentricity; in this case one distinguished axis can lie along the z axis and we shall treat this as a special case in Section 3.4.1A.

All graphs displayed in Sections 3.4.1 and 3.4.2 are presented with reference to the key given in Table 3.1.

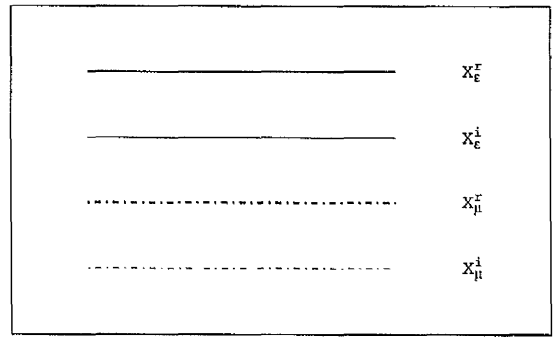

Table 3.1: Key for Figures 3.6–3.14. $X = \theta$, ϕ, p or q.

3.4.1 Dissipative biaxial dielectric

A. Isotropic ellipsoidal inclusions/isotropic spherical host

We begin by considering the homogenisation of a nondissipative isotropic host medium of permittivity $\underline{\underline{\epsilon}}_b = 1.2\epsilon_0\underline{\underline{I}}$ and spherical topology with a dissipative isotropic inclusion

medium of permittivity $\underline{\underline{\epsilon}}_a = (3+3i)\epsilon_0\underline{\underline{I}}$ and ellipsoidal geometry characterised by the shape dyadic $\underline{\underline{U}}_a = \mathrm{diag}(2,1,\gamma_a)$. The HCM permittivity $\underline{\underline{\epsilon}}_{HCM}$ was calculated as the ellipsoid eccentricity varied along the z axis. For this particular example (and no others) the identities (3.25) do not hold; instead here we take $\theta^{r,i}_{m\epsilon} = \theta^{r,i}_{\epsilon}$ and $\phi^{r,i}_{m\epsilon} = \phi^{r,i}_{\epsilon}$ and plot these angles as a function of γ in Figure 3.6. Three distinct regions are evident. For $\gamma_a < 1$, we have $\theta^{\chi}_{m\epsilon} = \pi - \theta^{\chi}_{n\epsilon}$ and $\phi^{\chi}_{m\epsilon} = \phi^{\chi}_{n\epsilon} = 0$, $(\chi = r,i)$; i.e., the unit vector pairs $\underline{u}^{r}_{m\epsilon,n\epsilon}$ and $\underline{u}^{i}_{m\epsilon,n\epsilon}$ both lie in the xz plane with the plane axes bisecting both $\theta^{r}_{m\epsilon,n\epsilon}$ and $\theta^{i}_{m\epsilon,n\epsilon}$. As γ_a enters the region $1 < \gamma_a < 2$, the unit vector pairs $\underline{u}^{r}_{m\epsilon,n\epsilon}$ and $\underline{u}^{i}_{m\epsilon,n\epsilon}$ come to lie in the xy plane and we have $\theta^{\chi}_{m\epsilon} = \theta^{\chi}_{n\epsilon} = \pi/2$ and $\phi^{\chi}_{m\epsilon} = -\phi^{\chi}_{n\epsilon}$, $(\chi = r,i)$. Finally for $\gamma_a > 2$, $\underline{u}^{r,i}_{m\epsilon,n\epsilon}$ all occupy the yz plane and $\theta^{\chi}_{m\epsilon} = \pi - \theta^{\chi}_{n\epsilon}$ and $\phi^{\chi}_{m\epsilon} = -\phi^{\chi}_{n\epsilon} = -\pi/2$, $(\chi = r,i)$. At points where the inclusion shape becomes spheroidal (i.e., $\gamma_a = 1,2$), the unit vectors $\underline{u}^{r,i}_{m\epsilon,n\epsilon}$ all lie on a common axis and the HCM becomes uniaxial. The scalar permittivity parameters $p^{r,i}_{\epsilon}$ and $q^{r,i}_{\epsilon}$ exhibit only a rather weak dependency on ellipsoid eccentricity and are not displayed. Since, for all values of γ_a, both the unit vector pair $\underline{u}^{r}_{m\epsilon,n\epsilon}$ and the pair $\underline{u}^{i}_{m\epsilon,n\epsilon}$ lie in a coordinate plane with the plane axes bisecting the angles between both pairs, we find that $\underline{\underline{\epsilon}}_{HCM}$ is diagonal and hence the HCM belongs to the biaxial orthorhombic class. This reflects the fact that in this case biaxiality arises from a geometrical structure based on three mutually perpendicular principal axes, namely the inclusion ellipsoid.

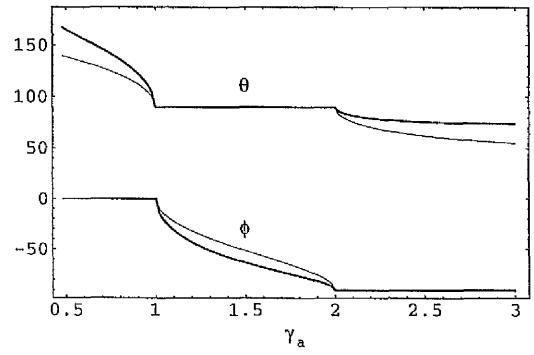

Figure 3.6: Dissipative ellipsoidal inclusion medium with nondissipative spherical host medium (both mediums isotropic dielectric). HCM unit vector angles $\theta^{r,i}_{\epsilon}$ and $\phi^{r,i}_{\epsilon}$ plotted against inclusion ellipsoid semi–axis γ_a. (Key: $X = \theta$, ϕ in Table 3.1).

B. Isotropic spheroidal inclusions/isotropic spheroidal host

Next we consider a second example where both the inclusion and host mediums are isotropic dielectric but in this instance each component medium presents one distinguished axis. We choose a host medium of permittivity $\underline{\underline{\epsilon}}_b = 1.2\epsilon_0\underline{\underline{I}}$ and of spheroidal topology characterised by $\underline{\underline{U}}_b = \mathrm{diag}(2,1,1)$, and homogenise with inclusions of dissipative permittivity $\underline{\underline{\epsilon}}_a = (3+3i)\epsilon_0\underline{\underline{I}}$ and of the same shape as the host medium particles

but with principal spheroid axis rotated by ψ_a in the xy plane, i.e.,

$$\underline{\underline{U}}_a = \begin{bmatrix} 2\cos^2\psi_a + \sin^2\psi_a & \sin\psi_a\cos\psi_a & 0 \\ \sin\psi_a\cos\psi_a & 2\sin^2\psi_a + \cos^2\psi_a & 0 \\ 0 & 0 & 1 \end{bmatrix}. \tag{3.26}$$

The defining angles $\theta_\epsilon^{r,i}$ and $\phi_\epsilon^{r,i}$ for the HCM unit vectors $\underline{u}_{m\epsilon,n\epsilon}^{r,i}$ are plotted as functions of the spheroid axis angle ψ_a in Figure 3.7. The HCM scalar permittivities $p_\epsilon^{r,i}$ and $q_\epsilon^{r,i}$ vary little with ψ_a and are not displayed. The variation of θ_ϵ^r and ϕ_ϵ^r (and a_ϵ^r and b_ϵ^r) with ψ_a is similar to that found for the non–dissipative dielectric case in Section 3.3.2, and the quantities arising from dissipative processes (θ_ϵ^i, ϕ_ϵ^i, a_ϵ^i and b_ϵ^i) behave in an analogous manner. At the endpoints $\psi_a = 0, \pi$, the unit vectors $\underline{u}_{m\epsilon,n\epsilon}^{r,i}$ all lie on a common line (the x axis) and the HCM has a uniaxial structure. At the midpoint $\psi_a = \pi/2$, we have $\phi_\epsilon^{r,i} = \pi/2$ and therefore $\underline{\underline{\epsilon}}_{HCM}$ has a diagonal form and the HCM is orthorhombic biaxial. In keeping with the previous example of ellipsoidal inclusions in Section 3.4.1, the orthorhombic case arises in this instance when the distinguished axes of the constituent mediums are orthogonal. Aside from these special cases, we observe $\theta_\epsilon^r \neq \theta_\epsilon^i \neq \phi_\epsilon^r \neq \phi_\epsilon^i$ and the biaxial HCM is of the monoclinic/triclinic type, in spite of the fact that the chosen values were such that $\mathrm{Re}\,\underline{\underline{\epsilon}}_a = \mathrm{Im}\,\underline{\underline{\epsilon}}_a$ (where $\underline{\underline{\epsilon}}_a = \mathrm{Re}\,\underline{\underline{\epsilon}}_a + i\,\mathrm{Im}\,\underline{\underline{\epsilon}}_a$, and $\mathrm{Re}\,\underline{\underline{\epsilon}}_a$, $\mathrm{Im}\,\underline{\underline{\epsilon}}_a$ are real–valued).

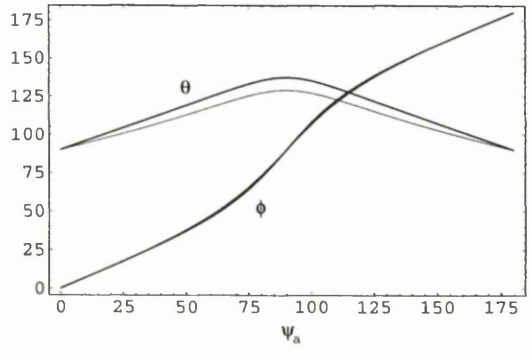

Figure 3.7: Dissipative spheroidal inclusion medium with nondissipative spheroidal host medium (both mediums isotropic dielectric). HCM unit vector angles $\theta_\epsilon^{r,i}$ and $\phi_\epsilon^{r,i}$ plotted against inclusion spheroid orientation angle ψ_a. (Key: $X = \theta$, ϕ in Table 3.1).

Greater differences between θ_ϵ^r and θ_ϵ^i, and between ϕ_ϵ^r and ϕ_ϵ^i, than those displayed in Figure 3.7 can be achieved by choosing $\mathrm{Re}\,\underline{\underline{\epsilon}}_a \neq \mathrm{Im}\,\underline{\underline{\epsilon}}_a$. We explore this matter further by repeating the homogenisation of Figure 3.7 but with an allowance made for dissipation in the host medium by taking $\underline{\underline{\epsilon}}_b = 1.2(1 + i\delta)\epsilon_0\underline{\underline{I}}$. For a spheroid inclusion angle of $\psi_a = 70°$, the HCM unit vector angles $\theta_\epsilon^{r,i}$ and $\phi_\epsilon^{r,i}$ and scalar permittivities $a_\epsilon^{r,i}$ and $b_\epsilon^{r,i}$ are plotted against δ in Figures 3.8 and 3.9 respectively. The point of interest occurs at $\delta = 1$ and we find,

$$\begin{aligned} &\mathrm{Re}\,\underline{\underline{\epsilon}}_b = \rho\,\mathrm{Im}\,\underline{\underline{\epsilon}}_b, \qquad \mathrm{Re}\,\underline{\underline{\epsilon}}_a = \rho\,\mathrm{Im}\,\underline{\underline{\epsilon}}_a \\ &\Longrightarrow \qquad \theta_\epsilon^r = \theta_\epsilon^i, \qquad \phi_\epsilon^r = \phi_\epsilon^i, \qquad p_\epsilon^r = p_\epsilon^i, \qquad q_\epsilon^r = q_\epsilon^i, \end{aligned} \tag{3.27}$$

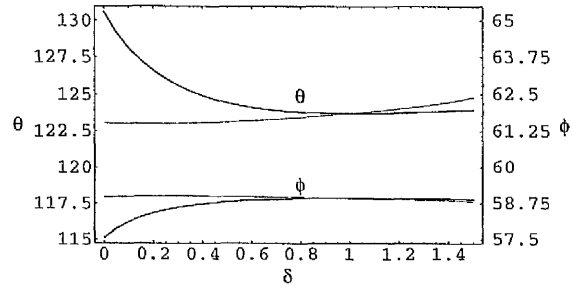

Figure 3.8: As for Figure 3.8 but with dissipative host medium. HCM unit vector angles $\theta_\epsilon^{r,i}$ and $\phi_\epsilon^{r,i}$ plotted against degree of host medium dissipation δ. (Key: $X = \theta$, ϕ in Table 3.1).

where ρ is a proportionality constant. At $\delta = 1$ the HCM is orthorhombic biaxial (since $\phi_\epsilon^r = \phi_\epsilon^i$), despite the distinguished axes of the constituent medium spheroids not being perpendicular. Furthermore, the structure at this point is a highly specialised form of orthorhombic for which $\underline{\underline{\epsilon}}_{HCM}$ is specified by only four real–valued parameters (θ_ϵ^r, ϕ_ϵ^r, p_ϵ^r and q_ϵ^r), although the HCM is both biaxial and dissipative.

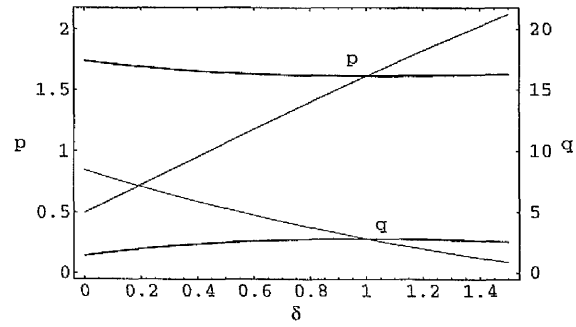

Figure 3.9: As for Figure 3.8 but with dissipative host medium. HCM scalar permittivities $p_\epsilon^{r,i}$ and $q_\epsilon^{r,i}$ plotted against degree of host medium dissipation δ. (Key: $X = p$, q in Table 3.1).

3.4.2 Dissipative biaxial dielectric–magnetic

We now extend our investigations to the case of dielectric–magnetic materials. Unlike the previous two examples in Section 3.4.1, here we consider constituents in which the distinguished axes have an electromagnetic, rather than topological, origin. We explore the homogenisation of a nondissipative uniaxial host medium with constitutive dyadics $\underline{\underline{\epsilon}}_b = \epsilon_0 \,\mathrm{diag}(3,1,1)$, $\underline{\underline{\mu}}_b = \mu_0 \,\mathrm{diag}(3,1,1)$, and a dissipative inclusion medium

specified by

$$\underline{\underline{\epsilon}}_a = \epsilon_0 \begin{bmatrix} 3(1+i)\cos^2\lambda_a + (1+i)\sin^2\lambda_a & 2(1+i)\sin\lambda_a\cos\lambda_a & 0 \\ 2(1+i)\sin\lambda_a\cos\lambda_a & 3(1+i)\sin^2\lambda_a + (1+i)\cos^2\lambda_a & 0 \\ 0 & 0 & 1+i \end{bmatrix}, \tag{3.28}$$

and

$$\underline{\underline{\mu}}_a = \mu_0 \begin{bmatrix} 3(2+i)\cos^2\lambda_a + (2+i)\sin^2\lambda_a & 2(2+i)\sin\lambda_a\cos\lambda_a & 0 \\ 2(2+i)\sin\lambda_a\cos\lambda_a & 3(2+i)\sin^2\lambda_a + (2+i)\cos^2\lambda_a & 0 \\ 0 & 0 & 2+i \end{bmatrix}, \tag{3.29}$$

where both host and inclusion mediums have a spherical topology. Notice that the distinguished axes for the inclusion permittivity and permeability dyadics are parallel and lie at angle λ_a in the xy plane to the distinguished axes of the corresponding host medium, which are also parallel. Plotted in Figures 3.10 and 3.11 as functions of λ_a are, respectively, the defining angles for the unit vector pairs $\underline{u}^{r,i}_{m\epsilon,n\epsilon,m\mu,n\mu}$ and the corresponding permittivity ($p^{r,i}_\epsilon$ and $q^{r,i}_\epsilon$) and permeability ($p^{r,i}_\mu$ and $q^{r,i}_\mu$) scalars. The general trends displayed by the graphed quantities with respect to λ_a are the same as those found in the analogous nondissipative case in Section 3.3.3. A uniaxial dielectric–magnetic HCM results when the distinguished axes of the constituent mediums are aligned (i.e., $\lambda_a = 0, \pi$). At the point $\lambda_a = \pi/2$, the unit vectors pairs $\underline{u}^{r,i}_{m\epsilon,n\epsilon,m\mu,n\mu}$ all lie in the xz plane with the plane axes bisecting the vector pairs $\underline{u}^r_{m\epsilon}, \underline{u}^i_{n\epsilon}$; $\underline{u}^i_{m\epsilon}, \underline{u}^i_{n\epsilon}$; $\underline{u}^r_{m\mu}, \underline{u}^r_{n\epsilon}$ and $\underline{u}^i_{m\mu}, \underline{u}^i_{n\mu}$; thus the HCM structure is orthorhombic biaxial with respect to both permittivity and permeability. With the exception of the special cases $\lambda_a = 0, \pi/2$ and π, all eight angles $\theta^{r,i}_{\epsilon,\mu}$ and $\phi^{r,i}_{\epsilon,\mu}$ and all eight scalars $p^{r,i}_{\epsilon,\mu}$ and $q^{r,i}_{\epsilon,\mu}$ have distinct values and the biaxial HCM is of the monoclinic/triclinic type as regards both $\underline{\underline{\epsilon}}_{HCM}$ and $\underline{\underline{\mu}}_{HCM}$. This most general biaxial dielectric–magnetic structure arises notwithstanding the numerical values of the constitutive dyadics of the component mediums being closely related; i.e., $(1/\epsilon_0)\mathrm{Re}\,\underline{\underline{\epsilon}}_a = (1/\epsilon_0)\mathrm{Im}\,\underline{\underline{\epsilon}}_a = (1/\mu_0)\mathrm{Im}\,\underline{\underline{\mu}}_a = (1/2\mu_0)\mathrm{Re}\,\underline{\underline{\mu}}_a$ for all values of λ_a, and $(1/\epsilon_0)\mathrm{Re}\,\underline{\underline{\epsilon}}_a = (1/\mu_0)\mathrm{Im}\,\underline{\underline{\mu}}_a = (1/\epsilon_0)\underline{\underline{\epsilon}}_b$ at $\lambda_a = 0$ and π. We note, in particular, that the inequalities $\theta^{r,i}_\epsilon \neq \theta^{r,i}_\mu$ and $\phi^{r,i}_\epsilon \neq \phi^{r,i}_\mu$ are not attributable to the presence of dissipation. On repeating these computations for the analogous nondissipative case, the distinctions between permittivity and permeability angles remain (i.e., $\theta^r_\epsilon \neq \theta^r_\mu$ and $\phi^r_\epsilon \neq \phi^r_\mu$) . In fact, further calculations (not presented here) reveal that the HCM unit vector angles $\theta^{r,i}_{\epsilon,\mu}$ and $\phi^{r,i}_{\epsilon,\mu}$ are largely independent of the degree of inclusion dissipation provided the host medium is nondissipative.

If both the inclusion and host mediums are taken to be dissipative then, depending on the ratios of real and imaginary parts of their constitutive dyadics, symmetries can arise in $\underline{\underline{\epsilon}}_{HCM}$ and $\underline{\underline{\mu}}_{HCM}$. To illustrate this point we repeat the homogenisations of Figures 3.10 and 3.11 but here with a more general host medium characterised by $\underline{\underline{\epsilon}}_b = \epsilon_0\,\mathrm{diag}(3+3i\delta, 1+i\delta, 1+i\delta)$, $\underline{\underline{\mu}}_b = \mu_0\,\mathrm{diag}(3+3i\delta, 1+i\delta, 1+i\delta)$ and with a fixed

angle for the inclusion distinguished axis of $\lambda_a = 50°$. The angles $\theta^{r,i}_{\epsilon,\mu}$ and scalars $p^{r,i}_{\epsilon,\mu}$ are plotted against δ in Figures 3.12 and 3.13 respectively. (The equivalent graphs for $\phi^{r,i}_{\epsilon,\mu}$ and $q^{r,i}_{\epsilon,\mu}$ show analogous behaviour to Figures 3.12 and 3.13, respectively, and are not displayed). The salient features of these two figures (and the corresponding graphs for $\phi^{r,i}_{\epsilon,\mu}$ and $q^{r,i}_{\epsilon,\mu}$ which are not displayed) may be summarised by

$$\begin{aligned} (1/\epsilon_0)\,\mathrm{Re}\,\underline{\underline{\epsilon}}_b = \rho(1/\epsilon_0)\,\mathrm{Im}\,\underline{\underline{\epsilon}}_b\,, \qquad (1/\epsilon_0)\,\mathrm{Re}\,\underline{\underline{\epsilon}}_a = \rho(1/\epsilon_0)\,\mathrm{Im}\,\underline{\underline{\epsilon}}_a \\ \Longrightarrow \qquad \theta^r_\epsilon = \theta^i_\epsilon\,, \qquad \phi^r_\epsilon = \phi^i_\epsilon\,, \qquad p^r_\epsilon = p^i_\epsilon\,, \qquad q^r_\epsilon = q^i_\epsilon\,, \end{aligned} \tag{3.30}$$

and

$$\begin{aligned} (1/\mu_0)\,\mathrm{Re}\,\underline{\underline{\mu}}_b = \sigma(1/\mu_0)\,\mathrm{Im}\,\underline{\underline{\mu}}_b\,, \qquad (1/\mu_0)\,\mathrm{Re}\,\underline{\underline{\mu}}_a = \sigma(1/\mu_0)\,\mathrm{Im}\,\underline{\underline{\mu}}_a \\ \Longrightarrow \qquad \theta^r_\mu = \theta^i_\mu\,, \qquad \phi^r_\mu = \phi^i_\mu\,, \end{aligned} \tag{3.31}$$

where ρ and σ are proportionality scalars. In an analogous manner to the case of spheroidal inclusions/spheroidal host medium presented in Figures 3.10 and 3.11, the biaxial HCM structure becomes orthorhombic with respect to permittivity when ratios of real and imaginary parts of $\underline{\underline{\epsilon}}_b$ and $\underline{\underline{\epsilon}}_a$ are equal. Furthermore, it is an especially symmetric form of biaxiality involving equalities between the scalar permittivities $p^{r,i}_\epsilon$ and $q^{r,i}_\epsilon$. An orthorhombic state with respect to permeability occurs when ratios of real and imaginary parts of $\underline{\underline{\mu}}_b$ and $\underline{\underline{\mu}}_a$ are equal; however, at this point $p^r_\epsilon \neq p^i_\epsilon$ and $q^r_\epsilon \neq q^i_\epsilon$. The graphs of p^r_ϵ and p^i_ϵ do intersect but not at $\delta = 0.5$ and not at the point where q^r_ϵ and q^i_ϵ intersect. (Presumably, the reason why the permittivity scalars $p^{r,i}_\epsilon$ and $q^{r,i}_\epsilon$ are equal at $\delta = 1$ but the permeability scalars $p^{r,i}_\mu$ and $q^{r,i}_\mu$ are not equal at $\delta = 0.5$ is that at $\delta = 1$, $\underline{\underline{\epsilon}}_a$ and $\underline{\underline{\epsilon}}_b$ have the same 'magnitude' — in the sense that the dyadic $\underline{\underline{\epsilon}}_a$ may be transformed into $\underline{\underline{\epsilon}}_b$ by rotating basis vectors by 50° in the xy plane — whereas at $\delta = 0.5$, $\underline{\underline{\mu}}_a$ and $\underline{\underline{\mu}}_b$ do not have the same 'magnitude').

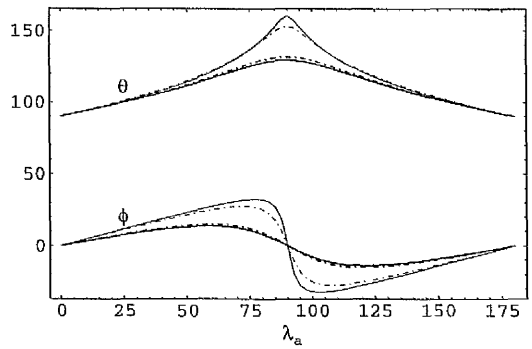

Figure 3.10: Dissipative inclusion medium with nondissipative host medium (both mediums uniaxial dielectric–magnetic). HCM unit vector angles $\theta^{r,i}_{\epsilon,\mu}$ and $\phi^{r,i}_{\epsilon,\mu}$ plotted against inclusion distinguished axis orientation angle λ_a. (Key: $X = \theta$, ϕ in Table 3.1).

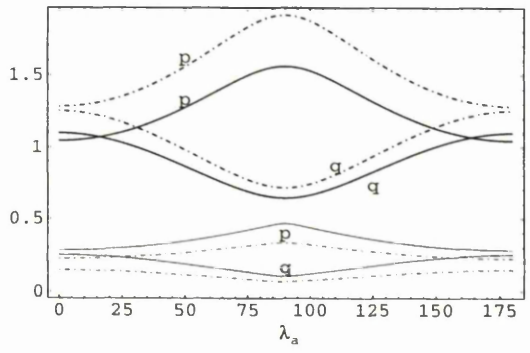

Figure 3.11: Dissipative inclusion medium with nondissipative host medium (both mediums uniaxial dielectric–magnetic). HCM scalar permittivities $p_\epsilon^{r,i}$ and $q_\epsilon^{r,i}$ and permeabilities $p_\mu^{r,i}$ and $q_\mu^{r,i}$ plotted against inclusion distinguished axis orientation angle λ_a. (Key: $X = p$, q in Table 3.1).

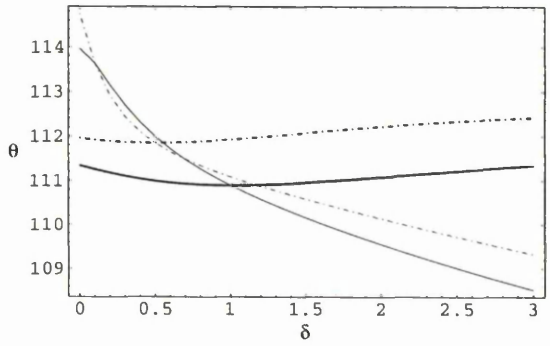

Figure 3.12: As for Figures 3.10 and 3.11 but with dissipative host medium. HCM unit vector polar angles $\theta_{\epsilon,\mu}^{r,i}$ plotted against degree of host medium dissipation δ. (Key: $X = \theta$ in Table 3.1).

Another type of symmetry in the constitutive dyadics $\underline{\underline{\epsilon}}_{HCM}$ and $\underline{\underline{\mu}}_{HCM}$ results when $\underline{\underline{\epsilon}}_a$ is a scalar multiple of $\underline{\underline{\mu}}_a$, and $\underline{\underline{\epsilon}}_b$ is the same scalar multiple of $\underline{\underline{\mu}}_b$, regardless of the ratios of their real and imaginary components. We consider an extension to the uniaxial inclusion/uniaxial host medium homogenisation of Figures 3.10 and 3.11 in which $\underline{\underline{\epsilon}}_a$ is defined by (3.28) with $\lambda_a = 50°$ and here we take $(1/\mu_0)\underline{\underline{\mu}}_a = (2/\epsilon_0)\underline{\underline{\epsilon}}_a$, and a host medium given by $\underline{\underline{\epsilon}}_b = \epsilon_0\,\mathrm{diag}(3+1.5i, 1+0.5i, 1+0.5i)$ and $(1/\mu_0)\underline{\underline{\mu}}_b = (\eta/\epsilon_0)\underline{\underline{\epsilon}}_b$. The variation of unit vector angles $\theta_{\epsilon,\mu}^{r,i}$ with increasing η is displayed in Figure 3.14. An equivalent figure (not shown) can be constructed for unit vector angles $\phi_{\epsilon,\mu}^{r,i}$ with the graphs of ϕ_ϵ^r and ϕ_μ^r, and of ϕ_ϵ^i and ϕ_μ^i, intersecting at the same η value as in Figure 3.14. The graphs indicate that

$$(1/\epsilon_0)\,\underline{\underline{\epsilon}}_b = \rho(1/\mu_0)\,\underline{\underline{\mu}}_b\,, \qquad (1/\epsilon_0)\,\underline{\underline{\epsilon}}_a = \rho(1/\mu_0)\,\underline{\underline{\mu}}_a$$
$$\Longrightarrow \qquad \theta_\epsilon^r = \theta_\mu^r\,, \quad \theta_\epsilon^i = \theta_\mu^i\,, \quad \phi_\epsilon^r = \phi_\mu^r\,, \quad \phi_\epsilon^i = \phi_\mu^i\,, \tag{3.32}$$

where ρ is a proportionality constant. Observe that, despite the symmetries in $\underline{\underline{\epsilon}}_{HCM}$ and $\underline{\underline{\mu}}_{HCM}$, the HCM is not of the orthorhombic biaxial type at $\eta = 2$ since $\phi^r_{\epsilon,\mu} \neq \phi^i_{\epsilon,\mu}$. No analogous results hold for the HCM scalar permittivities $p^{r,i}_{\epsilon}$ and $q^{r,i}_{\epsilon}$, and permeabilities $p^{r,i}_{\mu}$ and $q^{r,i}_{\mu}$.

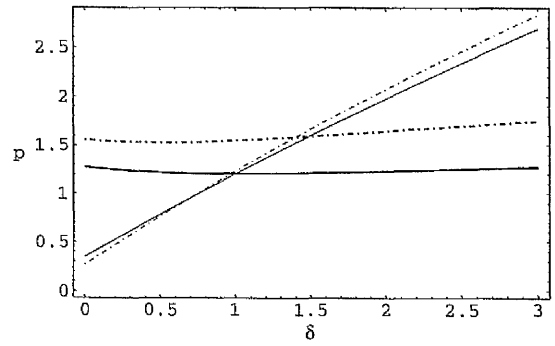

Figure 3.13: As for Figures 3.10 and 3.11 but with dissipative host medium. HCM scalar permittivities and permeabilities $p^{r,i}_{\epsilon,\mu}$ plotted against degree of host medium dissipation δ. (Key: $X = p$ in Table 3.1).

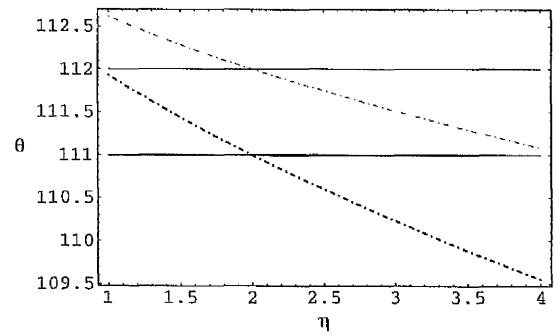

Figure 3.14: Dissipative inclusion medium with dissipative host medium (both mediums uniaxial dielectric–magnetic). HCM unit vector polar angles $\theta^{r,i}_{\epsilon,\mu}$ plotted against ratio of host medium permeability to host medium permittivity η. (Key: $X = \theta$ in Table 3.1).

3.5 Bianisotropic properties

Finally, in this section we explore in detail the conceptualisation of biaxial bianisotropic mediums through the process of homogenisation [15]. Biaxial bianisotropy is found to arise when (i) the component mediums undergoing homogenisation present two non-collinear distinguished axes and (ii) the most basic form of magnetoelectric coupling in the form of isotropic chirality is present in at least one of the component mediums. Two possible sources of directionality in the component mediums are considered:

topological and electromagnetic. Illustrative examples of these are investigated by considering the homogenisation of particulate components with non–spherical topologies and isotropic electromagnetic properties in Section 3.5.1, and uniaxial bianisotropic electromagnetic properties and spherical topologies in Section 3.5.2.

For all calculations presented in Sections 3.5.1 and 3.5.2, HCMs arise with constitutive dyadics (namely, $\underline{\underline{\epsilon}}_{HCM}$, $\underline{\underline{\xi}}_{HCM}$, $\underline{\underline{\zeta}}_{HCM}$ and $\underline{\underline{\mu}}_{HCM}$, related through the constitutive equations (2.5) and (2.6)) of a biaxial bianisotropic form. We make use of a generalisation of representation (3.7), (3.8) for their characterisation

$$\underline{\underline{\epsilon}}_{HCM} = \epsilon_0 \left\{ p^r_\epsilon \underline{\underline{I}} + q^r_\epsilon (\underline{u}^r_{m\epsilon}\underline{u}^r_{n\epsilon} + \underline{u}^r_{n\epsilon}\underline{u}^r_{m\epsilon}) + i \left[p^i_\epsilon \underline{\underline{I}} + q^i_\epsilon (\underline{u}^i_{m\epsilon}\underline{u}^i_{n\epsilon} + \underline{u}^i_{n\epsilon}\underline{u}^i_{m\epsilon}) \right] \right\}, \tag{3.33}$$

$$\underline{\underline{\xi}}_{HCM} = i\sqrt{\epsilon_0\mu_0} \left\{ p^r_\xi \underline{\underline{I}} + q^r_\xi (\underline{u}^r_{m\xi}\underline{u}^r_{n\xi} + \underline{u}^r_{n\xi}\underline{u}^r_{m\xi}) + i \left[p^i_\xi \underline{\underline{I}} + q^i_\xi (\underline{u}^i_{m\xi}\underline{u}^i_{n\xi} + \underline{u}^i_{n\xi}\underline{u}^i_{m\xi}) \right] \right\}, \tag{3.34}$$

$$\underline{\underline{\zeta}}_{HCM} = i\sqrt{\epsilon_0\mu_0} \left\{ p^r_\zeta \underline{\underline{I}} + q^r_\zeta (\underline{u}^r_{m\zeta}\underline{u}^r_{n\zeta} + \underline{u}^r_{n\zeta}\underline{u}^r_{m\zeta}) + i \left[p^i_\zeta \underline{\underline{I}} + q^i_\zeta (\underline{u}^i_{m\zeta}\underline{u}^i_{n\zeta} + \underline{u}^i_{n\zeta}\underline{u}^i_{m\zeta}) \right] \right\}, \tag{3.35}$$

$$\underline{\underline{\mu}}_{HCM} = \mu_0 \left\{ p^r_\mu \underline{\underline{I}} + q^r_\mu (\underline{u}^r_{m\mu}\underline{u}^r_{n\mu} + \underline{u}^r_{n\mu}\underline{u}^r_{m\mu}) + i \left[p^i_\mu \underline{\underline{I}} + q^i_\mu (\underline{u}^i_{m\mu}\underline{u}^i_{n\mu} + \underline{u}^i_{n\mu}\underline{u}^i_{m\mu}) \right] \right\}, \tag{3.36}$$

where $p^{r,i}_{\epsilon,\xi,\zeta,\mu}$ and $q^{r,i}_{\epsilon,\xi,\zeta,\mu}$ are real–valued scalars and we describe the real–valued unit vectors in terms of spherical polar coordinates as

$$\begin{aligned} \underline{u}^\chi_{\kappa\tau} &= \sin\theta^\chi_{\kappa\tau}\cos\phi^\chi_{\kappa\tau}\,\underline{u}_x + \sin\theta^\chi_{\kappa\tau}\sin\phi^\chi_{\kappa\tau}\,\underline{u}_y + \cos\theta^\chi_{\kappa\tau}\,\underline{u}_z\,, \\ &\qquad (\chi = r,i;\ \ \kappa = m,n;\ \ \tau = \epsilon,\xi,\zeta,\mu). \end{aligned} \tag{3.37}$$

Observe that a total of 45 real–valued parameters are required to specify the general biaxial bianisotropic structure given by (3.33)–(3.36); i.e, 12 for each independent constitutive dyadic (2 each for p^χ_τ and q^χ_τ and 4 each for $\theta^\chi_{\kappa\tau}$ and $\phi^\chi_{\kappa\tau}$ where $\chi = r,i;\ \kappa = m,n;\ \tau = \epsilon,\xi,\zeta,\mu$) less by 3 through the choice of coordinate frame.

The (non–isotropic) magnetoelectric coupling in the HCM is caused by the presence of (at least isotropic) magnetoelectric coupling in the constitutive relations of one of the constituent mediums. The HCM biaxiality, on the other hand, arises from the fact that the constituent mediums collectively possess two noncollinear distinguished axes. These axes originate from either the particulate topologies of the component mediums or from uniaxiality in their electromagnetic constitutive properties. In Sections 3.5.1 and 3.5.2, our choice of coordinate system is such that we consider only constituent mediums with distinguished axes lying in the xy plane. As a consequence, our calculations reveal that the HCM unit vector pairs $\underline{u}^\chi_{m\tau}$ and $\underline{u}^\chi_{n\tau}$ always lie in planes perpendicular to the xy plane with the xy plane bisecting the angle between $\underline{u}^\chi_{m\tau}$ and $\underline{u}^\chi_{n\tau}$. Therefore, we have the following identities

$$\theta^\chi_{m\tau} = \pi - \theta^\chi_{n\tau} = \theta^\chi_\tau\,, \quad \phi^\chi_{m\tau} = \phi^\chi_{n\tau} = \phi^\chi_\tau\,, \quad (\chi = r,i;\ \ \tau = \epsilon,\xi,\zeta,\mu). \tag{3.38}$$

Furthermore, an immediate simplification follows due to the fact that all component mediums we consider are reciprocal. Consequently, the computed HCM constitutive

dyadics are likewise reciprocal and results for the magnetoelectric dyadic $\underline{\underline{\zeta}}_{HCM}$ need not be explicitly presented since $\underline{\underline{\xi}}_{HCM} = -\underline{\underline{\zeta}}_{HCM}$. This last equality also guarantees that the Post constraint (1.19) [25]–[27], a structural constraint that needs to be fulfilled by all linear bianisotropic materials, is explicitly satisfied in all considered cases. We further remark that the condition of reciprocity reduces the number of real–valued parameters required to specify the biaxial structure given by (3.33)–(3.36) to 33.

All graphs in Sections 3.5.1 and 3.5.2 are presented with reference to the key given in Table 3.2.

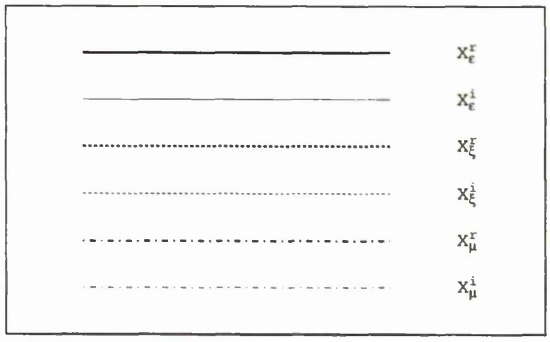

Table 3.2: Key for Figures 3.15–3.18. $X = \theta$, ϕ, p or q.

3.5.1 Isotropic ellipsoidal inclusions/isotropic spherical host

Consider ellipsoidal chiral inclusions characterised by the constitutive dyadics

$$\begin{aligned} \underline{\underline{\epsilon}}_a &= 3(1+i)\,\epsilon_0 \underline{\underline{I}}, \qquad \underline{\underline{\mu}}_a = 2(1+i)\,\mu_0 \underline{\underline{I}}, \\ \underline{\underline{\xi}}_a &= -\underline{\underline{\zeta}}_a = (1+i)\,i\sqrt{\epsilon_0\mu_0}\,\underline{\underline{I}}, \end{aligned} \tag{3.39}$$

their shape being specified by the dyadic $\underline{\underline{U}}_a = \mathrm{diag}(2, 1, 0.5)$. Our first numerical study concerns the homogenisation of such a medium with a dielectric–magnetic host medium specified by constitutive dyadics

$$\underline{\underline{\epsilon}}_b = 1.8(1+i\delta)\,\epsilon_0 \underline{\underline{I}}, \qquad \underline{\underline{\mu}}_b = 1.4(1+i\delta)\,\mu_0 \underline{\underline{I}}, \tag{3.40}$$

based on spherical topology. Notice that both component mediums are dissipative, as is apparent from the presence of imaginary components in (3.39) and (3.40). The parameter δ specifies the amount of dissipation in the dielectric–magnetic component.

Applying the Br homogenisation formalism, our calculations show that $\phi^{r,i}_{\epsilon,\mu,\xi,\zeta} = 0$ (regardless of the value of dissipation parameter δ); hence, the resulting HCM is orthorhombic biaxial with respect to all four constitutive dyadics $\underline{\underline{\epsilon}}_{HCM}$, $\underline{\underline{\mu}}_{HCM}$, $\underline{\underline{\xi}}_{HCM}$ and $\underline{\underline{\zeta}}_{HCM}$. Clearly, the orthorhombic state reflects the fact that biaxiality arises in this particular instance from a geometrical structure based on three mutually perpendicular principal axes, namely those of the inclusion ellipsoid. In general, however,

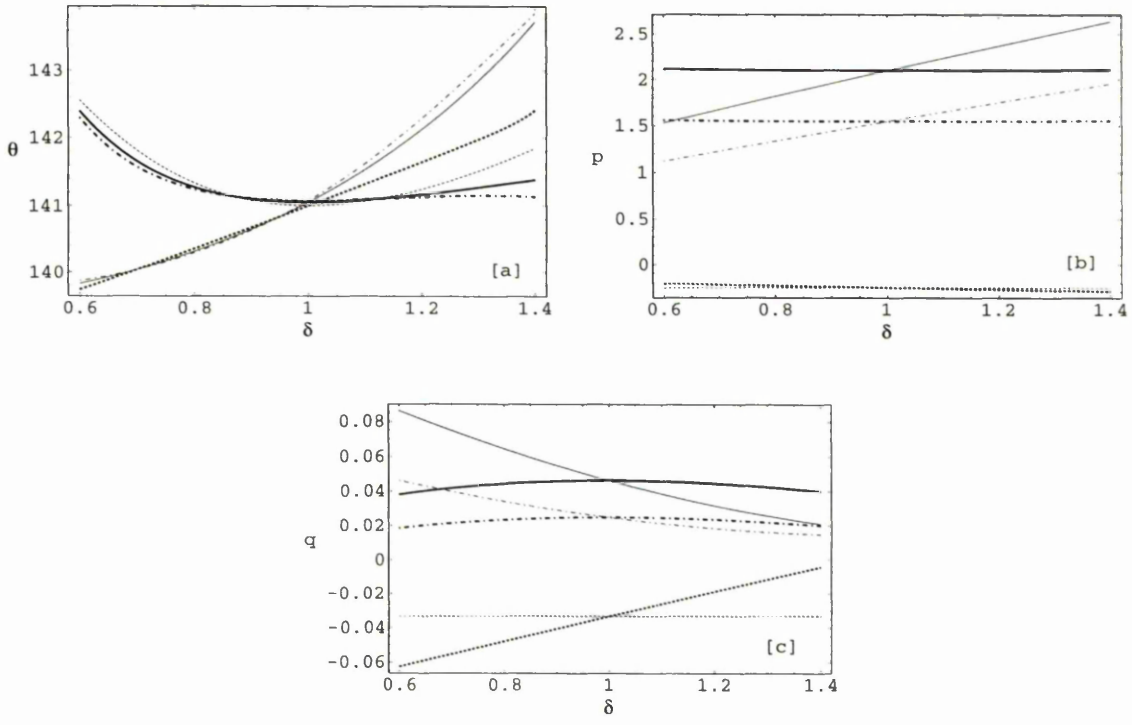

Figure 3.15: Chiral ellipsoidal inclusions homogenised with isotropic dielectric–magnetic spherical host medium. HCM (a) unit vector polar angles $\theta^{r,i}_{\epsilon,\xi,\mu}$ (degrees), and parameters (b) $p^{r,i}_{\epsilon,\mu}, p^{r}_{\xi}, -a^{i}_{\xi}$, and (c) $q^{r,i}_{\epsilon,\mu}, q^{r}_{\xi}, -b^{i}_{\xi}$, plotted against dissipation parameter δ. (Key in Table 3.2: $X = \theta$ for (a), $X = p$ for (b), $X = q$ for (c)).

the six unit vector angles $\theta^{r,i}_{\epsilon,\mu,\xi}$ are all different as may be observed in Figure 3.15(a) where these polar angles are plotted as functions of the host parameter δ; the HCM parameters $p^{r,i}_{\epsilon,\xi,\mu}$ and $q^{r,i}_{\epsilon,\xi,\mu}$ are likewise plotted against δ in Figures 3.15(b) and 3.15(c) respectively. In light of observations reported for dielectric–magnetic HCMs in Section 3.4, it might be anticipated that the HCM constitutive dyadics exhibit a high degree of symmetry at the point $\delta = 1$ where ratios of real and imaginary parts of all constitutive dyadics of the component mediums become equal. This is indeed the case for the bianisotropic HCM of Figure 3.15; the observed behaviour in the vicinity of $\delta = 1$ may be summarised as

$$\begin{aligned} &(1/\epsilon_0)\,\mathrm{Re}\,\underline{\underline{\epsilon}}_b = (1/\epsilon_0)\,\mathrm{Im}\,\underline{\underline{\epsilon}}_b\,, \qquad (1/\mu_0)\,\mathrm{Re}\,\underline{\underline{\mu}}_b = (1/\mu_0)\,\mathrm{Im}\,\underline{\underline{\mu}}_b \qquad \Longrightarrow \\ &\theta^{r}_{\tau} = \theta^{i}_{\tau}\,, \qquad \rho^{r}_{\epsilon} = \rho^{i}_{\epsilon}\,, \quad \rho^{r}_{\xi} = -\rho^{i}_{\xi} \quad \rho^{r}_{\mu} = \rho^{i}_{\mu}\,, \qquad (\tau = \epsilon, \xi, \mu;\ \rho = a, b), \end{aligned} \tag{3.41}$$

where $\underline{\underline{\tau}}_b = \mathrm{Re}\,\underline{\underline{\tau}}_b + i\,\mathrm{Im}\,\underline{\underline{\tau}}_b$ and $\mathrm{Re}\,\underline{\underline{\tau}}_b$, $\mathrm{Im}\,\underline{\underline{\tau}}_b$ are real–valued ($\tau = \epsilon, \mu$). Notice that close inspection of Figure 3.15(a) reveals $\theta^{r,i}_{\epsilon} \neq \theta^{r,i}_{\xi} \neq \theta^{r,i}_{\mu}$ at the point $\delta = 1$.

We briefly mention two further points without presenting graphical results. Firstly, further calculations demonstrate that an equally general biaxial bianisotropic HCM structure arises when the host medium in the homogenisation of Figure 3.15 is replaced with one which is nondissipative and non–magnetic, and indeed even when the host

medium is free space (i.e., vacuum). Secondly, a general monoclinic/triclinic biaxial bianisotropic HCM structure (i.e., one for which θ_τ^χ, ϕ_τ^χ, p_τ^χ and q_τ^χ $(\chi = r, i;\ \tau = \epsilon, \xi, \mu)$ all have distinct values) results when the homogenisation corresponding to that of Figure 3.15 is carried out for spheroidal chiral inclusions and an isotropic host medium of spheroidal topology. This general structure degenerates to the orthorhombic biaxial or uniaxial form when the orientation of inclusion spheroids is perpendicular or parallel, respectively, to that of the host medium spheroids. We further remark that analogous results arise when the topologies of the inclusion and host mediums are interchanged.

3.5.2 Uniaxial spherical inclusions/uniaxial spherical host

We turn our attention now to the homogenisation of dissipative uniaxial bianisotropic mediums based on spherical topologies. We choose an inclusion medium given by

$$\underline{\underline{\epsilon}}_a = 2\,\epsilon_0\,\underline{\underline{Y}}_a\,, \qquad \underline{\underline{\xi}}_a = -\underline{\underline{\zeta}}_a = \sqrt{\epsilon_0\mu_0}\,\underline{\underline{Y}}_a\,, \qquad \underline{\underline{\mu}}_a = 1.5\,\mu_0\,\underline{\underline{Y}}_a\,, \tag{3.42}$$

where

$$\underline{\underline{Y}}_a = (1+i)\begin{bmatrix} 2\cos^2\lambda_a + 1 & 2\sin\lambda_a\cos\lambda_a & 0 \\ 2\sin\lambda_a\cos\lambda_a & 2\sin^2\lambda_a + 1 & 0 \\ 0 & 0 & 1 \end{bmatrix}, \tag{3.43}$$

and a host medium given by

$$(1/\epsilon_0)\underline{\underline{\epsilon}}_b = (1/\mu_0)\underline{\underline{\mu}}_b = (-1/\sqrt{\epsilon_0\mu_0})\,\underline{\underline{\xi}}_b = (1/\sqrt{\epsilon_0\mu_0})\,\underline{\underline{\zeta}}_b = (1+i\delta)\,\mathrm{diag}\,(3,1,1). \tag{3.44}$$

The angle λ_a represents the angle by which the distinguished axes of the inclusion medium are rotated in the xy plane with respect to the host medium distinguished axes (the distinguished axes of each constitutive dyadic all being parallel for both component mediums). For the dissipation parameter $\delta = 2.5$, the corresponding HCM polar and azimuthal unit vector angles $\theta_{\epsilon,\xi,\mu}^{r,i}$ and $\phi_{\epsilon,\xi,\mu}^{r,i}$ and parameters $p_{\epsilon,\xi,\mu}^{r,i}$ and $q_{\epsilon,\xi,\mu}^{r,i}$ are displayed as functions of λ_a in Figure 3.16(a)–(d) respectively. When the distinguished axes of the uniaxial component mediums are aligned parallel or anti–parallel (i.e., $\lambda_a = 0$ or π), then we have $\theta_{\epsilon,\xi,\mu}^{r,i} = \phi_{\epsilon,\xi,\mu}^{r,i} = 0$ and the HCM acquires a uniaxial bianisotropic form. Also, when the distinguished axis of the host medium is perpendicular to that of the inclusion medium (i.e., $\lambda_a = \pi/2$), we see that $\phi_{\epsilon,\xi,\mu}^{r,i} = 0$ and a biaxial bianisotropic HCM structure which is orthorhombic with respect to all four of its constitutive dyadics emerges. In general, however, the computed biaxial HCM structure represented in Figure 3.16 is of the generalised monoclinic/triclinic type with angles $\theta_{\epsilon,\xi,\mu}^{r,i}$ and $\phi_{\epsilon,\xi,\mu}^{r,i}$, and scalars $p_{\epsilon,\xi,\mu}^{r,i}$ and $q_{\epsilon,\xi,\mu}^{r,i}$, all taking distinct values. This most general biaxial form arises in spite of the high degree of symmetry which is present between the various constitutive dyadics of the component mediums specified in (3.42).

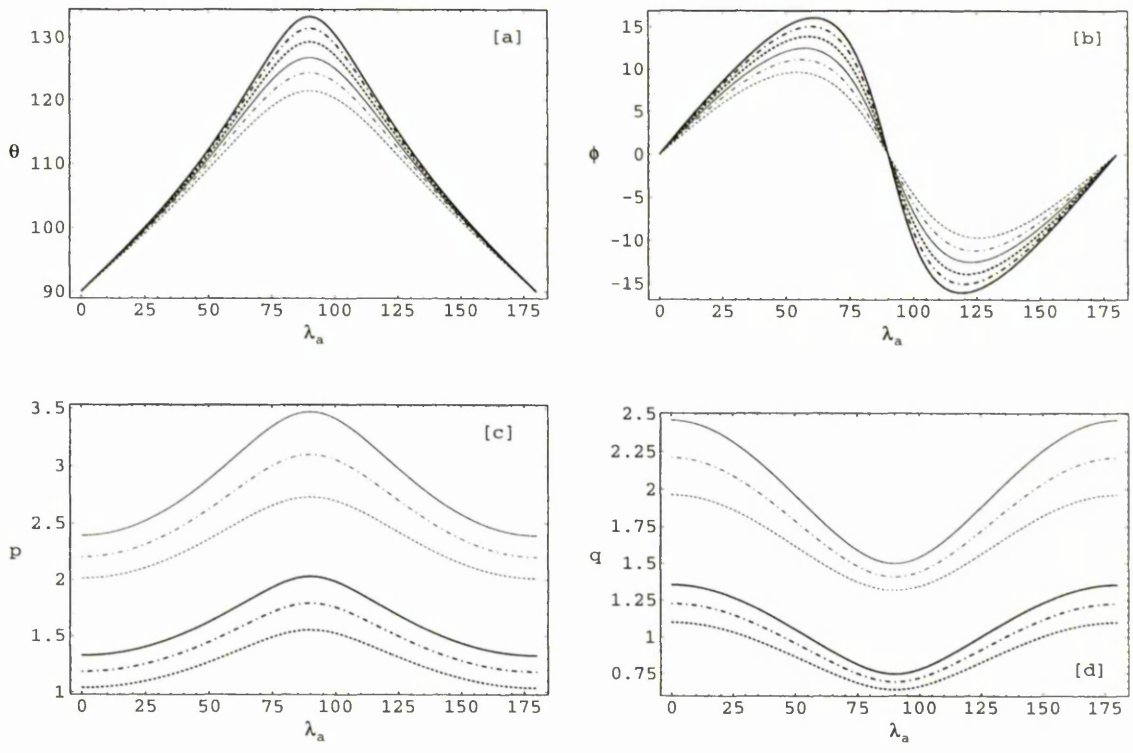

Figure 3.16: Uniaxial bianisotropic spherical inclusions homogenised with uniaxial bianisotropic spherical host medium. HCM unit vector (a) polar angles $\theta^{r,i}_{\epsilon,\xi,\mu}$ (degrees) and (b) azimuthal angles $\phi^{r,i}_{\epsilon,\xi,\mu}$ (degrees), and parameters (c) $p^{r,i}_{\epsilon,\xi,\mu}$ and (d) $q^{r,i}_{\epsilon,\xi,\mu}$ plotted against inclusion orientation angle λ_a. (Key in Table 3.2: $X = \theta$ for (a), $X = \phi$ for (b), $X = p$ for (c), $X = q$ for (d)).

It was earlier reported in Section 3.4 for biaxial dielectric–magnetic HCMs arising from uniaxial components that an orthorhombic HCM structure results when the ratios of the real and imaginary components of the host and inclusion medium constitutive dyadics are equal, despite the distinguished axes of the constituents being non–perpendicular. We investigate the generalisation of this result to bianisotropic HCMs by repeating the homogenisation of Figure 3.16 with the orientation angle λ_a fixed at 50° and allowing the dissipation parameter δ to vary. The resulting HCM constitutive parameters are plotted as functions of δ in Figure 3.17. At the point $\delta = 1$ we have

$$\mathrm{Re}\,\underline{\underline{\tau}}_b = \mathrm{Im}\,\underline{\underline{\tau}}_b\,, \qquad \mathrm{Re}\,\underline{\underline{\tau}}_a = \mathrm{Im}\,\underline{\underline{\tau}}_a\,, \qquad (\tau = \epsilon,\, \xi,\, \mu)\,, \tag{3.45}$$

and, from Figure 3.17(b), we observe $\phi^r_\tau = \phi^i_\tau$ $(\tau = \epsilon, \xi, \mu)$; i.e., the HCM is orthorhombic biaxial with respect to all four constitutive dyadics. We emphasise that this orthorhombic state is *not* associated with perpendicularity of the distinguished axes in the component mediums (i.e., $\lambda_a \neq \pi/2$). An equivalent orthorhombic state does not arise in the case of the homogenisation of Figure 3.16 since $\delta \neq 1$ in this instance. Furthermore, inspecting Figure 3.17(a), (b) and (c), we see that this is an

especially symmetric orthorhombic state for which $\theta_\tau^r = \theta_\tau^i$, $p_\tau^r = p_\tau^i$, and $q_\tau^r = q_\tau^i$ $(\tau = \epsilon, \xi, \mu)$.

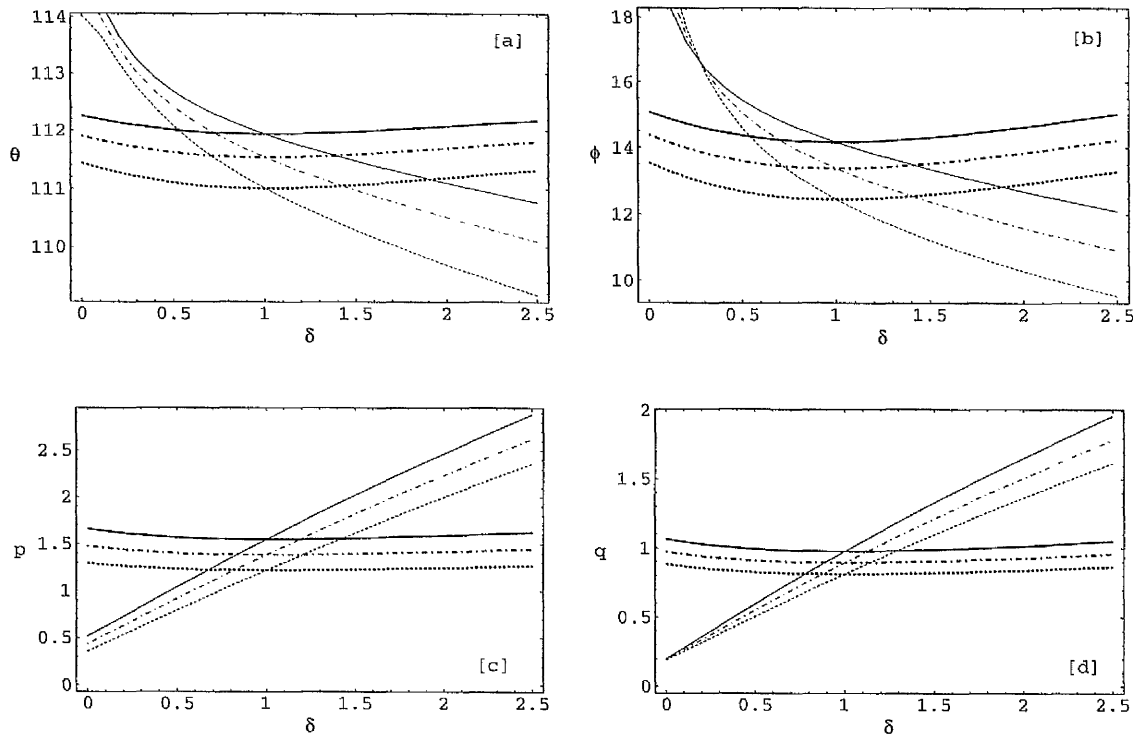

Figure 3.17: Uniaxial bianisotropic spherical inclusions homogenised with uniaxial bianisotropic spherical host medium. HCM unit vector (a) polar angles $\theta_{\epsilon,\xi,\mu}^{r,i}$ (degrees) and (b) azimuthal angles $\phi_{\epsilon,\xi,\mu}^{r,i}$ (degrees), and parameters (c) $p_{\epsilon,\xi,\mu}^{r,i}$ and (d) $q_{\epsilon,\xi,\mu}^{r,i}$ plotted against dissipation parameter δ. (Key in Table 3.2: $X = \theta$ for (a), $X = \phi$ for (b), $X = p$ for (c), $X = q$ for (d)).

A significant difference between the biaxial bianisotropic HCM represented by Figure 3.17, and the analogous biaxial dielectric–magnetic HCM reported in Section 3.4.2 (see Figures 3.12 and 3.13), is that in the present example the orthorhombic structure does not emerge if the ratios of real and imaginary parts of only one of the component constitutive dyadic–types are equal. That is, for example, here we have

$$\mathrm{Re}\,\underline{\underline{\epsilon}}_b = \mathrm{Im}\,\underline{\underline{\epsilon}}_b\,, \qquad \mathrm{Re}\,\underline{\underline{\epsilon}}_a = \mathrm{Im}\,\underline{\underline{\epsilon}}_a \qquad \not\Longrightarrow \qquad \phi_\epsilon^r = \phi_\epsilon^i\,, \tag{3.46}$$

in general.

We further explore the symmetric nature of the HCM constitutive dyadics by considering the case in which the constitutive dyadics of the component mediums are scalar multiples of one another. Continuing with the dissipative uniaxial bianisotropic inclusion/host medium example–type, we consider the homogenisation of components given by

$$\underline{\underline{\epsilon}}_a = \epsilon_0\,\underline{\underline{Y}}_a\,, \qquad \underline{\underline{\xi}}_a = -\underline{\underline{\zeta}}_a = 0.5\,\sqrt{\epsilon_0\mu_0}\,\underline{\underline{Y}}_a\,, \qquad \underline{\underline{\mu}}_a = 1.5\,\mu_0\,\underline{\underline{Y}}_a\,, \tag{3.47}$$

where

$$\underline{\underline{Y}}_a = (2 + 0.5i) \begin{bmatrix} \cos^2 \lambda_a + 1 & \sin \lambda_a \cos \lambda_a & 0 \\ \sin \lambda_a \cos \lambda_a & \sin^2 \lambda_a + 1 & 0 \\ 0 & 0 & 1 \end{bmatrix}, \tag{3.48}$$

and

$$\underline{\underline{\epsilon}}_b = \epsilon_0 \underline{\underline{Y}}_b, \qquad \underline{\underline{\xi}}_b = -\underline{\underline{\zeta}}_b = (\sqrt{\epsilon_0 \mu_0}/\eta)\, \underline{\underline{Y}}_b, \qquad \underline{\underline{\mu}}_b = \eta\, \mu_0 \underline{\underline{Y}}_b, \tag{3.49}$$

with

$$\underline{\underline{Y}}_b = (1 + 0.5i)\, \mathrm{diag}\,(3, 1, 1). \tag{3.50}$$

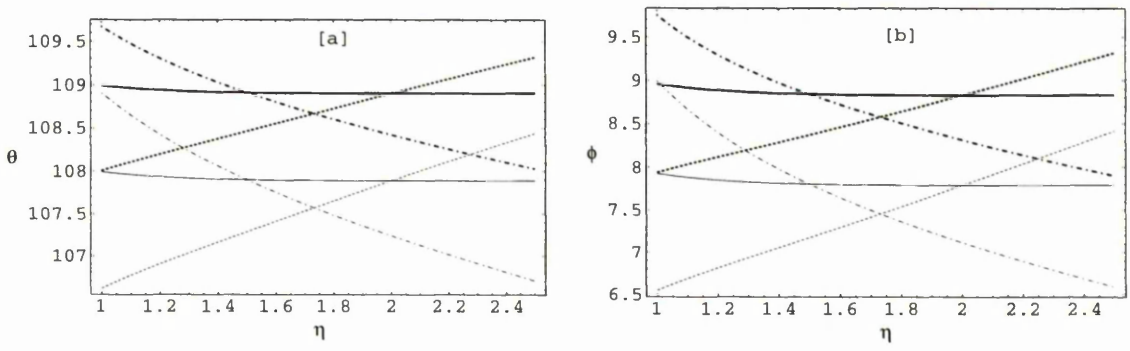

Figure 3.18: Uniaxial bianisotropic spherical inclusions homogenised with uniaxial bianisotropic spherical host medium. HCM unit vector (a) polar angles $\theta^{r,i}_{\epsilon,\xi,\mu}$ (degrees) and (b) azimuthal angles $\phi^{r,i}_{\epsilon,\xi,\mu}$ (degrees) plotted against ratio of host medium permeability to host medium permittivity η. (Key in Table 3.2: $X = \theta$ for (a), $X = \phi$ for (b)).

As earlier, both component phases are assumed to have spherical topology; and we take the angle λ_a in the xy plane between the inclusion and host medium distinguished axes to be 50°. The defining polar and azimuthal angles calculated for the HCM unit vector pairs $\underline{u}^{r,i}_{m\epsilon,\xi,\mu}$ and $\underline{u}^{r,i}_{n\epsilon,\xi,\mu}$ are plotted as functions of η in Figures 3.18(a) and 3.18(b) respectively. The points of greatest interest occur at $\eta = 1.5, \sqrt{3}$ and 2; we summarise the salient features of Figure 3.18 at these points as

$$(1/\epsilon_0)\, \underline{\underline{\epsilon}}_b = r(1/\mu_0)\, \underline{\underline{\mu}}_b, \qquad (1/\epsilon_0)\, \underline{\underline{\epsilon}}_a = r(1/\mu_0)\, \underline{\underline{\mu}}_a \qquad \Longrightarrow$$
$$\theta^r_\epsilon = \theta^r_\mu, \qquad \theta^i_\epsilon = \theta^i_\mu, \qquad \phi^r_\epsilon = \phi^r_\mu, \qquad \phi^i_\epsilon = \phi^i_\mu, \tag{3.51}$$

$$(1/\epsilon_0)\, \underline{\underline{\epsilon}}_b = s(1/i\sqrt{\epsilon_0 \mu_0})\, \underline{\underline{\xi}}_b, \qquad (1/\epsilon_0)\, \underline{\underline{\epsilon}}_a = s(1/i\sqrt{\epsilon_0 \mu_0})\, \underline{\underline{\xi}}_a \qquad \Longrightarrow$$
$$\theta^r_\epsilon = \theta^r_\xi, \qquad \theta^i_\epsilon = \theta^i_\xi, \qquad \phi^r_\epsilon = \phi^r_\xi, \qquad \phi^i_\epsilon = \phi^i_\xi \tag{3.52}$$

$$(1/i\sqrt{\epsilon_0 \mu_0})\, \underline{\underline{\xi}}_b = t(1/\mu_0)\, \underline{\underline{\mu}}_b, \qquad (1/i\sqrt{\epsilon_0 \mu_0})\, \underline{\underline{\xi}}_a = t(1/\mu_0)\, \underline{\underline{\mu}}_a \qquad \Longrightarrow$$
$$\theta^r_\xi = \theta^r_\mu, \qquad \theta^i_\xi = \theta^i_\mu, \qquad \phi^r_\xi = \phi^r_\mu, \qquad \phi^i_\xi = \phi^i_\mu, \tag{3.53}$$

where r, s and t are proportionality scalars. As was the case for the corresponding homogenisations for the dielectric–magnetic HCM (see Figure 3.9 in Section 3.4.2),

we observe that the biaxial bianisotropic HCM structure is not orthorhombic at $\eta = 1.5, \sqrt{3}$ and 2, notwithstanding the symmetries outlined in (3.51)–(3.53). Analogous results do not arise for the scalar quantities $p^{r,i}_{\epsilon,\xi,\mu}$ and $q^{r,i}_{\epsilon,\xi,\mu}$ and these are not presented.

3.6 Concluding remarks

For dielectric mediums it is well established in Sections 3.3 and 3.4 that, through the process of homogenisation, an effective medium biaxial with respect to permittivity arises provided the component mediums present two noncollinear distinguished axes. If the distinguished axes of the component mediums are perpendicular, or alternatively if the ratios of real and imaginary parts of the permittivity dyadics of the host and inclusion mediums are equal, then an orthorhombic biaxial structure results, for which the complex HCM permittivity dyadic can be diagonalised. Otherwise, the biaxial dielectric HCMs have a monoclinic/triclinic structure — a structure characterised as having a complex permittivity dyadic with principal axes of real and imaginary parts which do not coincide. The generalisation of these results to the homogenisation of dielectric–magnetic mediums gives rise to richer HCM structures in which orthorhombic dielectric and magnetic forms may be realised independently of one another. Generalising further — through the introduction of magnetoelectric coupling — vastly increases the range and complexity of HCM structures which may be conceptualised from relatively simple component mediums. Even with the restriction to reciprocal mediums, a generalised biaxial bianisotropic HCM form emerges which requires 33 real–valued parameters in order to completely specify its constitutive dyadics. With such a large parameter space, only illustrative examples giving insights into the structure and symmetries of the constitutive properties were practicably presented here. A highly symmetric biaxial bianisotropic HCM, orthorhombic with respect to all of its constitutive dyadics, is achievable through balancing real and imaginary components of the component medium constitutive dyadics, even though the distinguished axes presented by constituents are not orthogonal. Further simplifications of the biaxial bianisotropic HCM form arise where the constitutive dyadics of the component mediums are scalar multiples of each other.

Chapter 4

The Strong–Property–Fluctuation Theory

4.1 Introduction

In general, the electromagnetic response of a composite medium depends upon the topological and distributional details of the component phases as well as their physical properties. In the widely–used MG homogenisation formalism and its incremental and differential variants, as well as the Br homogenisation formalism, allowance can be made for ellipsoidal component phase topology; however, the distributions of the component phases are characterised solely through their volume fractions [1, 3, 10]. In order to incorporate a more extensive statistical description of the composite microstructure, higher–order spatial correlation functions are required.

A homogenisation formalism which, in principle, can accommodate spatial correlation functions of arbitrarily high order is the *strong–property–fluctuation theory* (SPFT). In the SPFT, a preliminary ansatz is made about the nature of the composite; the ansatz is used to perturbatively calculate corrections in orders of statistical cumulants of the spatial distribution of the constituent phases. Solutions are expressed in terms of a so–called *mass operator* which—due to the process of iteration—has an infinite series representation. In the usual SPFT implementation, the second–order truncation of the mass operator—known as the *bilocal approximation*—is adopted. A covariance function and its associated correlation length characterise the distributional statistics of the component phases in the bilocally–approximated SPFT. In particular, within a region of linear dimensions given by the correlation length, and of shape determined by the covariance function, the correlated responses of scattering centres result in an attenuation of the macroscopic coherent field. On the other hand, the responses of scattering centres separated by distances much greater than the correlation length are statistically independent. In the limiting case of zero correlation length, the SPFT reduces to the Br homogenisation formalism.

The SPFT has been successively developed for isotropic dielectric [53], anisotropic

dielectric [54], and chiral–in–chiral [55] composite materials. Under the bilocal approximation, the SPFT is developed in Section 4.2 for the most general linear class of composite materials [16], namely bianisotropic composites. Detailed numerical calculations which consider the influence of ellipsoidal topology, orientation diversity and correlation length are presented in Section 4.3 [17]. In Section 4.4, the influence of the covariance function is explored through a study concerning the homogenisation of ellipsoidal metallic inclusions with a non–conducting host medium [18]. Finally, by explicitly calculating the third–order mass operator term, the convergence of the bilocally–approximated SPFT is demonstrated in Section 4.5 for isotropic chiral HCMs, as well as for chiroferrite composites which are both weakly uniaxial and weakly gyrotropic [19].

4.2 Formalism for bianisotropic composites

The SPFT is presented for the homogenisation of a two–constituent bianisotropic composite [16]. Following a general presentation of the statistical parameters used to describe bianisotropic composites, we introduce the notion of a *bianisotropic comparison medium* (BCM). The BCM is a local homogeneous medium which serves as our initial ansatz in the iterative process resulting in the SPFT estimate of constitutive properties. We develop the *Dyson equation* for the average electromagnetic field in terms of the *mass operator*, and present the bilocally–approximated mass operator. Next we derive the relation between the constitutive dyadics of the exact effective medium (which includes all correlation effects) and the Dyson equation. We then consider the case where principal electromagnetic wavelengths are long compared with the correlation length, and the composite medium can therefore be regarded as homogeneous. Finally we implement the SPFT, under the long–wavelength and bilocal approximations, for the case of reciprocal bianisotropic composites based on ellipsoidal topology.

4.2.1 Generalities

We begin the analysis with the frequency–dependent version of the source–free Maxwell curl equations

$$\nabla \times \underline{E}(\underline{r}) = i\omega \underline{B}(\underline{r}), \tag{4.1}$$

$$\nabla \times \underline{H}(\underline{r}) = -i\omega \underline{D}(\underline{r}), \tag{4.2}$$

and the constitutive relations of a nonhomogeneous bianisotropic medium, given in the notation of (1.21) and (1.22) as

$$\underline{\mathbf{C}}(\underline{r}) = \underline{\underline{\mathbf{K}}}(\underline{r}) \cdot \underline{\mathbf{F}}(\underline{r}), \tag{4.3}$$

with

$$\underline{\underline{\mathbf{K}}}(\underline{r}) = \begin{bmatrix} \underline{\underline{\epsilon}}(\underline{r}) & \underline{\underline{\xi}}(\underline{r}), \\ \underline{\underline{\zeta}}(\underline{r}) & \underline{\underline{\mu}}(\underline{r}) \end{bmatrix}. \tag{4.4}$$

Combining (4.1), (4.2) and (4.3), we have

$$\underline{\underline{\mathbf{L}}}(\nabla) \cdot \underline{\mathbf{F}}(\underline{r}) = -i\omega \underline{\underline{\mathbf{K}}}(\underline{r}) \cdot \underline{\mathbf{F}}(\underline{r}) \,, \tag{4.5}$$

where the linear differential operator $\underline{\underline{\mathbf{L}}}(\nabla)$ is defined in (1.15).

We consider a two–phase composite consisting of two bianisotropic constituent phases mixed at the microscopic, but not molecular, length scale. Let all space be partitioned into disjoint parts V_a and V_b containing the phases labelled a and b, respectively. For $\underline{r} \in V_\ell$, $(\ell = a, b)$, we write

$$\underline{\underline{\epsilon}}(\underline{r}) = \underline{\underline{\epsilon}}_\ell \,, \quad \underline{\underline{\xi}}(\underline{r}) = \underline{\underline{\xi}}_\ell \,, \quad \underline{\underline{\zeta}}(\underline{r}) = \underline{\underline{\zeta}}_\ell \,, \quad \underline{\underline{\mu}}(\underline{r}) = \underline{\underline{\mu}}_\ell \,, \qquad \underline{r} \in V_\ell \,, \tag{4.6}$$

so that

$$\underline{\underline{\mathbf{K}}}(\underline{r}) = \underline{\underline{\mathbf{K}}}_\ell \,, \qquad \underline{r} \in V_\ell \,. \tag{4.7}$$

We introduce two characteristic functions θ_ℓ as

$$\theta_\ell(\underline{r}) = \begin{cases} 1 & \underline{r} \in V_\ell \\ \\ 0 & \underline{r} \notin V_\ell \end{cases} ; \tag{4.8}$$

thus,

$$\theta_a(\underline{r}) + \theta_b(\underline{r}) = 1 \,, \qquad \underline{r} \in V_a \cup V_b \,. \tag{4.9}$$

Any of the $\underline{r}$–dependent constitutive quantities can be expressed *everywhere* in terms of the characteristic functions $\theta_\ell(\underline{r})$; for example,

$$\underline{\underline{\mathbf{K}}}(\underline{r}) = \underline{\underline{\mathbf{K}}}_a \theta_a(\underline{r}) + \underline{\underline{\mathbf{K}}}_b \theta_b(\underline{r}) \,, \qquad \underline{r} \in V_a \cup V_b \,. \tag{4.10}$$

Throughout this work, we use the concept of ensemble–averaging, i.e., averaging over a large number of different samples of the two–phase composite, and we denote ensemble averages by $\langle\ \rangle$. The complete statistical information about the composite is contained in *moments* of the characteristic function $\theta_a(\underline{r})$. The nth moment is the expectation value $\langle \theta_a(\underline{r}_1) \ldots \theta_a(\underline{r}_n) \rangle$ and represents the probability for $\underline{r}_1, \ldots, \underline{r}_n$ being inside V_a; equivalently, we may use b instead of a due to (4.9). We assume that, on average, the composite is homogeneous.

The first moment for the phase a is its volume fraction

$$f_a = \langle \theta_a(\underline{r}) \rangle \,, \tag{4.11}$$

which is constant with respect to $\underline{r}$. The same holds for the volume fraction $f_b = \langle \theta_b(\underline{r}) \rangle$ of phase b. Obviously, $f_a + f_b = 1$.

The two volume fractions f_a and f_b contain only minimal geometrical information about the composite. A more detailed description is provided by the second moment $\langle\theta_a(\underline{r})\theta_a(\underline{r}')\rangle$ of $\theta_a(\underline{r})$, or, equivalently, by the second *cumulant* or covariance

$$\begin{aligned}\Gamma(\underline{R}) &= \langle\theta_a(\underline{r})\theta_a(\underline{r}')\rangle - \langle\theta_a(\underline{r})\rangle\langle\theta_a(\underline{r}')\rangle \\ &\equiv \langle\theta_b(\underline{r})\theta_b(\underline{r}')\rangle - \langle\theta_b(\underline{r})\rangle\langle\theta_b(\underline{r}')\rangle\,, \end{aligned} \tag{4.12}$$

where $\underline{R} = \underline{r} - \underline{r}'$. If the composite is disordered, it is usually possible to define a correlation length L such that $\Gamma(\underline{R})$ is negligible for $|\,\underline{R}\,| \gg L$; i.e., on scales larger than L, the composite may be considered homogeneous.

The formulation of SPFT requires the introduction of a bianisotropic comparison medium (BCM), which allows an approximate treatment of electromagnetic fields arising in $V_a \cup V_b$. The constitutive dyadics $\underline{\underline{\epsilon}}_{BCM}$, $\underline{\underline{\xi}}_{BCM}$, $\underline{\underline{\zeta}}_{BCM}$ and $\underline{\underline{\mu}}_{BCM}$ of this medium are not $\underline{r}$–dependent; hence it is not only homogeneous but also spatially *local*. The BCM will later on serve as the preliminary ansatz for the SPFT and will be shown in Section 4.2.2 to actually be in agreement with the Br homogenisation formalism. Electromagnetic wave propagation in the BCM is described by

$$\underline{\underline{\mathbf{L}}}(\nabla) \cdot \underline{\mathbf{F}}_{BCM}(\underline{r}) = -i\omega\underline{\underline{\mathbf{K}}}_{BCM} \cdot \underline{\mathbf{F}}_{BCM}(\underline{r})\,, \tag{4.13}$$

where

$$\underline{\underline{\mathbf{K}}}_{BCM} = \begin{bmatrix} \underline{\underline{\epsilon}}_{BCM} & \underline{\underline{\xi}}_{BCM} \\ \underline{\underline{\zeta}}_{BCM} & \underline{\underline{\mu}}_{BCM} \end{bmatrix}, \qquad \underline{\mathbf{F}}_{BCM}(\underline{r}) = \begin{bmatrix} \underline{E}_{BCM}(\underline{r}) \\ \underline{H}_{BCM}(\underline{r}) \end{bmatrix}, \tag{4.14}$$

with $\underline{\mathbf{F}}_{BCM}(\underline{r})$ denoting the local spatially–averaged electromagnetic field. We introduce the 6×6 dyadic Green function $\underline{\underline{\mathbf{G}}}_{BCM}(\underline{r} - \underline{r}')$ which satisfies the differential equation

$$\left(\underline{\underline{\mathbf{L}}}(\nabla) + i\omega\underline{\underline{\mathbf{K}}}_{BCM}\right) \cdot \underline{\underline{\mathbf{G}}}_{BCM}(\underline{r} - \underline{r}') = \underline{\underline{\mathbf{I}}}\,\delta(\underline{r} - \underline{r}'), \tag{4.15}$$

where $\delta(\underline{r} - \underline{r}')$ is the Dirac delta function. The singular behaviour of $\underline{\underline{\mathbf{G}}}_{BCM}(\underline{r} - \underline{r}')$ in the limit $\underline{r} \to \underline{r}'$ can be conveniently isolated through

$$\underline{\underline{\mathbf{G}}}_{BCM}(\underline{R}) = \mathcal{P}\underline{\underline{\mathbf{G}}}_{BCM}(\underline{R}) + \underline{\underline{\mathbf{D}}}\,\delta(\underline{R}), \tag{4.16}$$

where $\mathcal{P}$ is the principal value operation excluding a certain infinitesimal region centred on $\underline{R} = \underline{0}$ and $\underline{\underline{\mathbf{D}}}$ is the corresponding depolarisation dyadic of the specified region in the BCM [29]. The dyadic $\underline{\underline{\mathbf{D}}}$ is fixed at a later stage in the analysis.

4.2.2 The Dyson equation

With the foregoing generalities established, we now proceed to derive the central equation in the SPFT: the *Dyson equation*. From (4.5) we obtain

$$\left(\underline{\underline{\mathbf{L}}}(\nabla) + i\omega\underline{\underline{\mathbf{K}}}_{BCM}\right) \cdot \underline{\mathbf{F}}(\underline{r}) = -i\omega\left(\underline{\underline{\mathbf{K}}}(\underline{r}) - \underline{\underline{\mathbf{K}}}_{BCM}\right) \cdot \underline{\mathbf{F}}(\underline{r})\,. \tag{4.17}$$

By virtue of (4.13) and (4.15), the solution of (4.17) may be represented by the following *Fredholm equation of the third kind* [56]

$$\underline{\mathbf{F}}(\underline{r}) = \underline{\mathbf{F}}_{BCM}(\underline{r}) - i\omega \int \underline{\underline{\mathbf{G}}}_{BCM}(\underline{r}-\underline{r}') \cdot \left(\underline{\underline{\mathbf{K}}}(\underline{r}') - \underline{\underline{\mathbf{K}}}_{BCM}\right) \cdot \underline{\mathbf{F}}(\underline{r}')\, d^3\underline{r}' \,. \qquad (4.18)$$

Clearly, $\underline{\mathbf{F}}_{BCM}(\underline{r})$ now serves as a solution of the homogeneous version of (4.17), i.e., $\underline{\mathbf{F}}_{BCM}(\underline{r})$ is the *complementary function.*

Equation (4.18) cannot be evaluated perturbatively when the constitutive parameters in $\underline{\underline{\mathbf{K}}}(\underline{r})$ fluctuate strongly. This is due to secular terms produced by the singularities of the dyadic Green function $\underline{\underline{\mathbf{G}}}_{BCM}(\underline{R})$ in the source region. The singularities can be removed from the right side of (4.18) by taking advantage of (4.16); thus,

$$\begin{aligned} \underline{\mathbf{F}}(\underline{r}) \;=\; & \underline{\mathbf{F}}_{BCM}(\underline{r}) - i\omega\mathcal{P} \int \underline{\underline{\mathbf{G}}}_{BCM}(\underline{r}-\underline{r}') \cdot \left(\underline{\underline{\mathbf{K}}}(\underline{r}') - \underline{\underline{\mathbf{K}}}_{BCM}\right) \cdot \underline{\mathbf{F}}(\underline{r}')\, d^3\underline{r}' \\ & -i\omega\underline{\underline{\mathbf{D}}} \cdot \left(\underline{\underline{\mathbf{K}}}(\underline{r}) - \underline{\underline{\mathbf{K}}}_{BCM}\right) \cdot \underline{\mathbf{F}}(\underline{r}) \,. \end{aligned} \qquad (4.19)$$

Next, after introducing the *exciting field*

$$\underline{\mathbf{F}}_{exc}(\underline{r}) = \left[\underline{\underline{\mathbf{I}}} + i\omega\underline{\underline{\mathbf{D}}} \cdot \left(\underline{\underline{\mathbf{K}}}(\underline{r}) - \underline{\underline{\mathbf{K}}}_{BCM}\right)\right] \cdot \underline{\mathbf{F}}(\underline{r}) \,, \qquad (4.20)$$

we rewrite the integral equation (4.19) as

$$\underline{\mathbf{F}}_{exc}(\underline{r}) = \underline{\mathbf{F}}_{BCM}(\underline{r}) + \mathcal{P} \int \underline{\underline{\mathbf{G}}}_{BCM}(\underline{r}-\underline{r}') \cdot \underline{\underline{\boldsymbol{\chi}}}(\underline{r}') \cdot \underline{\mathbf{F}}_{exc}(\underline{r}')\, d^3\underline{r}' \,, \qquad (4.21)$$

with a generalised *polarisability dyadic* defined as

$$\underline{\underline{\boldsymbol{\chi}}}(\underline{r}) = -i\omega \left(\underline{\underline{\mathbf{K}}}(\underline{r}) - \underline{\underline{\mathbf{K}}}_{BCM}\right) \cdot \left[\underline{\underline{\mathbf{I}}} + i\omega\underline{\underline{\mathbf{D}}} \cdot \left(\underline{\underline{\mathbf{K}}}(\underline{r}) - \underline{\underline{\mathbf{K}}}_{BCM}\right)\right]^{-1} . \qquad (4.22)$$

The next steps are canonical: We calculate the ensemble–average $\langle\, \underline{\mathbf{F}}_{exc}(\underline{r}) \,\rangle$ of the exciting field by ensemble–averaging both sides of the integral equation (4.21). For this purpose, we formally represent (4.21) in terms of its Born series as

$$\begin{aligned} & \underline{\mathbf{F}}_{exc}(\underline{r}) = \\ & \underline{\mathbf{F}}_{BCM}(\underline{r}) + \mathcal{P} \int \underline{\underline{\mathbf{G}}}_{BCM}(\underline{r}-\underline{r}') \cdot \underline{\underline{\boldsymbol{\chi}}}(\underline{r}') \cdot \underline{\mathbf{F}}_{BCM}(\underline{r}')\, d^3\underline{r}' \\ & + \mathcal{P} \int \underline{\underline{\mathbf{G}}}_{BCM}(\underline{r}-\underline{r}') \cdot \underline{\underline{\boldsymbol{\chi}}}(\underline{r}') \cdot \left(\mathcal{P} \int \underline{\underline{\mathbf{G}}}_{BCM}(\underline{r}'-\underline{r}'') \cdot \underline{\underline{\boldsymbol{\chi}}}(\underline{r}'') \cdot \underline{\mathbf{F}}_{BCM}(\underline{r}'')\, d^3\underline{r}''\right) d^3\underline{r}' \\ & + \mathcal{P} \int \underline{\underline{\mathbf{G}}}_{BCM}(\underline{r}-\underline{r}') \cdot \underline{\underline{\boldsymbol{\chi}}}(\underline{r}') \cdot \Big[\mathcal{P} \int \underline{\underline{\mathbf{G}}}_{BCM}(\underline{r}'-\underline{r}'') \cdot \underline{\underline{\boldsymbol{\chi}}}(\underline{r}'') \\ & \cdot \left(\mathcal{P} \int \underline{\underline{\mathbf{G}}}_{BCM}(\underline{r}''-\underline{r}''') \cdot \underline{\underline{\boldsymbol{\chi}}}(\underline{r}''') \cdot \underline{\mathbf{F}}_{BCM}(\underline{r}''')\, d^3\underline{r}'''\right) d^3\underline{r}'' \Big]\, d^3\underline{r}' + \cdots \,, \end{aligned} \qquad (4.23)$$

and average each term of the series separately [6]. By ensemble–averaging the terms of (4.23) separately and re–ordering terms using a Feynman–diagrammatic technique [57], the Dyson equation

$$\langle\, \underline{\mathbf{F}}_{exc}(\underline{r}) \,\rangle = \underline{\mathbf{F}}_{BCM}(\underline{r}) + \mathcal{P} \int \underline{\underline{\mathbf{G}}}_{BCM}(\underline{r}-\underline{r}') \cdot \left(\int \underline{\underline{\boldsymbol{\Sigma}}}(\underline{r}'-\underline{r}'') \cdot \langle\, \underline{\mathbf{F}}_{exc}(\underline{r}'') \,\rangle d^3\underline{r}''\right) d^3\underline{r}' \,, \qquad (4.24)$$

is developed. The *mass operator* $\underline{\underline{\Sigma}}(\underline{r}' - \underline{r}'')$ has an infinite series representation, the terms of which comprise products over $\mathcal{P}\,\underline{\underline{G}}_{BCM}(\underline{r}' - \underline{r}'')$ and the statistical cumulants of $\underline{\underline{\chi}}(\underline{r}' - \underline{r}'')$. For later convenience, we express

$$\underline{\underline{\Sigma}}(\underline{R}) = \underline{\underline{\Sigma}}_0(\underline{R}) + \underline{\underline{\Sigma}}_1(\underline{R}) + \underline{\underline{\Sigma}}_2(\underline{R}) + \underline{\underline{\Sigma}}_3(\underline{R}) + \cdots , \tag{4.25}$$

where the subscript j in $\underline{\underline{\Sigma}}_j(\underline{R})$ refers to the order of $\underline{\underline{\chi}}(\underline{R})$.

For practical purposes, an approximate evaluation of the mass operator is necessary. The lowest–order truncation of the mass operator series; i.e.,

$$\underline{\underline{\Sigma}}(\underline{R}) \approx \underline{\underline{\Sigma}}_0(\underline{R}) = \underline{\underline{0}}, \tag{4.26}$$

leads to the trivial result $\underline{\underline{K}}_{Dy0} = \underline{\underline{K}}_{BCM}$. The BCM is conventionally chosen so that the first–order mass operator approximation does not add to the zero–order approximation [53]–[55]. Thus, we have the condition

$$\langle\, \underline{\underline{\chi}}(\underline{r}) \,\rangle = \underline{\underline{0}}, \tag{4.27}$$

and $\underline{\underline{\Sigma}}_1(\underline{R}) = \underline{\underline{0}}$ correspondingly. The condition (4.27) removes the secular terms from the Born series expansion [58]. Substituting (4.10), (4.11) and (4.22) into (4.27), we obtain

$$\begin{aligned} &\left(\underline{\underline{K}}_a - \underline{\underline{K}}_{BCM}\right) \cdot \left[\underline{\underline{I}} + i\omega\underline{\underline{D}} \cdot \left(\underline{\underline{K}}_a - \underline{\underline{K}}_{BCM}\right)\right]^{-1} f_a \;+ \\ &\left(\underline{\underline{K}}_b - \underline{\underline{K}}_{BCM}\right) \cdot \left[\underline{\underline{I}} + i\omega\underline{\underline{D}} \cdot \left(\underline{\underline{K}}_b - \underline{\underline{K}}_{BCM}\right)\right]^{-1} f_b \;=\; \underline{\underline{0}}, \end{aligned} \tag{4.28}$$

which is the Br equation for bianisotropic composites [31]. Thus, we see that electromagnetic wave propagation in $V_a \cup V_b$ can indeed be approximately described by means of the BCM.

The most widely–adopted procedure is to implement the second–order truncation of the mass operator series, whence

$$\underline{\underline{\Sigma}}(\underline{r} - \underline{r}') \approx \underline{\underline{\Sigma}}_2(\underline{r} - \underline{r}') = \langle\, \underline{\underline{\chi}}(\underline{r}) \cdot \mathcal{P}\underline{\underline{G}}_{BCM}(\underline{r} - \underline{r}') \cdot \underline{\underline{\chi}}(\underline{r}') \,\rangle , \tag{4.29}$$

which is known as the *bilocal approximation* [59]. Since

$$\underline{\underline{\chi}}(\underline{r}) = \underline{\underline{\chi}}_a\, \theta_a(\underline{r}) + \underline{\underline{\chi}}_b \theta_b(\underline{r}) , \tag{4.30}$$

(4.29) leads to

$$\underline{\underline{\Sigma}}(\underline{R}) = \Gamma(\underline{R}) \left(\underline{\underline{\chi}}_a - \underline{\underline{\chi}}_b\right) \cdot \mathcal{P}\underline{\underline{G}}_{BCM}(\underline{R}) \cdot \left(\underline{\underline{\chi}}_a - \underline{\underline{\chi}}_b\right), \tag{4.31}$$

after some algebraic manipulations exploiting (4.27), the covariance $\Gamma(\underline{R})$ having been introduced in (4.12).

Higher–order mass operator approximations and the issue of convergence are explored in Section 4.5.

4.2.3 Nonlocal effective medium

In order to complete the SPFT formulation, we go on to determine the relation between the ensemble–averaged fields $\langle\, \underline{\mathbf{C}}(\underline{r}) \,\rangle$ and $\langle\, \underline{\mathbf{F}}(\underline{r}) \,\rangle$. The ensemble–average of the constitutive relation (4.3) may be stated as

$$\langle\, \underline{\mathbf{C}}(\underline{r}) \,\rangle = \langle\, \underline{\underline{\mathbf{K}}}(\underline{r}) \cdot \underline{\mathbf{F}}(\underline{r}) \,\rangle \,. \tag{4.32}$$

The relationship between $\langle\, \underline{\underline{\mathbf{K}}}(\underline{r}) \cdot \underline{\mathbf{F}}(\underline{r}) \,\rangle$ and $\langle\, \underline{\mathbf{F}}(\underline{r}) \,\rangle$ must be linear, because the composite is linear. Furthermore, this relation has to be of the form of a convolution integral

$$\langle\, \underline{\underline{\mathbf{K}}}(\underline{r}) \cdot \underline{\mathbf{F}}(\underline{r}) \,\rangle = \int \underline{\underline{\mathbf{K}}}_{Dy}(\underline{R}) \cdot \langle\, \underline{\mathbf{F}}(\underline{r} - \underline{R}) \,\rangle \, d^3\underline{R}, \tag{4.33}$$

due to translational invariance. The dyadic $\underline{\underline{\mathbf{K}}}_{Dy}(\underline{R})$ contains the constitutive properties of the effective medium consistent with the SPFT. In general, $\underline{\underline{\mathbf{K}}}_{Dy}(\underline{R})$ is *spatially nonlocal* and, therefore, signifies spatial dispersion.

Equations (4.20) and (4.22) yield

$$\underline{\underline{\boldsymbol{\chi}}}(\underline{r}) \cdot \underline{\mathbf{F}}_{exc}(\underline{r}) = -i\omega \left(\underline{\underline{\mathbf{K}}}(\underline{r}) - \underline{\underline{\mathbf{K}}}_{BCM} \right) \cdot \underline{\mathbf{F}}(\underline{r}) \,, \tag{4.34}$$

whence

$$\langle\, \underline{\underline{\boldsymbol{\chi}}}(\underline{r}) \cdot \underline{\mathbf{F}}_{exc}(\underline{r}) \,\rangle = -i\omega \left(\langle\, \underline{\underline{\mathbf{K}}}(\underline{r}) \cdot \underline{\mathbf{F}}(\underline{r}) \,\rangle - \underline{\underline{\mathbf{K}}}_{BCM} \cdot \langle\, \underline{\mathbf{F}}(\underline{r}) \,\rangle \right) . \tag{4.35}$$

The ensemble–averaged counterpart of (4.20) is given by

$$\langle\, \underline{\mathbf{F}}_{exc}(\underline{r}) \,\rangle = \left(\underline{\underline{\mathbf{I}}} - i\omega \underline{\underline{\mathbf{D}}} \cdot \underline{\underline{\mathbf{K}}}_{BCM} \right) \cdot \langle\, \underline{\mathbf{F}}(\underline{r}) \,\rangle + i\omega \underline{\underline{\mathbf{D}}} \cdot \langle\, \underline{\underline{\mathbf{K}}}(\underline{r}) \cdot \underline{\mathbf{F}}(\underline{r}) \,\rangle \,. \tag{4.36}$$

Furthermore, on taking the ensemble average of (4.21) and comparing it with the Dyson equation (4.24), we get

$$\langle\, \underline{\underline{\boldsymbol{\chi}}}(\underline{r}) \cdot \underline{\mathbf{F}}_{exc}(\underline{r}) \,\rangle = \int \underline{\underline{\boldsymbol{\Sigma}}}(\underline{r} - \underline{r}') \cdot \langle\, \underline{\mathbf{F}}_{exc}(\underline{r}') \,\rangle d^3\underline{r}' \,. \tag{4.37}$$

Finally, after rearranging (4.35)–(4.37) and inserting the ensemble–averaged constitutive relation (4.32) in (4.33), we obtain

$$\begin{aligned} &\langle\, \underline{\mathbf{C}}(\underline{r}) \,\rangle + \int \underline{\underline{\boldsymbol{\Sigma}}}(\underline{r} - \underline{r}') \cdot \underline{\underline{\mathbf{D}}} \cdot \langle\, \underline{\mathbf{C}}(\underline{r}') \,\rangle \, d^3\underline{r}' = \\ &\underline{\underline{\mathbf{K}}}_{BCM} \cdot \langle\, \underline{\mathbf{F}}(\underline{r}) \,\rangle - \frac{1}{i\omega} \int \underline{\underline{\boldsymbol{\Sigma}}}(\underline{r} - \underline{r}') \cdot \left(\underline{\underline{\mathbf{I}}} - i\omega \underline{\underline{\mathbf{D}}} \cdot \underline{\underline{\mathbf{K}}}_{BCM} \right) \cdot \langle\, \underline{\mathbf{F}}(\underline{r}') \,\rangle \, d^3\underline{r}'. \end{aligned} \tag{4.38}$$

This integral equation gives a linear relation between $\langle\, \underline{\mathbf{C}}(\underline{r}) \,\rangle$ and $\langle\, \underline{\mathbf{F}}(\underline{r}) \,\rangle$. Its solution for $\langle\, \underline{\mathbf{C}}(\underline{r}) \,\rangle$ enables the emergence of the desired constitutive dyadic $\underline{\underline{\mathbf{K}}}_{Dy}(\underline{R})$ of the nonlocal effective medium.

Since the integral equation (4.38) is of the convolution type, it can be solved by the Fourier transform technique [60]. Therefore, we define the following quantities:

$$\underline{\tilde{\mathbf{F}}}(\underline{q}) = \int \langle\, \underline{\mathbf{F}}(\underline{r}) \,\rangle \exp(-i\,\underline{q}\cdot\underline{r})\; d^3\underline{r}\,, \tag{4.39}$$

$$\underline{\tilde{\mathbf{C}}}(\underline{q}) = \int \langle\, \underline{\mathbf{C}}(\underline{r}) \,\rangle \exp(-i\,\underline{q}\cdot\underline{r})\; d^3\underline{r}\,, \tag{4.40}$$

$$\underline{\underline{\tilde{\Sigma}}}(\underline{q}) = \int \underline{\underline{\Sigma}}(\underline{r}) \exp(-i\,\underline{q}\cdot\underline{r})\; d^3\underline{r}\,, \tag{4.41}$$

$$\underline{\underline{\tilde{\mathbf{K}}}}_{Dy}(\underline{q}) = \int \underline{\underline{\mathbf{K}}}_{Dy}(\underline{r}) \exp(-i\,\underline{q}\cdot\underline{r})\; d^3\underline{r}\,, \tag{4.42}$$

$\underline{q}$ being the three–dimensional spatial frequency vector. The Fourier–transformed version of (4.38) reads as follows

$$\left(\underline{\underline{\mathbf{I}}} + \underline{\underline{\tilde{\Sigma}}}(\underline{q})\cdot\underline{\underline{\mathbf{D}}}\right)\cdot\underline{\tilde{\mathbf{C}}}(\underline{q}) = \left[\underline{\underline{\mathbf{K}}}_{BCM} - \frac{1}{i\omega}\underline{\underline{\tilde{\Sigma}}}(\underline{q})\cdot\left(\underline{\underline{\mathbf{I}}} - i\omega\underline{\underline{\mathbf{D}}}\cdot\underline{\underline{\mathbf{K}}}_{BCM}\right)\right]\cdot\underline{\tilde{\mathbf{F}}}(\underline{q})\,. \tag{4.43}$$

But $\underline{\tilde{\mathbf{C}}}(\underline{q}) = \underline{\underline{\tilde{\mathbf{K}}}}_{Dy}(\underline{q})\cdot\underline{\tilde{\mathbf{F}}}(\underline{q})$ by virtue of the foregoing relations; hence, (4.43) yields

$$\underline{\underline{\tilde{\mathbf{K}}}}_{Dy}(\underline{q}) = \underline{\underline{\mathbf{K}}}_{BCM} - \frac{1}{i\omega}\left(\underline{\underline{\mathbf{I}}} + \underline{\underline{\tilde{\Sigma}}}(\underline{q})\cdot\underline{\underline{\mathbf{D}}}\right)^{-1}\cdot\underline{\underline{\tilde{\Sigma}}}(\underline{q})\,. \tag{4.44}$$

The constitutive dyadic $\underline{\underline{\mathbf{K}}}_{Dy}(\underline{r})$ then emerges as the inverse Fourier integral

$$\underline{\underline{\mathbf{K}}}_{Dy}(\underline{r}) = \frac{1}{(2\pi)^3}\int \underline{\underline{\tilde{\mathbf{K}}}}_{Dy}(\underline{q}) \exp(i\,\underline{q}\cdot\underline{r})\; d^3\underline{q}\,. \tag{4.45}$$

The Dyson equation (4.24) involves the ensemble–averaged exciting field $\langle\, \underline{\mathbf{F}}_{exc}(\underline{r}) \,\rangle$. In order to determine the ensemble–averaged electromagnetic field $\langle\, \underline{\mathbf{F}}(\underline{r}) \,\rangle$ itself, we take the ensemble average of (4.5) and use (4.33) to get

$$\underline{\underline{\mathbf{L}}}(\nabla)\cdot\langle\, \underline{\mathbf{F}}(\underline{r}) \,\rangle + i\omega\int \underline{\underline{\mathbf{K}}}_{Dy}(\underline{R})\cdot\langle\, \underline{\mathbf{F}}(\underline{r}-\underline{R}) \,\rangle\; d^3\underline{R} = \underline{\mathbf{0}}\,. \tag{4.46}$$

The Fourier–transformed version of this equation is

$$\left[\begin{pmatrix} \underline{0} & i\underline{q}\times\underline{\underline{I}} \\ -i\underline{q}\times\underline{\underline{I}} & \underline{0} \end{pmatrix} + i\omega\underline{\underline{\tilde{\mathbf{K}}}}_{Dy}(\underline{q})\right]\cdot\underline{\tilde{\mathbf{F}}}(\underline{q}) = \underline{\mathbf{0}}\,, \tag{4.47}$$

from which $\underline{\tilde{\mathbf{F}}}(\underline{q})$ may be extracted by standard dyadic techniques [33]. Thus, depending on a specific choice for the evaluation of $\underline{\underline{\mathbf{D}}}$, the SPFT homogenisation formulation is now complete in the bilocal approximation.

4.2.4 Local effective medium

When the principal electromagnetic wavelengths are much larger than the correlation length L, we can achieve a *macroscopic* description of the composite as a homogeneous local continuum [1]. Although it has a different provenance, this description is

conceptually no different from that available from the MG and the Br formalisms: the mixture is considered homogeneous in the *long–wavelength approximation.*

Suppose the long–wavelength approximation is appropriate. Let us then introduce the macroscopic fields $\underline{\mathbf{C}}_{macro}(\underline{r})$ and $\underline{\mathbf{F}}_{macro}(\underline{r})$ by *spatially* averaging the microscopic fields $\langle\, \underline{\mathbf{C}}(\underline{r}) \,\rangle$ and $\langle\, \underline{\mathbf{F}}(\underline{r}) \,\rangle$ over a region V; thus,

$$\underline{\mathbf{C}}_{macro}(\underline{r}) = \frac{1}{V} \int_V \langle\, \underline{\mathbf{C}}(\underline{r} + \underline{r}'') \,\rangle d^3\underline{r}'' \,, \tag{4.48}$$

$$\underline{\mathbf{F}}_{macro}(\underline{r}) = \frac{1}{V} \int_V \langle\, \underline{\mathbf{F}}(\underline{r} + \underline{r}'') \,\rangle d^3\underline{r}'' \,. \tag{4.49}$$

The minimum linear cross–sectional extent of the region V must be larger than L, but smaller than the maximum principal electromagnetic wavelength. Inserting (4.32) and (4.33) into (4.48), we find

$$\begin{aligned} \underline{\mathbf{C}}_{macro}(\underline{r}) &= \frac{1}{V} \int_V \left(\int \underline{\underline{\mathbf{K}}}_{Dy}(\underline{R}) \cdot \langle\, \underline{\mathbf{F}}(\underline{r} + \underline{r}'' - \underline{R}) \,\rangle d^3\underline{R} \right) d^3\underline{r}'' \\ &= \int \underline{\underline{\mathbf{K}}}_{Dy}(\underline{R}) \cdot \underline{\mathbf{F}}_{macro}(\underline{r} - \underline{R}) \; d^3\underline{R} \\ &\approx \int \underline{\underline{\mathbf{K}}}_{Dy}(\underline{R}) \cdot \underline{\mathbf{F}}_{macro}(\underline{r}) \; d^3\underline{R} \,. \end{aligned} \tag{4.50}$$

This leads to the macroscopic constitutive relation

$$\underline{\mathbf{C}}_{macro}(\underline{r}) = \tilde{\underline{\underline{\mathbf{K}}}}_{Dy}(\underline{0}) \cdot \underline{\mathbf{F}}_{macro}(\underline{r}) \,. \tag{4.51}$$

The constitutive properties of a two–phase bianisotropic composite in the long–wavelength approximation are thus specified by the dyadic $\tilde{\underline{\underline{\mathbf{K}}}}_{Dy}(\underline{0}) \equiv \underline{\underline{\mathbf{K}}}_{Dy0}$. Evidently from (4.44), (4.41) and (4.31), the key step in estimating $\underline{\underline{\mathbf{K}}}_{Dy0}$ is the evaluation of

$$\tilde{\underline{\underline{\mathbf{\Sigma}}}}(\underline{0}) = \int \underline{\underline{\mathbf{\Sigma}}}(\underline{R}) \; d^3\underline{R} = \left(\underline{\underline{\chi}}_a - \underline{\underline{\chi}}_b \right) \cdot \left[\mathcal{P} \int \Gamma(\underline{R}) \, \underline{\underline{\mathbf{G}}}_{BCM}(\underline{R}) d^3\underline{R} \right] \cdot \left(\underline{\underline{\chi}}_a - \underline{\underline{\chi}}_b \right) . \tag{4.52}$$

We note that the presence of $\Gamma(\underline{R})$ within the above principal value integration is justified, because $\Gamma(\underline{0}) = f_a(1 - f_a) = f_b(1 - f_b)$ cannot be null–valued for non–trivial problems.

Although an explicit expression for $\underline{\underline{\mathbf{G}}}_{BCM}(\underline{R})$ cannot be written down, its Fourier transform

$$\tilde{\underline{\underline{\mathbf{G}}}}_{BCM}(\underline{q}) = \int \underline{\underline{\mathbf{G}}}_{BCM}(\underline{R}) \exp(-i \, \underline{q} \cdot \underline{R}) \; d^3\underline{R} \,, \tag{4.53}$$

can be obtained by taking the Fourier transforms of both sides of (4.15). Thus,

$$\tilde{\underline{\underline{\mathbf{G}}}}_{BCM}(\underline{q}) = \frac{1}{i\omega} \frac{\text{adj} \left(\tilde{\underline{\underline{\mathbf{A}}}}_{BCM}(\underline{q}) \right)}{\det \tilde{\underline{\underline{\mathbf{A}}}}_{BCM}(\underline{q})} \,, \tag{4.54}$$

where

$$\tilde{\underline{\underline{\mathbf{A}}}}_{BCM}(\underline{q}) = \begin{bmatrix} \underline{\underline{0}} & (\underline{q}/\omega) \times \underline{\underline{I}} \\ -(\underline{q}/\omega) \times \underline{\underline{I}} & \underline{\underline{0}} \end{bmatrix} + \underline{\underline{\mathbf{K}}}_{BCM} \,. \tag{4.55}$$

For later convenience, we note that (4.55) can be manipulated to deliver $\underline{\underline{\tilde{G}}}_{BCM}(\underline{q})$ in the following general form

$$\underline{\underline{\tilde{G}}}_{BCM}(\underline{q}) = \frac{1}{i\omega}\left(\frac{\underline{\underline{T}}_4(\hat{\underline{q}})(\frac{q}{\omega})^4 + \underline{\underline{T}}_3(\hat{\underline{q}})(\frac{q}{\omega})^3 + \underline{\underline{T}}_2(\hat{\underline{q}})(\frac{q}{\omega})^2 + \underline{\underline{T}}_1(\hat{\underline{q}})(\frac{q}{\omega}) + \underline{\underline{T}}_0(\hat{\underline{q}})}{t_4(\hat{\underline{q}})(\frac{q}{\omega})^4 + t_3(\hat{\underline{q}})(\frac{q}{\omega})^3 + t_2(\hat{\underline{q}})(\frac{q}{\omega})^2 + t_1(\hat{\underline{q}})(\frac{q}{\omega}) + t_0(\hat{\underline{q}})}\right). \tag{4.56}$$

Here, $\underline{\underline{T}}_n(\hat{\underline{q}})$ are 6×6 dyadic functions, and $t_n(\hat{\underline{q}})$ are scalar functions ($n = 0, 1, 2, 3, 4$) of the unit spatial frequency vector $\hat{\underline{q}}$. Furthermore, $\underline{\underline{\tilde{G}}}_{BCM}(\underline{q})$ may be partitioned as [29, 62]

$$\underline{\underline{\tilde{G}}}_{BCM}(\underline{q}) = \underline{\underline{\tilde{G}}}^{0}_{BCM}(\underline{q}) + \underline{\underline{\tilde{G}}}^{\infty}_{BCM}(\hat{\underline{q}}), \tag{4.57}$$

where

$$\underline{\underline{\tilde{G}}}^{\infty}_{BCM}(\hat{\underline{q}}) = \lim_{q\to\infty} \underline{\underline{\tilde{G}}}_{BCM}(\underline{q}) = \frac{1}{i\omega}\frac{\underline{\underline{T}}_4(\hat{\underline{q}})}{t_4(\hat{\underline{q}})} \tag{4.58}$$

and (suppressing the dependencies of $\underline{\underline{T}}_n$ and t_n on $\hat{\underline{q}}$)

$$\underline{\underline{\tilde{G}}}^{0}_{BCM}(\underline{q}) = \frac{(t_4\underline{\underline{T}}_3 - t_3\underline{\underline{T}}_4)(\frac{q}{\omega})^3 + (t_4\underline{\underline{T}}_2 - t_2\underline{\underline{T}}_4)(\frac{q}{\omega})^2 + (t_4\underline{\underline{T}}_1 - t_1\underline{\underline{T}}_4)(\frac{q}{\omega}) + (t_4\underline{\underline{T}}_0 - t_0\underline{\underline{T}}_4)}{i\omega\, t_4\left[t_4(\frac{q}{\omega})^4 + t_3(\frac{q}{\omega})^3 + t_2(\frac{q}{\omega})^2 + t_1(\frac{q}{\omega}) + t_0\right]}. \tag{4.59}$$

Explicit coordinate–free representations of $\underline{\underline{\tilde{G}}}_{BCM}(\underline{q})$ are already available for chiral [55], general dielectric [62], and dielectric–magnetic [63] mediums; we consider the structure of $\underline{\underline{\tilde{G}}}_{BCM}(\underline{q})$ for reciprocal biaxial bianisotropic mediums in Section 4.2.5.

In order to advance our analysis, we have to specify the depolarisation dyadic $\underline{\underline{D}}$; we do so by considering the topology of the composite. Let V^e_η be an ellipsoidal region, centred at the origin of our coordinate system, of size determined by the linear measure η and of shape specified by the real symmetric dyadic $\underline{\underline{U}}$, as specified in equation (1.24). We imagine that both constituent phases are distributed as conformal ellipsoids of surfaces parameterised by the shape dyadic $\underline{\underline{U}}$. We mean here that both constituent phases are present with a distribution of η such that there is no vacant space in the composite medium. The same fractal–like topology is inherent in the MG and Br homogenisation formalisms, although it is rarely mentioned. Having selected $\underline{\underline{U}}$, we determine $\underline{\underline{D}}$ as [29]

$$\begin{aligned}\underline{\underline{D}} &= \lim_{\delta\to 0}\int_{V^e_\delta} \underline{\underline{G}}_{BCM}(\underline{R})\, d^3\underline{R} \\ &= abc \lim_{\delta\to 0}\int_{V^s_\delta} \underline{\underline{G}}_{BCM}(\underline{\underline{U}}\cdot\underline{H})\, d^3\underline{H},\end{aligned} \tag{4.60}$$

where the spherical region V^s_δ has radius δ, $\underline{H} = \underline{\underline{U}}^{-1}\cdot\underline{R}$, and a, b and c are the positive eigenvalues of $\underline{\underline{U}}$. The covariance $\Gamma(\underline{R})$ is chosen to reflect the ellipsoidal

topology relating to $\underline{\underline{\mathbf{D}}}$. Accordingly, we adopt the physically–motivated [61]

$$\Gamma(\underline{R}) = \Gamma_0(\underline{R}) = \begin{cases} f_a f_b & \underline{R} \in V_L^e \\ \\ 0 & \underline{R} \notin V_L^e \end{cases}, \tag{4.61}$$

where L is the correlation length. Covariance functions in the form of step functions, for both isotropic [64, 65] and anisotropic [53] types, have been considered in previous SPFT analyses. Alternative choices of covariance functions are explored in Section 4.4.

Let $V_{L-\delta}^e = V_L^e - V_\delta^e$ and $V_{L-\delta}^s = V_L^s - V_\delta^s$. The principal value integration in (4.52) now proceeds through the introduction of the Fourier transform of $\underline{\underline{\mathbf{G}}}_{BCM}(\underline{R})$, facilitated by the changes of variable $\underline{H} = \underline{\underline{U}}^{-1} \cdot \underline{R}$ and $\underline{v} = \underline{\underline{U}} \cdot \underline{w}$ (where $\underline{H}$, $\underline{v}$ and $\underline{w}$ are dummy vector variables), as follows

$$\begin{aligned} &\frac{(2\pi)^3}{f_a f_b} \mathcal{P} \int \Gamma_0(\underline{R})\, \underline{\underline{\mathbf{G}}}_{BCM}(\underline{R})\, d^3\underline{R} \\ &\quad = \lim_{\delta \to 0} \int_{V_{L-\delta}^e} \left[\int_{\underline{w}} \underline{\underline{\tilde{\mathbf{G}}}}_{BCM}(\underline{w}) \exp(i\underline{w} \cdot \underline{R})\, d^3\underline{w} \right] d^3\underline{R} \\ &\quad = \lim_{\delta \to 0} \int_{\underline{v}} \underline{\underline{\tilde{\mathbf{G}}}}_{BCM}(\underline{\underline{U}}^{-1} \cdot \underline{v}) \left[\int_{V_{L-\delta}^s} \exp(i\underline{v} \cdot \underline{H})\, d^3\underline{H} \right] d^3\underline{v} \\ &\quad = \int_{\underline{v}} \underline{\underline{\tilde{\mathbf{G}}}}_{BCM}(\underline{\underline{U}}^{-1} \cdot \underline{v}) \left[\frac{4\pi}{v^2} \left(\frac{\sin vL}{v} - L\cos vL \right) \right] d^3\underline{v} \\ &\qquad - \lim_{\delta \to 0} \int_{\underline{v}} \underline{\underline{\tilde{\mathbf{G}}}}_{BCM}(\underline{\underline{U}}^{-1} \cdot \underline{v}) \left[\frac{4\pi}{v^2} \left(\frac{\sin v\delta}{v} - \delta\cos v\delta \right) \right] d^3\underline{v}\,. \end{aligned} \tag{4.62}$$

Now, from [62] we have

$$\underline{\underline{\mathbf{D}}} = \frac{1}{(2\pi)^3} \lim_{\delta \to 0} \int_{\underline{v}} \underline{\underline{\tilde{\mathbf{G}}}}_{BCM}(\underline{\underline{U}}^{-1} \cdot \underline{v}) \left[\frac{4\pi}{v^2} \left(\frac{\sin v\delta}{v} - \delta\cos v\delta \right) \right] d^3\underline{v} \tag{4.63}$$

$$= \frac{1}{(2\pi)^3} \int_{\underline{v}} \underline{\underline{\tilde{\mathbf{G}}}}^{\infty}_{BCM}(\underline{\underline{U}}^{-1} \cdot \underline{v}) \left[\frac{4\pi}{v^2} \left(\frac{\sin vE}{v} - E\cos vE \right) \right] d^3\underline{v}\,, \tag{4.64}$$

for $E > 0$. Thus, combining (4.62)–(4.64) along with (4.57), we find

$$\mathcal{P} \int \Gamma_0(\underline{R})\, \underline{\underline{\mathbf{G}}}_{BCM}(\underline{R})\, d^3\underline{R} = \frac{f_a f_b}{2\pi^2} \int \underline{\underline{\tilde{\mathbf{G}}}}^{0}_{BCM}(\underline{\underline{U}}^{-1} \cdot \underline{v}) \left(\frac{\sin vL}{v} - L\cos vL \right) \frac{1}{v^2}\, d^3\underline{v}\,. \tag{4.65}$$

Although very cumbersome for reproduction here, a straightforward analysis shows that the determinant of $\underline{\underline{\tilde{\mathbf{A}}}}_{BCM}(\underline{w})$ is quadratic in w^2 for reciprocal bianisotropic mediums (i.e., $\underline{\underline{\epsilon}} = \underline{\underline{\epsilon}}^T$, $\underline{\underline{\xi}} = -\underline{\underline{\zeta}}^T$ and $\underline{\underline{\mu}} = \underline{\underline{\mu}}^T$) and general dielectric/magnetic mediums (i.e., $\underline{\underline{\xi}} = \underline{\underline{\zeta}} = \underline{\underline{0}}$). Consequently, provided the numerator of $\underline{\underline{\tilde{\mathbf{G}}}}^{0}_{BCM}(\underline{w})$ is an even function of w, the integration in (4.65) with respect to v may be evaluated by conventional calculus of residues for such mediums . However, for the general bianisotropic case,

the determinant of $\underline{\underline{\tilde{\mathbf{A}}}}_{BCM}(\underline{w})$ is not an even function of w and alternative methods may be required to compute the integral (4.65).

In addition to being central to the calculation of $\underline{\underline{\mathbf{K}}}_{Dy0}$, the integral (4.65) provides a correction to the depolarisation dyadic $\underline{\underline{\mathbf{D}}}$ when the exclusion region V_L^e is of finite size. This is also reflected in the fact that $\underline{\underline{\mathbf{K}}}_{Dy0}$ represents a modification of $\underline{\underline{\mathbf{K}}}_{BCM}$; indeed,

$$\underline{\underline{\mathbf{K}}}_{Dy0} = \underline{\underline{\mathbf{K}}}_{BCM} - \frac{1}{i\omega}\left(\underline{\underline{\mathbf{I}}} + \underline{\underline{\tilde{\boldsymbol{\Sigma}}}}(\underline{0}) \cdot \underline{\underline{\mathbf{D}}}\right)^{-1} \cdot \underline{\underline{\tilde{\boldsymbol{\Sigma}}}}(\underline{0}) \,. \tag{4.66}$$

The evaluation of this key equation (4.66) is central to the remainder of this chapter.

4.2.5 Implementation of the long–wavelength approximation

In order to illustrate the implementation of the long–wavelength approximation in the bilocal SPFT framework, we consider a two–phase composite for which both constituent phases belong to the general class of reciprocal biaxial bianisotropic mediums. The constitutive dyadics $\underline{\underline{\epsilon}}_p$, $\underline{\underline{\xi}}_p = -\underline{\underline{\zeta}}_p$ and $\underline{\underline{\mu}}_p$ of the constituent phases are taken to have the same eigenvectors, i.e.,

$$\underline{\underline{\epsilon}}_p = \begin{bmatrix} \epsilon_x^p & 0 & 0 \\ 0 & \epsilon_y^p & 0 \\ 0 & 0 & \epsilon_z^p \end{bmatrix}, \quad \underline{\underline{\xi}}_p = \begin{bmatrix} \xi_x^p & 0 & 0 \\ 0 & \xi_y^p & 0 \\ 0 & 0 & \xi_z^p \end{bmatrix} = -\underline{\underline{\zeta}}_p, \quad \underline{\underline{\mu}}_p = \begin{bmatrix} \mu_x^p & 0 & 0 \\ 0 & \mu_y^p & 0 \\ 0 & 0 & \mu_z^p \end{bmatrix}, \tag{4.67}$$

where all diagonal entries are complex–valued.

As emphasised in the Section 4.2.4, the crucial step in applying the long–wavelength approximation is the calculation of the volume integral (4.65). We now proceed to evaluate the integration with respect to v in (4.65) by means of residue calculus, exploiting symmetries in the integrand along the way. We begin by considering the singularities of $\underline{\underline{\tilde{\mathbf{G}}}}^0_{BCM}(\underline{v})$, i.e., the zeros of $t_4(\hat{\underline{v}})\det\underline{\underline{\tilde{\mathbf{A}}}}_{BCM}(\underline{v})$. Taking the determinant of (4.55), we find

$$\det\underline{\underline{\tilde{\mathbf{A}}}}_{BCM}(\underline{v}) = t_4(\hat{\underline{v}})(v/\omega)^4 + t_2(\hat{\underline{v}})(v/\omega)^2 + t_0 \,, \tag{4.68}$$

$$t_4(\hat{\underline{v}}) = (\hat{\underline{v}} \cdot \underline{\underline{\epsilon}}_{BCM} \cdot \hat{\underline{v}})(\hat{\underline{v}} \cdot \underline{\underline{\mu}}_{BCM} \cdot \hat{\underline{v}}) + (\hat{\underline{v}} \cdot \underline{\underline{\xi}}_{BCM} \cdot \hat{\underline{v}})(\hat{\underline{v}} \cdot \underline{\underline{\xi}}_{BCM} \cdot \hat{\underline{v}}) \,, \tag{4.69}$$

$$\begin{aligned} t_2(\hat{\underline{v}}) = \mathrm{tr}\Big[&(\hat{\underline{v}} \times \mathrm{adj}(\underline{\underline{\epsilon}}_{BCM})) \cdot (\hat{\underline{v}} \times \mathrm{adj}(\underline{\underline{\mu}}_{BCM})) \\ &-(\hat{\underline{v}} \times \mathrm{adj}(\underline{\underline{\xi}}_{BCM})) \cdot (\hat{\underline{v}} \times \mathrm{adj}(\underline{\underline{\xi}}_{BCM}))\Big] \\ &+\hat{\underline{v}} \cdot \Big[\underline{\underline{\epsilon}}_{BCM} \cdot \underline{\underline{F}}(\underline{\underline{\xi}}_{BCM}, \underline{\underline{\xi}}_{BCM}) \cdot \underline{\underline{\mu}}_{BCM} \\ &-\underline{\underline{\xi}}_{BCM} \cdot \underline{\underline{F}}(\underline{\underline{\epsilon}}_{BCM}, \underline{\underline{\mu}}_{BCM}) \cdot \underline{\underline{\xi}}_{BCM}\Big] \cdot \hat{\underline{v}} \,, \end{aligned} \tag{4.70}$$

$$t_0 = \det\left(\underline{\underline{\Pi}}\right) , \tag{4.71}$$

$$\underline{\underline{F}}(\underline{\underline{m}}, \underline{\underline{n}}) = \left[(\mathrm{tr}\,\underline{\underline{m}})\,\underline{\underline{I}} - \underline{\underline{m}}\right] \cdot \left[(\mathrm{tr}\,\underline{\underline{n}})\,\underline{\underline{I}} - \underline{\underline{n}}\right] - \left[(\mathrm{tr}\,\underline{\underline{m}} \cdot \underline{\underline{n}})\,\underline{\underline{I}} - \underline{\underline{m}} \cdot \underline{\underline{n}}\right] , \tag{4.72}$$

$$\underline{\underline{\Pi}} = \underline{\underline{\epsilon}}_{BCM} \cdot \underline{\underline{\mu}}_{BCM} + \underline{\underline{\xi}}_{BCM} \cdot \underline{\underline{\xi}}_{BCM} , \tag{4.73}$$

where $\underline{\underline{m}}$ and $\underline{\underline{n}}$ are arbitrary 3×3 dyadics. The issues of the location and nature of the singularities of $\underline{\underline{\tilde{G}}}^{0}_{BCM}(\underline{v})$ are rather involved in the most general setting; see Cottis & Kondylis [66] for a detailed discussion in the case of an anisotropic dielectric medium. We refrain from considering pathological special cases here: that is, for all values of $\hat{\underline{v}}$ we assume that

(i) $t_4(\hat{\underline{v}}) \neq 0$, and

(ii) the v^2 roots of $\det \underline{\underline{\tilde{A}}}_{BCM}(\underline{v})$ are distinct, i.e., $\kappa_+ \neq \kappa_-$ where

$$\kappa_\pm = \omega^2 \left(\frac{-t_2(\hat{\underline{v}}) \pm \sqrt{t_2^2(\hat{\underline{v}}) - 4t_4(\hat{\underline{v}})t_0}}{2t_4(\hat{\underline{v}})} \right) . \tag{4.74}$$

We note that the possibility $\kappa_+ = \kappa_-$ is most likely to arise when we have isotropic constituent phases combined with spherical topology; but SPFT in this instance has been treated by Michel & Lakhtakia [55].

With the foregoing simplifications in place, we find that the singularities of $\underline{\underline{\tilde{G}}}^{0}_{BCM}(\underline{v})$ occur as simple poles at

$$v = \sqrt{\kappa_+},\ -\sqrt{\kappa_+},\ \sqrt{\kappa_-},\ -\sqrt{\kappa_-} . \tag{4.75}$$

Therefore, for definiteness, we take both $\sqrt{\kappa_+}$ and $\sqrt{\kappa_-}$ to lie in the upper half of the complex v–plane (inclusive of the real axis).

We next turn our attention to symmetries of $\underline{\underline{\tilde{G}}}^{0}_{BCM}(\underline{v})$. For reciprocal biaxial bianisotropic mediums, the numerator of $\underline{\underline{\tilde{G}}}^{0}_{BCM}(\underline{v})$ is a dyadic function that is cubic in v. However, by a straightforward — albeit lengthy — utilization of (4.55), we find that the odd terms in the numerator of $\underline{\underline{\tilde{G}}}^{0}_{BCM}(\underline{v})$ integrate to zero with respect to the angular variables in (4.65). The remaining even terms $\underline{\underline{\mathbf{T}}}_n(\hat{\underline{v}})$, $(n = 0, 2, 4)$, in the notation of (4.59), are conveniently expressed in terms of four 3×3 dyadics $\underline{\underline{T}}^{\lambda}_n(\hat{\underline{v}})$, $(\lambda = ee, em, me, mm)$, as follows

$$\underline{\underline{\mathbf{T}}}_n(\hat{\underline{v}}) = \begin{bmatrix} \underline{\underline{T}}^{ee}_n(\hat{\underline{v}}) & \underline{\underline{T}}^{em}_n(\hat{\underline{v}}) \\ \\ \underline{\underline{T}}^{me}_n(\hat{\underline{v}}) & \underline{\underline{T}}^{mm}_n(\hat{\underline{v}}) \end{bmatrix} , \qquad n = 0, 2, 4 . \tag{4.76}$$

By symmetry considerations, only the diagonal entries of $\underline{\underline{T}}^{\lambda}_n$ give rise to non–zero integrals in (4.65). Thus, in evaluating (4.65), we can replace $\underline{\underline{\tilde{G}}}^{0}_{BCM}(\underline{v})$ by

$$\frac{1}{i\omega} \left(\frac{\underline{\underline{\mathbf{\Lambda}}}(\hat{\underline{v}})(v/\omega)^2 + \underline{\underline{\mathbf{\Upsilon}}}(\hat{\underline{v}})}{t_4(\hat{\underline{v}})(v/\omega)^4 + t_2(\hat{\underline{v}})(v/\omega)^2 + t_0} \right) , \tag{4.77}$$

where we have

$$\left[\underline{\underline{\mathbf{\Lambda}}}(\hat{\underline{v}}) \right]_{\ell j} = \begin{cases} \left[\underline{\underline{\mathbf{T}}}_2(\hat{\underline{v}}) \right]_{\ell j} - \dfrac{t_2(\hat{\underline{v}})}{t_4(\hat{\underline{v}})} \left[\underline{\underline{\mathbf{T}}}_4(\hat{\underline{v}}) \right]_{\ell j} , & \ell \,(\mathrm{mod}\, 3) \equiv j \,(\mathrm{mod}\, 3), \\ \\ 0, & \ell \,(\mathrm{mod}\, 3) \not\equiv j \,(\mathrm{mod}\, 3), \end{cases} \tag{4.78}$$

and

$$\left[\underline{\underline{\Upsilon}}(\hat{\underline{v}})\right]_{\ell j} = \begin{cases} \left[\underline{\underline{\mathbf{T}}}_0(\hat{\underline{v}})\right]_{\ell j} - \dfrac{t_0}{t_4(\hat{\underline{v}})}\left[\underline{\underline{\mathbf{T}}}_4(\hat{\underline{v}})\right]_{\ell j}, & \ell\,(\mathrm{mod}\,3) \equiv j\,(\mathrm{mod}\,3), \\ 0, & \ell\,(\mathrm{mod}\,3) \not\equiv j\,(\mathrm{mod}\,3), \end{cases} \tag{4.79}$$

for $\ell, j = 1, 2, \ldots, 6$; and $[\underline{\underline{\mathbf{T}}}_n]_{\ell j}$ denotes the ℓj^{th} entry of the 6×6 dyadic $\underline{\underline{\mathbf{T}}}_n$.

The dyadics $\underline{\underline{\mathbf{T}}}_0(\hat{\underline{v}})$ and $\underline{\underline{\mathbf{T}}}_4(\hat{\underline{v}})$ are readily extracted from the adjoint of $\underline{\underline{\tilde{\mathbf{A}}}}_{BCM}(\underline{v})$. They are given in coordinate–free form as

$$\underline{\underline{\mathbf{T}}}_0(\hat{\underline{v}}) = \begin{bmatrix} \underline{\underline{\mu}}_{BCM} \cdot \mathrm{adj}\left(\underline{\underline{\Pi}}\right) & -\underline{\underline{\xi}}_{BCM} \cdot \mathrm{adj}\left(\underline{\underline{\Pi}}\right) \\ \underline{\underline{\xi}}_{BCM} \cdot \mathrm{adj}\left(\underline{\underline{\Pi}}\right) & \underline{\underline{\epsilon}}_{BCM} \cdot \mathrm{adj}\left(\underline{\underline{\Pi}}\right) \end{bmatrix}, \tag{4.80}$$

and

$$\underline{\underline{\mathbf{T}}}_4(\hat{\underline{v}}) = \begin{bmatrix} \left(\hat{\underline{v}} \cdot \underline{\underline{\mu}}_{BCM} \cdot \hat{\underline{v}}\right) \hat{\underline{v}}\,\hat{\underline{v}} & -\left(\hat{\underline{v}} \cdot \underline{\underline{\xi}}_{BCM} \cdot \hat{\underline{v}}\right) \hat{\underline{v}}\,\hat{\underline{v}} \\ \left(\hat{\underline{v}} \cdot \underline{\underline{\xi}}_{BCM} \cdot \hat{\underline{v}}\right) \hat{\underline{v}}\,\hat{\underline{v}} & \left(\hat{\underline{v}} \cdot \underline{\underline{\epsilon}}_{BCM} \cdot \hat{\underline{v}}\right) \hat{\underline{v}}\,\hat{\underline{v}} \end{bmatrix}. \tag{4.81}$$

The dyadic $\underline{\underline{\mathbf{T}}}_2(\hat{\underline{v}})$ has a more complex structure, but only its diagonal components are needed to evaluate (4.65)

$$\begin{aligned} \left[\underline{\underline{T}}_2^{ee}(\hat{\underline{v}})\right]_{\ell\ell} &= \Big[\left(2\,\underline{\underline{\epsilon}} \cdot \mathrm{adj}(\underline{\underline{\mu}}) - \mathrm{tr}\left(\underline{\underline{\epsilon}} \cdot \mathrm{adj}(\underline{\underline{\mu}})\right) \underline{\underline{I}} + \underline{\underline{\mu}} \cdot \underline{\underline{F}}(\underline{\underline{\xi}}, \underline{\underline{\xi}})\right) \cdot \hat{\underline{v}}\,\hat{\underline{v}} \\ &\quad - \underline{\underline{F}}(\underline{\underline{\mu}}, \underline{\underline{\xi}} \cdot \underline{\underline{\xi}} \cdot \hat{\underline{v}}\,\hat{\underline{v}}) - (\hat{\underline{v}} \cdot \underline{\underline{\epsilon}} \cdot \hat{\underline{v}})\,\mathrm{adj}(\underline{\underline{\mu}}) \Big]_{\ell\ell}, \quad \ell = 1, 2, 3, \end{aligned} \tag{4.82}$$

$$\begin{aligned} \left[\underline{\underline{T}}_2^{em}(\hat{\underline{v}})\right]_{\ell\ell} &= \Big[\left(\underline{\underline{F}}(\underline{\underline{\epsilon}}, \underline{\underline{\mu}}) \cdot \underline{\underline{\xi}} - \det(\underline{\underline{\xi}})\,\underline{\underline{I}}\right) \cdot \hat{\underline{v}}\,\hat{\underline{v}} \\ &\quad - \underline{\underline{F}}(\underline{\underline{\epsilon}} \cdot \underline{\underline{\mu}} \cdot \hat{\underline{v}}\,\hat{\underline{v}}, \underline{\underline{\xi}}) - (\hat{\underline{v}} \cdot \underline{\underline{\xi}} \cdot \hat{\underline{v}})\,\mathrm{adj}(\underline{\underline{\xi}}) \Big]_{\ell\ell}, \quad \ell = 1, 2, 3, \end{aligned} \tag{4.83}$$

$$\begin{aligned} \left[\underline{\underline{T}}_2^{me}(\hat{\underline{v}})\right]_{\ell\ell} &= -\Big[\left(\underline{\underline{F}}(\underline{\underline{\epsilon}}, \underline{\underline{\mu}}) \cdot \underline{\underline{\xi}} - \det(\underline{\underline{\xi}})\,\underline{\underline{I}}\right) \cdot \hat{\underline{v}}\,\hat{\underline{v}} \\ &\quad - \underline{\underline{F}}(\underline{\underline{\epsilon}} \cdot \underline{\underline{\mu}} \cdot \hat{\underline{v}}\,\hat{\underline{v}}, \underline{\underline{\xi}}) - (\hat{\underline{v}} \cdot \underline{\underline{\xi}} \cdot \hat{\underline{v}})\,\mathrm{adj}(\underline{\underline{\xi}}) \Big]_{\ell\ell}, \quad \ell = 1, 2, 3, \end{aligned} \tag{4.84}$$

$$\begin{aligned} \left[\underline{\underline{T}}_2^{mm}(\hat{\underline{v}})\right]_{\ell\ell} &= \Big[\left(2\,\mathrm{adj}(\underline{\underline{\epsilon}}) \cdot \underline{\underline{\mu}} - \mathrm{tr}\left(\mathrm{adj}(\underline{\underline{\epsilon}}) \cdot \underline{\underline{\mu}}\right) \underline{\underline{I}} + \underline{\underline{\epsilon}} \cdot \underline{\underline{F}}(\underline{\underline{\xi}}, \underline{\underline{\xi}})\right) \cdot \hat{\underline{v}}\,\hat{\underline{v}} \\ &\quad - \underline{\underline{F}}(\underline{\underline{\epsilon}}, \underline{\underline{\xi}} \cdot \underline{\underline{\xi}} \cdot \hat{\underline{v}}\,\hat{\underline{v}}) - (\hat{\underline{v}} \cdot \underline{\underline{\mu}} \cdot \hat{\underline{v}})\,\mathrm{adj}(\underline{\underline{\epsilon}}) \Big]_{\ell\ell}, \quad \ell = 1, 2, 3. \end{aligned} \tag{4.85}$$

Residue calculus thereby results in the following evaluation of the integral with respect to v in (4.65)

$$\begin{aligned} \int \underline{\underline{\tilde{\mathbf{G}}}}^{0}_{BCM}(\underline{\underline{U}}^{-1} \cdot \underline{v}) \left(\frac{\sin vL}{v} - L\cos vL\right) \frac{1}{v^2}\, d^3\underline{v} = \frac{\pi\omega^3}{2i} \int \frac{1}{t_4(\underline{\underline{U}}^{-1} \cdot \hat{\underline{v}})} \Bigg\{ \frac{1}{\kappa_+ - \kappa_-} \\ \times \left[\mathrm{e}^{iLv}\,(1 - iLv) \left(\frac{\underline{\underline{\mathbf{\Lambda}}}(\underline{\underline{U}}^{-1} \cdot \hat{\underline{v}})}{\omega^2} + \frac{\underline{\underline{\Upsilon}}(\underline{\underline{U}}^{-1} \cdot \hat{\underline{v}})}{v^2} \right) \right]_{v=\sqrt{\kappa_-}}^{v=\sqrt{\kappa_+}} + \frac{\underline{\underline{\Upsilon}}(\underline{\underline{U}}^{-1} \cdot \hat{\underline{v}})}{\kappa_+\,\kappa_-} \Bigg\}\, d\Omega, \end{aligned} \tag{4.86}$$

where $d\Omega = \sin\theta\, d\theta\, d\phi$. Thus, (4.65) reduces to a surface integral which, in general, must be handled numerically.

An expression equivalent to (4.86) can be developed without explicit reference to the components $\underline{\underline{\mathbf{T}}}_n(\underline{\hat{v}})$ of the adjoint dyadic of $\underline{\underline{\tilde{\mathbf{A}}}}_{BCM}(\underline{v})$. This derivation — though less instructive — leads to a surface integral more amenable to numerical evaluation than that of (4.86). Introducing

$$\underline{\underline{\mathbf{N}}}(\underline{v}) = \frac{\text{adj}\left(\underline{\underline{\tilde{\mathbf{A}}}}_{BCM}(\underline{v})\right) - \det\left(\underline{\underline{\tilde{\mathbf{A}}}}_{BCM}(\underline{v})\right) \underline{\underline{\tilde{\mathbf{G}}}}^{\infty}_{BCM}(\underline{\hat{v}})}{(\underline{\hat{v}} \cdot \underline{\underline{\epsilon}}_{BCM} \cdot \underline{\hat{v}})(\underline{\hat{v}} \cdot \underline{\underline{\mu}}_{BCM} \cdot \underline{\hat{v}}) + (\underline{\hat{v}} \cdot \underline{\underline{\xi}}_{BCM} \cdot \underline{\hat{v}})(\underline{\hat{v}} \cdot \underline{\underline{\xi}}_{BCM} \cdot \underline{\hat{v}})}\,, \tag{4.87}$$

we find that

$$\int \underline{\underline{\tilde{\mathbf{G}}}}^{0}_{BCM}(\underline{\underline{U}}^{-1} \cdot \underline{v}) \left(\frac{\sin vL}{v} - L\cos vL\right) \frac{1}{v^2}\, d^3\underline{v} = \frac{\pi\omega^3}{4i} \int \left\{ \frac{1}{\kappa_+ - \kappa_-} \right.$$
$$\left. \times \left[\frac{\mathrm{e}^{iLv}}{v^2}(1 - iLv)\left(\underline{\underline{\mathbf{N}}}(\underline{\underline{U}}^{-1} \cdot \underline{v}) + \underline{\underline{\mathbf{N}}}(-\underline{\underline{U}}^{-1} \cdot \underline{v})\right) \right]_{v=\sqrt{\kappa_-}}^{v=\sqrt{\kappa_+}} + \frac{2\,\underline{\underline{\mathbf{N}}}(0)}{\kappa_+\,\kappa_-} \right\} d\Omega\,. \tag{4.88}$$

The specification of the bilocal SPFT equations in the long–wavelength approximation for reciprocal biaxial bianisotropic composites with spherical topology is completed by the following expression for the corresponding depolarisation dyadic [29]

$$\underline{\underline{\mathbf{D}}} = \frac{1}{4\pi i\omega} \int \frac{1}{t_4(\underline{\underline{U}}^{-1} \cdot \underline{\hat{v}})}\, \underline{\underline{\mathbf{T}}}_4(\underline{\underline{U}}^{-1} \cdot \underline{\hat{v}})\, d\Omega\,. \tag{4.89}$$

Thus, the constitutive dyadic $\underline{\underline{\mathbf{K}}}_{Dy0}$ of the local effective medium is fully specified through (4.66), (4.52), (4.86), (4.88) and (4.89).

Finally in this section, we consider the long–wavelength regime $|L\sqrt{\kappa_\pm}| \ll 1$. Retaining terms only of $\mathcal{O}(L\sqrt{\kappa_\pm})$, we see that the integrals (4.86) and (4.88) become null–valued. This is consistent with the finding reported for chiral mediums that the bilocally–approximated SPFT does not yield a correction to the Br homogenisation formalism in the static limit [64]. However, on retaining terms up to $\mathcal{O}(L^2\kappa_\pm)$, the $\mathrm{e}^{iLv}(1 - iLv)$ term in the integrand of (4.86) and (4.88) reduces to $1 + (Lv)^2/2$; hence the principal value integration (4.65) becomes

$$\mathcal{P} \int \Gamma(\underline{R})\, \underline{\underline{\mathbf{G}}}_{BCM}(\underline{R})\, d^3\underline{R} = \frac{-i\omega f_a f_b L^2}{8\pi} \int \frac{\underline{\underline{\mathbf{\Lambda}}}(\underline{\underline{U}}^{-1} \cdot \underline{\hat{v}})}{t_4(\underline{\underline{U}}^{-1} \cdot \underline{\hat{v}})}\, d\Omega\,. \tag{4.90}$$

For constituent mediums with real–valued constitutive parameters $\underline{\underline{\mathbf{K}}}_p$, the integrand of (4.90) is correspondingly real–valued. Thus, it is clear from (4.66), (4.52), (4.22) and (4.89) that scattering losses cannot be predicted under the long–wavelength approximation represented by (4.90). A similar result was reported for SPFT applied to chiral mediums [64].

4.3 Parametric numerical studies

We now apply the bilocally–approximated SPFT developed in Section 4.2 to detailed numerical investigations of three different classes of HCM [17]. Specifically, we explore

the influence of the correlation length in Section 4.3.1 where an isotropic chiral HCM is studied; direct comparison of results with earlier SPFT analyses is made. The effects of the component phase topology and orientation diversity are considered for a biaxial bianisotropic HCM and a chiroferrite HCM in Sections 4.3.2 and 4.3.3, respectively. The HCMs of Sections 4.3.1 and 4.3.2 belong to the reciprocal biaxial bianisotropic category of materials; accordingly, we calculate the constitutive dyadic $\underline{\underline{\mathbf{K}}}_{Dy0}$ for these HCMs via the numerical evaluation of (4.88) (or, equivalently, (4.86)). However, the chiroferrite HCM encountered in Section 4.3.3 is inherently nonreciprocal and in this case direct numerical evaluation of (4.65) is necessary to calculate $\underline{\underline{\mathbf{K}}}_{Dy0}$.

An angular frequency ω of $2\pi \times 10^{10}$ rad s^{-1} was used for all calculations reported in this section.

4.3.1 Isotropic chiral HCM

In order to allow direct comparison with the SPFT analyses of Michel & Lakhtakia [55], [65], we choose the phase a to be an isotropic chiral medium described by the constitutive dyadic

$$\underline{\underline{\mathbf{K}}}_a = \begin{bmatrix} \epsilon_0\epsilon_a\,\underline{\underline{I}} & i\sqrt{\epsilon_0\mu_0}\,\xi_a\,\underline{\underline{I}} \\ -i\sqrt{\epsilon_0\mu_0}\,\xi_a\,\underline{\underline{I}} & \mu_0\mu_a\,\underline{\underline{I}} \end{bmatrix}, \tag{4.91}$$

where $\epsilon_a = 2.304$, $\xi_a = 0.724$ and $\mu_a = 1.728$. The phase b is simply taken to be free space itself. Spherical component phase topology is assumed. For this isotropic example, the effective medium is characterised by the constitutive dyadic

$$\underline{\underline{\mathbf{K}}}_{Dy0} = \begin{bmatrix} \epsilon_0\epsilon_{Dy0}\,\underline{\underline{I}} & i\sqrt{\epsilon_0\mu_0}\,\xi_{Dy0}\,\underline{\underline{I}} \\ -i\sqrt{\epsilon_0\mu_0}\,\xi_{Dy0}\,\underline{\underline{I}} & \mu_0\mu_{Dy0}\,\underline{\underline{I}} \end{bmatrix}. \tag{4.92}$$

The computed values of $\epsilon_{Dy0}, \xi_{Dy0}$ and μ_{Dy0} are plotted as functions of correlation length L in Figure 4.1 for three different values of volume fraction f_a. All three effective constitutive scalars exhibit a similar dependency on L: their imaginary parts increase sharply from zero as the correlation length increases from zero, whereas their real parts remain almost constant. Upon converting from the present Tellegen notation to the Drude–Born–Federov notation [33], the computed values of the effective constitutive scalars at $f_a = 0.3$ are found to be in complete agreement with those values calculated previously [65]. We note that the derivation presented by Michel & Lakhtakia [55] proceeded in a somewhat different manner to that in Section 4.2, as an explicit expression for the dyadic Green function is available for chiral mediums. Over the range $0.3 \leq f_a \leq 0.5$, the graphs in Figure 4.1 clearly demonstrate that the degree of attenuation (due to scattering losses) increases as the volumetric proportion of phase a increases. In this context, the extended MG [67, 68] and the extended Br [69] homogenisation formalisms also predict attenuation losses, but in terms of finite inclusion–size and not in terms of a correlation length. We note that some disagreement [70] has recently emerged on the completeness of certain extensions of the MG and the Br formalisms.

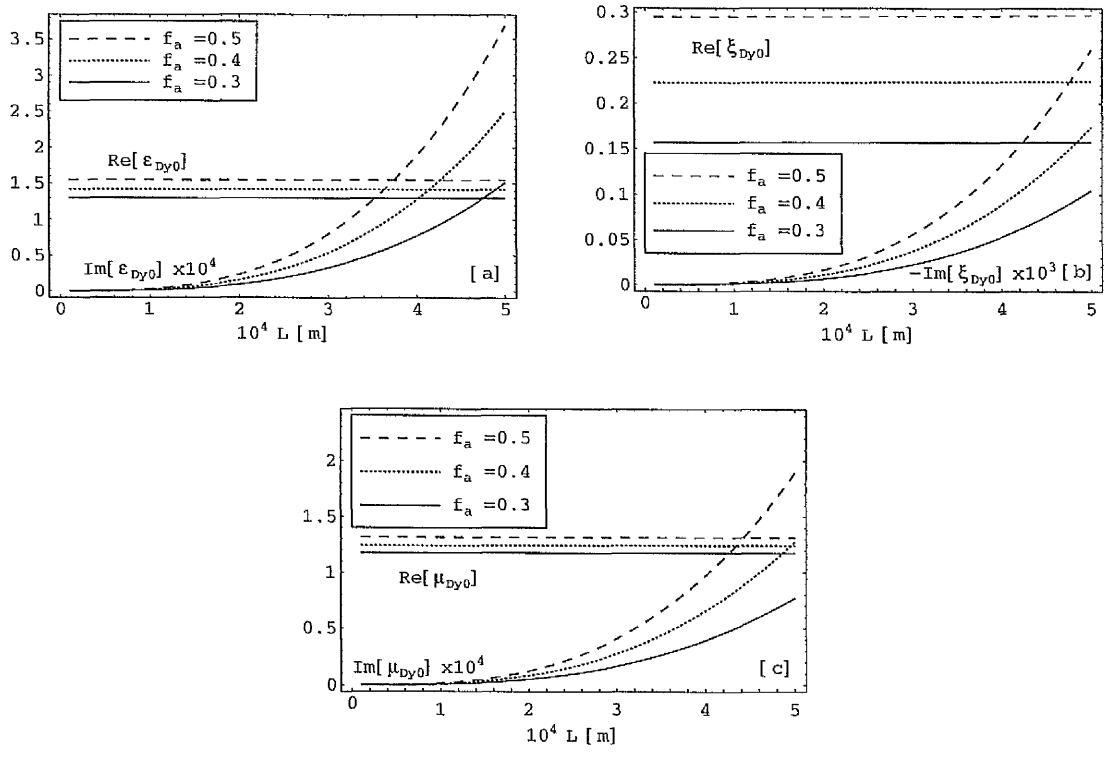

Figure 4.1: The effective constitutive scalars of an isotropic chiral composite plotted as functions of the correlation length L for $f_a = 0.3, 0.4$ and 0.5.

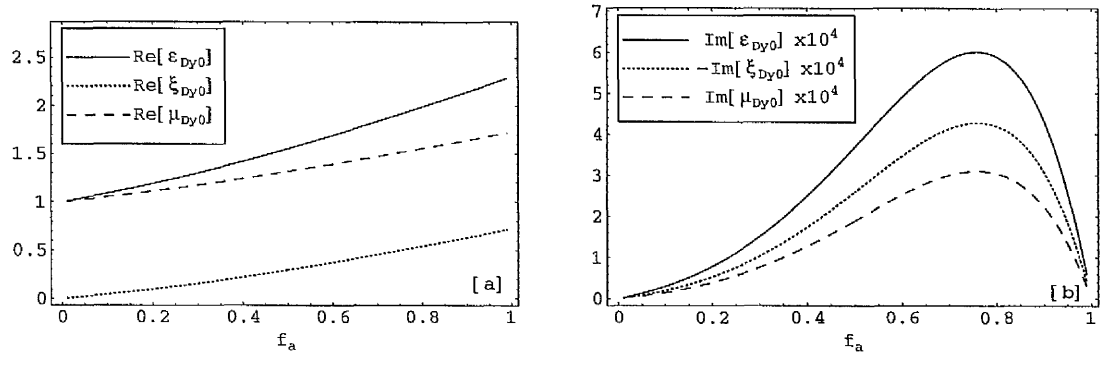

Figure 4.2: The (a) real and (b) imaginary parts of the effective constitutive scalars of an isotropic chiral composite plotted as functions f_a for a correlation length $L = 5 \times 10^{-4}$ m.

This issue is pursued further in Figure 4.2 where, for a fixed correlation length $L = 5 \times 10^{-4}$ m, the constitutive scalars of the effective medium are plotted as functions of f_a. The maximum degree of attenuation, as indicated by the magnitude of the imaginary parts of the effective constitutive scalars, occurs at $f_a \approx 0.75$. Beyond this value of f_a, fewer scattering centres are present in the composite. The real parts of the effective constitutive scalars follow an almost linear progression between the values they must hold at $f_a = 0$ and $f_a = 1$.

4.3.2 Biaxial bianisotropic HCM

We focus attention here on a biaxial bianisotropic composite medium constituted by a biaxial dielectric medium and an isotropic chiral medium. Biaxial constitutive properties — which encompass the orthorhombic, monoclinic and triclinic crystal classifications — abound in nature, and have been the focus of recent MG and Br homogenisation investigations [13]–[15], as described in detail in Chapter 3. In this section we estimate the constitutive dyadic $\underline{\underline{\mathbf{K}}}_{Dy0}$ of a biaxial bianisotropic HCM by means of the SPFT; for comparison, estimates of the HCM constitutive dyadics $\underline{\underline{\mathbf{K}}}_{Br}$ and $\underline{\underline{\mathbf{K}}}_{IMG}$ calculated using, respectively, the Br and IMG homogenisation formalisms are also presented. Henceforth in this section, the subscript $p = Dy0, Br, IMG$.

The constituent mediums are (i) a biaxial dielectric medium described by

$$\underline{\underline{\epsilon}}_a = \epsilon_0 \begin{bmatrix} \epsilon_a^x \cos^2\psi + \epsilon_a^y \sin^2\psi & (\epsilon_a^x - \epsilon_a^y)\sin\psi\cos\psi & 0 \\ (\epsilon_a^x - \epsilon_a^y)\sin\psi\cos\psi & \epsilon_a^x \sin^2\psi + \epsilon_a^y \cos^2\psi & 0 \\ 0 & 0 & \epsilon_a^z \end{bmatrix}, \quad \underline{\underline{\mu}}_a = \mu_0 \underline{\underline{I}}, \tag{4.93}$$

and (ii) an isotropic chiral medium with the following constitutive dyadics

$$\underline{\underline{\epsilon}}_b = \epsilon_0\,\epsilon_b\,\underline{\underline{I}}, \qquad \underline{\underline{\xi}}_b = -\underline{\underline{\zeta}}_b = i\sqrt{\epsilon_0\,\mu_0}\,\xi_b\,\underline{\underline{I}}, \qquad \underline{\underline{\mu}}_b = \mu_0\,\mu_b\,\underline{\underline{I}}. \tag{4.94}$$

The parameter values selected for calculations are as follows: $\epsilon_a^x = 4 + i\,0.4$, $\epsilon_a^y = 3 + i\,0.3$, $\epsilon_a^z = 1.5 + i\,0.15$; $\epsilon_b = 2.5 + i\,0.5$, $\xi_b = 1 + i\,0.2$ and $\mu_b = 1.75 + i\,0.35$. The ellipsoidal topology was captured by the shape dyadic

$$\underline{\underline{U}} = \frac{1}{\sqrt[3]{U_x\,U_y\,U_z}}\,\mathrm{diag}(U_x,\,U_y,\,U_z), \qquad (U_x, U_y, U_z > 0). \tag{4.95}$$

where $U_x = 1 + \delta$, $U_y = 1$, $U_z = 1 - (\delta/2)$ and δ is the *eccentricity parameter*. Thus, the principal axes of $\underline{\underline{\epsilon}}_a$ are rotated with respect to the principal axes of $\underline{\underline{U}}$ by the angle ψ in the xy plane. A sample of calculated results is presented in Figure 4.3.

We begin by considering the effect of the correlation length L. The constitutive properties of the HCM were estimated for $f_a = 0.3$, $\delta = 0.5$, $\psi = 0$, whilst L ranged from 0.0 to 0.0015 m. The HCM constitutive dyadics were found to have the form

$$\underline{\underline{\epsilon}}_p = \epsilon_0\,\mathrm{diag}\,(\,\epsilon_p^x\,,\,\epsilon_p^y\,,\,\epsilon_p^z\,)\,, \tag{4.96}$$

$$\underline{\underline{\xi}}_p = -\underline{\underline{\zeta}}_p = i\sqrt{\epsilon_0\,\mu_0}\,\mathrm{diag}\,(\,\xi_p^x\,,\,\xi_p^y\,,\,\xi_p^z\,)\,, \tag{4.97}$$

$$\underline{\underline{\mu}}_p = \mu_0\,\mathrm{diag}\,(\,\mu_p^x\,,\,\mu_p^y\,,\,\mu_p^z\,)\,. \tag{4.98}$$

The real parts and imaginary parts of μ_p^x, μ_p^y and μ_p^z are plotted as functions of the correlation length L in Figures 4.3(a) and 4.3(b), respectively. With respect to L, the HCM constitutive quantities not displayed in Figures 4.3(a) and 4.3(b) behave in a broadly analogous manner to those which are. The Br and IMG values are independent of correlation length. Furthermore, the SPFT and Br values are identical when $L = 0$; but the SPFT values deviate rapidly from the Br values as L increases.

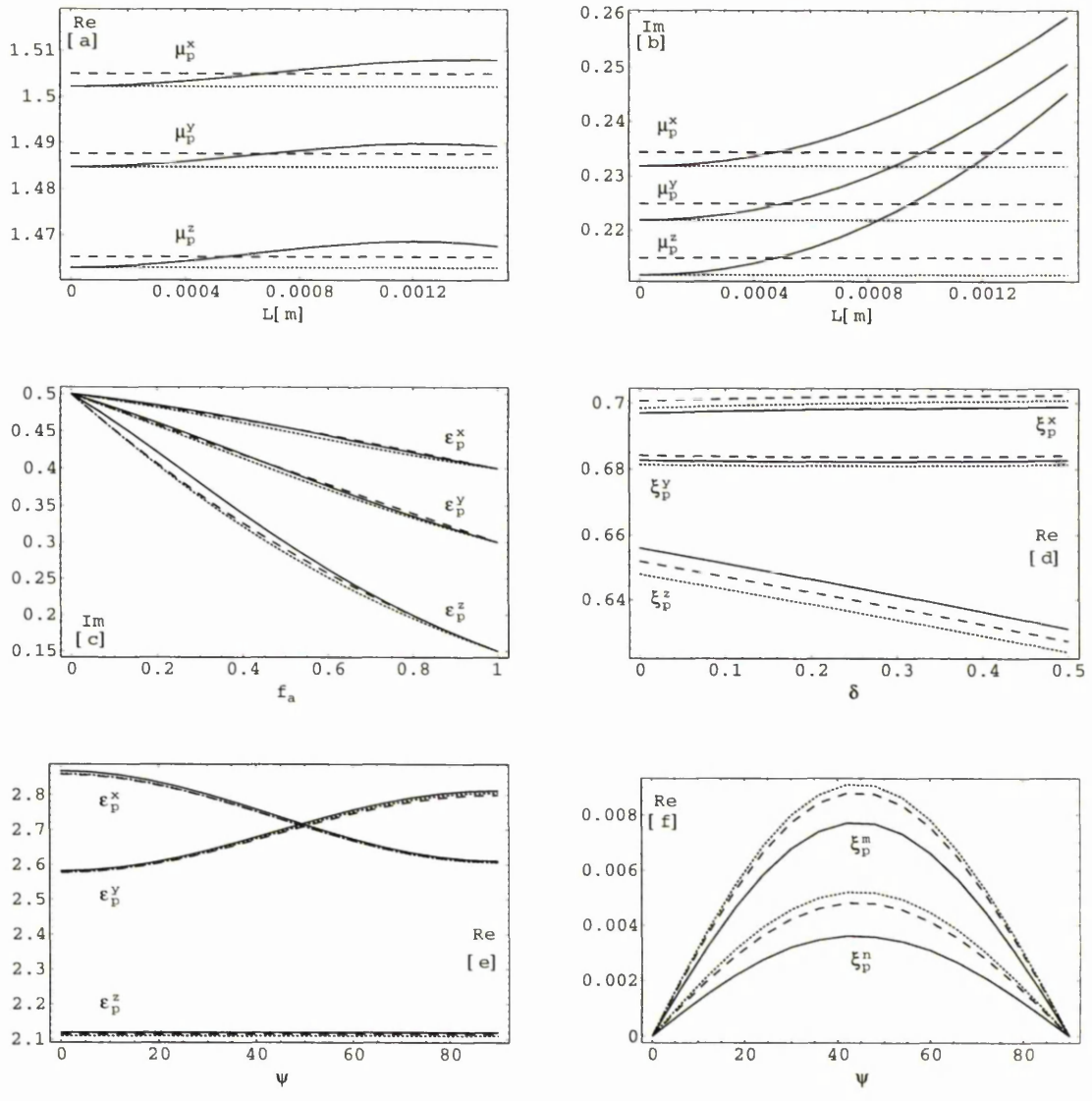

Figure 4.3: Representative plots of the estimated effective constitutive parameters of a biaxial bianisotropic composite medium as functions of the correlation length L in (a) and (b); volume fraction f_a in (c); eccentricity parameter δ in (d); and orientation angle ψ in (e) and (f). Key: solid line for $p = Dy0$; dotted line for $p = Br$; dashed line for $p = IMG$.

This is because the actions of increased numbers of scattering centres (i.e., the inclusions) become correlated as L increases, and, consequently, the number of significant multiple–scattering events escalates.

Next, using $f_a \in [0, 1]$ as an independent variable we estimated the constitutive dyadics of the HCM with $L = 0.001\,\mathrm{m}$, $\delta = 0.5$ and $\psi = 0$. The 3×3 diagonal dyadic form (4.96)–(4.98) was found to hold for all three formalisms. As functions of the volume fraction, the constitutive parameters estimated by the SPFT, Br and IMG formalisms all behave similarly. Representative graphs are provided by those

displayed in Figure 4.3(c) for the imaginary parts of ϵ_p^x, ϵ_p^y and ϵ_p^z. Notice that the *simplest* homogenisation formalism — whereby the HCM constitutive parameter values are estimated as the volume–weighted averages of the constitutive parameters of the constituent mediums — results in a linear relationship between the values which the HCM constitutive parameters must take at $f_a = 0$ and $f_a = 1$. Therefore, the nonlinearity of each of the graphs in Figure 4.3(c) is a measure of the deviation of the respective SPFT, Br and IMG homogenisation formalisms from the simplest formalism. Comparisons between the Br and IMG estimates as functions of f_a have been extensively reported for various types of composite mediums [8]–[10].

We turn now to the influence of the inclusion shape. The HCM constitutive dyadics were estimated as functions of the eccentricity parameter $\delta \in [0, 0.5]$, while the parameters $L = 0.001\,\mathrm{m}$, $f_a = 0.3$ and $\psi = 0$ were kept fixed. Once again, (4.96)–(4.98) describe the form of the computed HCM constitutive dyadics. An increase in the eccentricity of the ellipsoidal shape underlying the topology of the composite medium was found to have the distinct effect of increasing the contrast between the diagonal elements of the 3×3 constitutive dyadics. This is illustrated in Figure 4.3(d) by representative parameter values, provided by the real parts of ξ_p^x, ξ_p^y and ξ_p^z.

Lastly in this section, we consider the dependency of the HCM constitutive parameters on the orientation diversity between the principal axes of $\underline{\underline{\epsilon}}_a$ and $\underline{\underline{U}}$, as quantified by the angle ψ. Calculations were carried out for $0 \leq \psi \leq \pi/2$, with $L = 0.001$ m, $f_a = 0.3$ and $\delta = 0.5$. Instead of conforming to (4.96)–(4.98), the constitutive dyadics of the HCM were now found to be of the more general form

$$\underline{\underline{\epsilon}}_p = \epsilon_0 \begin{bmatrix} \epsilon_p^x & \epsilon_p^t & 0 \\ \epsilon_p^t & \epsilon_p^y & 0 \\ 0 & 0 & \epsilon_p^z \end{bmatrix}, \qquad \underline{\underline{\mu}}_p = \mu_0 \begin{bmatrix} \mu_p^x & \mu_p^t & 0 \\ \mu_p^t & \mu_p^y & 0 \\ 0 & 0 & \mu_p^z \end{bmatrix}, \tag{4.99}$$

$$\underline{\underline{\xi}}_p = -\underline{\underline{\zeta}}_p^T = i\sqrt{\epsilon_0\,\mu_0} \begin{bmatrix} \xi_p^x & \xi_p^m & 0 \\ \xi_p^n & \xi_p^y & 0 \\ 0 & 0 & \xi_p^z \end{bmatrix}. \tag{4.100}$$

We remark that the surface integral evaluation (4.88) is also applicable for mediums of the type (4.99)–(4.100), but not for more general forms of bianisotropic biaxial medium. Our calculations show that the off–diagonal elements in (4.99)–(4.100) disappear when either $\psi = 0$ or $\psi = \pi/2$, and electromagnetic response characteristics of the HCM are then in accordance with (4.96)–(4.98).

The influence of ψ is revealed in Figure 4.3(e) for the real parts of ϵ_p^x, ϵ_p^y and ϵ_p^z; and in Figure 4.3(f) for the real parts of ξ_p^m and ξ_p^n. The relative permittivity scalars ϵ_p^x, ϵ_p^y and ϵ_p^t are strongly influenced by the orientation of the principal axes of $\underline{\underline{\epsilon}}_a$ in the xy plane, but ϵ_p^z is not. A similar relationship is demonstrated by the magnetoelectric constitutive scalars of the HCM; however, the permeability parameters are considerably less sensitive to ψ than their dielectric counterparts are.

4.3.3 Chiroferrite HCM

The homogenisation of a chiroferrite composite medium, formed by mixing a magnetically–biased ferrite with an isotropic chiral medium, is considered here. Chiroferrites, together with chiroplasmas, were theoretically conceived as composite materials [12]; and, subsequently, their constitutive relations were rigorously developed [34]. Both chiroferrite [35] and chiroplasma [11] HCMs have been developed using the MG and the Br formalisms. Further details are provided in Chapter 2.

The constituent mediums are (i) a gyrotropic magnetic medium characterised by

$$\underline{\underline{\epsilon}}_a = \epsilon_0\,\epsilon_a\,\underline{\underline{I}}\,, \qquad \underline{\underline{\mu}}_a = \mu_0\left[\mu_a\,\underline{\underline{I}} - i\mu_a^g\,\hat{\underline{u}}_z \times \underline{\underline{I}} + (\mu_a^u - \mu_a)\,\hat{\underline{u}}_z\,\hat{\underline{u}}_z\right]\,, \quad (4.101)$$

and (ii) an isotropic chiral medium with constitutive dyadics as given by (4.94). The following parameter values were chosen: $\epsilon_a = 1.2+i\,0.4$, $\mu_a = 4.5+i\,1.5$, $\mu_a^g = 2.4+i\,0.8$, $\mu_a^u = 1.8+i\,0.6$; $\epsilon_b = 2.5+i\,0.5$, $\xi_b = 1+i\,0.2$ and $\mu_b = 1.75+i\,0.35$. Both constituent mediums a and b are assumed to have ellipsoidal topologies described by the shape dyadic

$$\begin{aligned}\underline{\underline{U}} \;=\; & \frac{1}{(U_x\,U_y\,U_z)^{1/3}}\left\{\left[U_x\cos^2\alpha + U_y\sin^2\alpha + (U_z - U_x)\sin^2\beta\right]\,\hat{\underline{u}}_x\,\hat{\underline{u}}_x\right. \\ & + \left(U_x\sin^2\alpha + U_y\cos^2\alpha\right)\,\hat{\underline{u}}_y\,\hat{\underline{u}}_y + \left(U_x\sin^2\beta + U_z\cos^2\beta\right)\,\hat{\underline{u}}_z\,\hat{\underline{u}}_z \\ & + \left[(U_x - U_y)\sin\alpha\cos\alpha\right]\left(\hat{\underline{u}}_x\,\hat{\underline{u}}_y + \hat{\underline{u}}_y\,\hat{\underline{u}}_x\right) \\ & \left. + \left[(U_x - U_z)\sin\beta\cos\beta\right]\left(\hat{\underline{u}}_x\,\hat{\underline{u}}_z + \hat{\underline{u}}_z\,\hat{\underline{u}}_x\right)\right\}, \end{aligned} \quad (4.102)$$

where $U_x = 1+\delta$, $U_y = 1$ and $U_z = 1-(\delta/2)$. Thus, for $\beta = 0$, the angle α represents the rotation of the ellipsoid principal axes in the xy plane about the z axis; while the angle β represents the rotation of the ellipsoid principal axes in the xz plane about the y axis when $\alpha = 0$. Representative plots are presented in Figure 4.4.

With $f_a = 0.3$, $\delta = 0.5$, and $\alpha = \beta = 0$ fixed, estimates of the HCM constitutive parameters were computed as functions of the correlation length $L \in [0,\, 0.0015]$ m. The permittivity and the permeability dyadics of the HCM were found to possess the respective forms

$$\underline{\underline{\epsilon}}_p = \epsilon_0\begin{bmatrix} \epsilon_p^{11} & \epsilon_p^{12} & 0 \\ -\epsilon_p^{12} & \epsilon_p^{22} & 0 \\ 0 & 0 & \epsilon_p^{33}\end{bmatrix}, \qquad \underline{\underline{\mu}}_p = \mu_0\begin{bmatrix} \mu_p^{11} & \mu_p^{12} & 0 \\ -\mu_p^{12} & \mu_p^{22} & 0 \\ 0 & 0 & \mu_p^{33}\end{bmatrix}; \quad (4.103)$$

whereas the effective magnetoelectric dyadics have the more general form

$$\underline{\underline{\xi}}_p = i\sqrt{\epsilon_0\,\mu_0}\begin{bmatrix} \xi_p^{11} & \xi_p^{12} & 0 \\ \xi_p^{21} & \xi_p^{22} & 0 \\ 0 & 0 & \xi_p^{33}\end{bmatrix}, \quad \underline{\underline{\zeta}}_p = i\sqrt{\epsilon_0\,\mu_0}\begin{bmatrix} -\xi_p^{11} & \xi_p^{21} & 0 \\ \xi_p^{12} & -\xi_p^{22} & 0 \\ 0 & 0 & -\xi_p^{33}\end{bmatrix}. \quad (4.104)$$

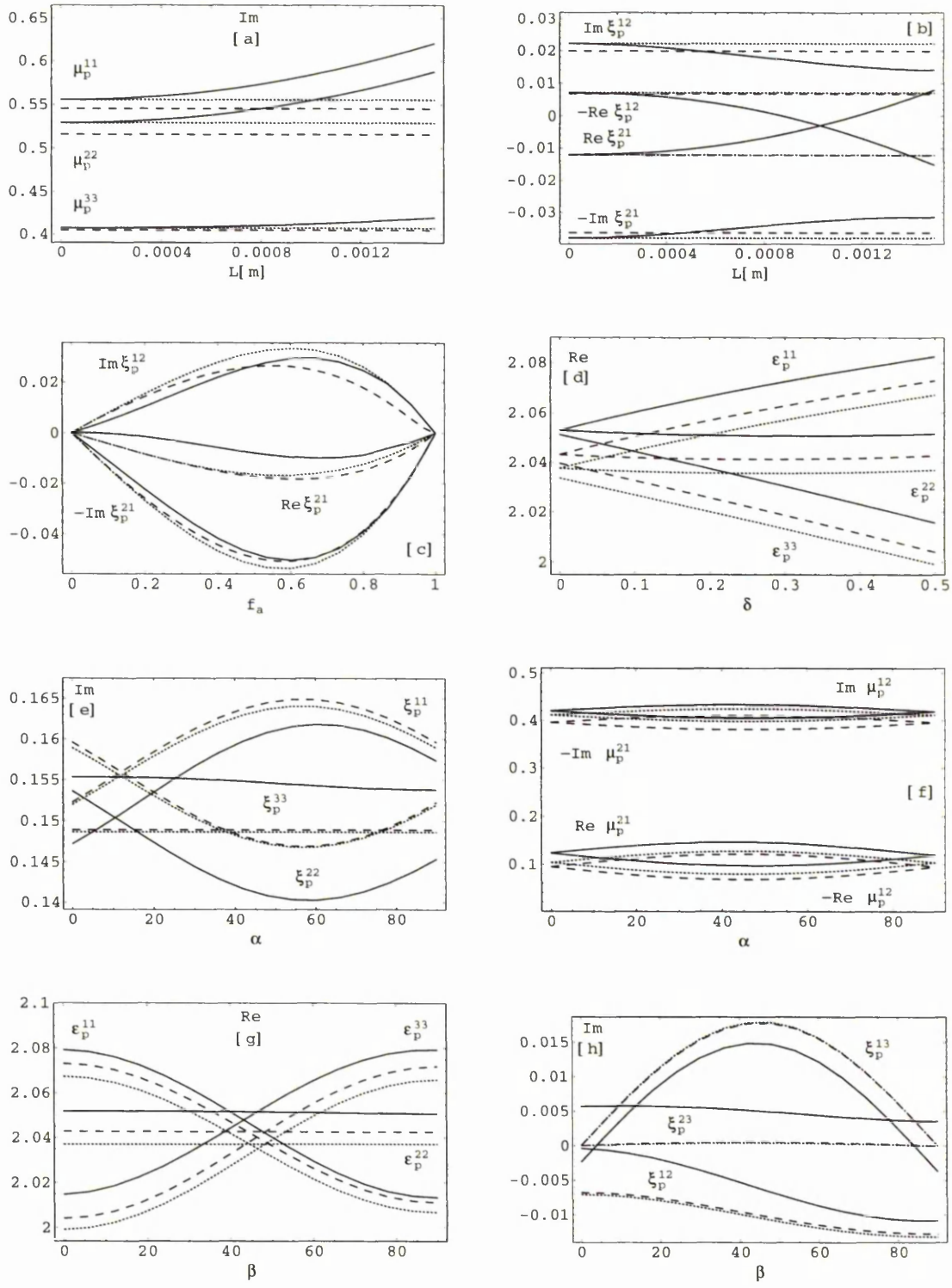

Figure 4.4: Representative plots of the estimated effective constitutive parameters of a chiroferrite composite medium as functions of the correlation length L in (a) and (b); volume fraction f_a in (c); ellipsoid eccentricity parameter δ in (d); orientation angle α in (e) and (f); and orientation angle β in (g) and (h). Key: solid line for $p = Dy0$; dotted line for $p = Br$; dashed line for $p = IMG$.

Equations (4.103) and (4.104) show that the considered composite medium is more general than the so–called *Faraday chiral mediums*, as exemplified by chiroferrites and chiroplasmas endowed with spherical microstructural topology [34]. We note that the constitutive dyadics of chiroplasmas possessing non–spherical topology [11] have the same structure as (4.103) and (4.104). See Chapter 2 for further details.

As in Sections 4.3.1 and 4.3.2, the SPFT calculations are acutely sensitive to the correlation length, while those computed using the Br and IMG formalisms are independent of L. This is illustrated by the representative plots of the imaginary parts of μ_p^x, μ_p^y and μ_p^z; and ξ_p^{12} and ξ_p^{21} in Figures 4.4(a) and 4.4(b), respectively. Once again, the escalation in the magnitudes of the SPFT estimates with increasing L is a manifestation of the rising number of multiple–scattering events within V_L^e.

Next, we consider the influence of the volume fraction $f_a \in [0,\ 1]$ on the constitutive properties of the chosen HCM. Calculations were made for $L = 0.001$ m, $\delta = 0.5$ and $\alpha = \beta = 0$; and the results conformed to (4.103) and (4.104). The computed diagonal entries of all four 3×3 constitutive dyadics display an approximately linear behaviour with respect to f_a, between the values they must take at the endpoints $f_a = 0$ (where $\underline{\underline{\mathbf{K}}}_p = \underline{\underline{\mathbf{K}}}_b$) and $f_a = 1$ (where $\underline{\underline{\mathbf{K}}}_p = \underline{\underline{\mathbf{K}}}_a$). Considerable nonlinearity with respect to f_a is apparent for the off–diagonal entries of the constitutive dyadics in (4.103) and (4.104), but the magnitudes of these terms are rather small in comparison with those of the diagonal entries. As representative examples, the real and imaginary parts of ξ_p^{21} as well as the imaginary parts of ξ_p^{12} are plotted against f_a in Figure 4.4(c).

The HCM constitutive parameters were then estimated as functions of the eccentricity parameter $\delta \in [0,\ 0.5]$, with $L = 0.001$ m, $f_a = 0.3$ and $\alpha = \beta = 0$. Equations (4.103) and (4.104) were satisfied by the results. At $\delta = 0$, we get $\tau_p^{11} = \tau_p^{22}$ ($\tau = \epsilon, \mu, \xi$) and $\xi_p^{12} = -\xi_p^{21}$; i.e., the HCM is a Faraday chiral medium [34] if the topology is spherical. By way of a representative example, in Figure 4.4(d) the real parts of ϵ_p^{11}, ϵ_p^{22} and ϵ_p^{33} are displayed as functions of δ. As was observed in Section 4.3.2, increased contrast between the diagonal elements of the 3×3 constitutive dyadics of the HCM is achieved at higher degrees of asphericity of the ellipsoidal inclusions.

Finally, we come to the influence of the orientation diversity on the effective constitutive dyadics of the chosen HCM. We selected $L = 0.001$ m, $f_a = 0.3$ and $\delta = 0.5$. First, we set $\beta = 0$ and determined that the constitutive dyadics of the HCM possess the form

$$\underline{\underline{\epsilon}}_p = \epsilon_0 \begin{bmatrix} \epsilon_p^{11} & \epsilon_p^{12} & 0 \\ \epsilon_p^{21} & \epsilon_p^{22} & 0 \\ 0 & 0 & \epsilon_p^{33} \end{bmatrix}, \qquad \underline{\underline{\xi}}_p = i\sqrt{\epsilon_0\,\mu_0} \begin{bmatrix} \xi_p^{11} & \xi_p^{12} & 0 \\ \xi_p^{21} & \xi_p^{22} & 0 \\ 0 & 0 & \xi_p^{33} \end{bmatrix}, \tag{4.105}$$

$$\underline{\underline{\zeta}}_p = i\sqrt{\epsilon_0\,\mu_0} \begin{bmatrix} \zeta_p^{11} & \zeta_p^{12} & 0 \\ \zeta_p^{21} & \zeta_p^{22} & 0 \\ 0 & 0 & -\xi_p^{33} \end{bmatrix}, \qquad \underline{\underline{\mu}}_p = \mu_0 \begin{bmatrix} \mu_p^{11} & \mu_p^{12} & 0 \\ \mu_p^{21} & \mu_p^{22} & 0 \\ 0 & 0 & \mu_p^{33} \end{bmatrix}, \tag{4.106}$$

for $\alpha \in [0,\, \pi/2]$. Then, for $\alpha = 0$ and $\beta \in [0,\, \pi/2]$, we found that

$$\underline{\underline{\epsilon}}_p = \epsilon_0 \begin{bmatrix} \epsilon_p^{11} & \epsilon_p^{12} & \epsilon_p^{13} \\ -\epsilon_p^{12} & \epsilon_p^{22} & \epsilon_p^{23} \\ \epsilon_p^{13} & -\epsilon_p^{23} & \epsilon_p^{33} \end{bmatrix}, \quad \underline{\underline{\xi}}_p = i\sqrt{\epsilon_0\,\mu_0} \begin{bmatrix} \xi_p^{11} & \xi_p^{12} & \xi_p^{13} \\ \xi_p^{21} & \xi_p^{22} & \xi_p^{23} \\ \xi_p^{31} & \xi_p^{32} & \xi_p^{33} \end{bmatrix}, \tag{4.107}$$

$$\underline{\underline{\zeta}}_p = i\sqrt{\epsilon_0\,\mu_0} \begin{bmatrix} -\xi_p^{11} & \xi_p^{21} & -\xi_p^{31} \\ \xi_p^{12} & -\xi_p^{22} & \xi_p^{32} \\ -\xi_p^{13} & \xi_p^{23} & -\xi_p^{33} \end{bmatrix}, \quad \underline{\underline{\mu}}_p = \mu_0 \begin{bmatrix} \mu_p^{11} & \mu_p^{12} & \mu_p^{13} \\ -\mu_p^{12} & \mu_p^{22} & \mu_p^{23} \\ \mu_p^{12} & -\mu_p^{23} & \mu_p^{33} \end{bmatrix}. \tag{4.108}$$

Both sets of constitutive dyadics are more general than the ones specified through (4.103) and (4.104), except when (i) $\alpha = 0$ and either $\beta = 0$ or $\beta = \pi/2$, or (ii) $\beta = 0$ and either $\alpha = 0$ or $\alpha = \pi/2$.

Illustrative examples of the effects of orientation diversity are provided in Figures 4.4(e) and 4.4(f), wherein the imaginary parts of ξ_p^{11}, ξ_p^{22} and ξ_p^{33} as well as the real and the imaginary parts of μ_p^{12} and μ_p^{21}, respectively, are plotted against α when $\beta = 0$. Likewise, in Figures 4.4(g) and 4.4(h) are plotted the real parts of ϵ_p^{11}, ϵ_p^{22} and ϵ_p^{33}, and the imaginary parts of ξ_p^{12}, ξ_p^{13} and ξ_p^{23}, respectively, as functions of β when $\alpha = 0$. The τ_p^{11} and τ_p^{22} diagonal entries of the effective 3×3 constitutive dyadics are greatly dependent on α, whereas the τ_p^{33} values are not, $(\tau = \epsilon, \xi, \zeta, \mu)$. Analogously, the τ_p^{11} and τ_p^{33} diagonal entries of the 3×3 constitutive dyadics are highly sensitive to β, whereas the τ_p^{22} values are not, $(\tau = \epsilon, \xi, \mu)$.

4.4 Influence of covariance

We now consider the covariance function in the SPFT. In the SPFT developed in Section 4.2, the specific choice $\Gamma(\underline{R}) = \Gamma_0(\underline{R})$ (4.61) was made for the covariance function. Here we shall derive results for more general choices of covariance function and investigate the influence of the covariance function in a specific homogenisation example. Specifically, we consider the homogenisation of an assembly of metallic ellipsoidal inclusions, randomly distributed but similarly oriented, in a non–conducting host medium. Our study is an extension of an earlier investigation by Sherwin *et al.* [50] in which the same homogenisation scenario was explored using the Br homogenisation formalism. Their results highlighted the importance of the underlying component phase topology in determining the constitutive parameters of the composite medium. Most notably, abrupt changes in the effective permittivity of the composite medium as the volume fraction of inclusions was increased—indicative of a *percolation threshold* [5, 71]—were found to be particularly sensitive to the eccentricity of the ellipsoidal topology.

4.4.1 Theoretical results

We recall from (4.66) and (4.52) that the key step in calculating the SPFT–estimated HCM constitutive dyadic $\underline{\underline{\mathbf{K}}}_{Dy0}$ is the evaluation of the principal value integral

$$\underline{\underline{\mathbf{P}}}^{\Gamma} = \frac{1}{8\pi^3} \lim_{\delta \to 0} \int_{V_\infty - V_\delta^e} \Gamma(\underline{R}) \left(\int_{\underline{q}} \underline{\underline{\tilde{\mathbf{G}}}}_{BCM}(\underline{q}) \exp(i\underline{q} \cdot \underline{R})\, d^3\underline{q} \right) d^3\underline{R}, \quad (4.109)$$

where V_∞ denotes all space. For the case of the step function covariance $\Gamma_0(\underline{R})$ (4.61), we showed in Section 4.2.5 that (4.109) reduces to the surface integral

$$\underline{\underline{\mathbf{P}}}^{\Gamma_0} = \frac{\omega^3 f_a f_b}{4\pi i} \int \frac{1}{t_4(\underline{\underline{U}}^{-1} \cdot \hat{\underline{p}})} \left\{ \frac{1}{\kappa_+ - \kappa_-} \times \right.$$
$$\left. \left[e^{iLp} (1 - iLp) \left(\frac{\underline{\underline{\mathbf{\Lambda}}}(\underline{\underline{U}}^{-1} \cdot \hat{\underline{p}})}{\omega^2} + \frac{\underline{\underline{\mathbf{\Upsilon}}}(\underline{\underline{U}}^{-1} \cdot \hat{\underline{p}})}{p^2} \right) \right]_{p=\sqrt{\kappa_-}}^{p=\sqrt{\kappa_+}} + \frac{\underline{\underline{\mathbf{\Upsilon}}}(\underline{\underline{U}}^{-1} \cdot \hat{\underline{p}})}{\kappa_+ \kappa_-} \right\} d\Omega, \quad (4.110)$$

which requires numerical evaluation, in general. Here we present results analogous to (4.110) for the exponential covariances

$$\Gamma_1(\underline{R}) = f_a f_b \exp(-\sigma\, |\underline{\underline{U}}^{-1} \cdot \underline{R}|), \quad (4.111)$$
$$\Gamma_2(\underline{R}) = f_a f_b \exp(-\sigma\, |\underline{\underline{U}}^{-1} \cdot \underline{R}|^2), \quad (4.112)$$

where $\sigma > 0$. Notice that each of the covariance functions (4.61), (4.111) and (4.112) reflects the ellipsoidal topology of the component phases insofar as each is spherically symmetric with respect to the coordinate frame of $\underline{S} = \underline{\underline{U}}^{-1} \cdot \underline{R}$. The treatments for covariance functions (4.111) and (4.112) follow by residue calculus in the manner detailed in Section 4.2.5, with (4.109) yielding

$$\underline{\underline{\mathbf{P}}}^{\Gamma_1} = \frac{\omega f_a f_b}{4\pi i} \int \left\{ \frac{\sigma^2 \underline{\underline{\mathbf{\Lambda}}}(\underline{\underline{U}}^{-1} \cdot \hat{\underline{p}}) + \omega^2 \underline{\underline{\mathbf{\Upsilon}}}(\underline{\underline{U}}^{-1} \cdot \hat{\underline{p}})}{t_4(\underline{\underline{U}}^{-1} \cdot \hat{\underline{p}})\, (\sqrt{\kappa_+} + i\sigma)^2 (\sqrt{\kappa_-} + i\sigma)^2} - \right.$$
$$\left. \frac{2i\sigma \left[\sqrt{\kappa_+}\sqrt{\kappa_-}\, \underline{\underline{\mathbf{\Lambda}}}(\underline{\underline{U}}^{-1} \cdot \hat{\underline{p}}) - \omega^2 \underline{\underline{\mathbf{\Upsilon}}}(\underline{\underline{U}}^{-1} \cdot \hat{\underline{p}}) \right] \left(\frac{1}{\sqrt{\kappa_+} + \sqrt{\kappa_-}} \right)}{t_4(\underline{\underline{U}}^{-1} \cdot \hat{\underline{p}})\, (\sqrt{\kappa_+} + i\sigma)^2 (\sqrt{\kappa_-} + i\sigma)^2} \right\} d\Omega, \quad (4.113)$$

and

$$\underline{\underline{\mathbf{P}}}^{\Gamma_2} = \frac{f_a f_b \omega}{8i\pi\sigma} \int \frac{1}{(\kappa_+ - \kappa_-)\, t_4(\underline{\underline{U}}^{-1} \cdot \hat{\underline{p}})} \times$$
$$\left[\left(m^2 \underline{\underline{\mathbf{\Lambda}}}(\underline{\underline{U}}^{-1} \cdot \hat{\underline{p}}) + \omega^2 \underline{\underline{\mathbf{\Upsilon}}}(\underline{\underline{U}}^{-1} \cdot \hat{\underline{p}}) \right) \exp(-\frac{m^2}{8\sigma})\, D_{-2}(\frac{-i\, m}{\sqrt{2\sigma}}) \right]_{m=\sqrt{\kappa_-}}^{m=\sqrt{\kappa_+}} d\Omega, \quad (4.114)$$

where

$$D_{-2}(z) = \exp(-\frac{z^2}{4}) - \left(\sqrt{\frac{\pi}{2}}\, z \exp(\frac{z^2}{4}) \operatorname{erfc}(\frac{z}{\sqrt{2}}) \right), \quad (4.115)$$

is the second–order parabolic cylinder function and erfc denotes the complementary error function [72]. The results (4.113) and (4.114) hold provided the BCM belongs to the general category of reciprocal biaxial bianisotropic mediums; the same restriction applies to (4.110).

4.4.2 Numerical results and discussion

Pursuing the homogenisation example previously investigated using the Br formalism by Sherwin *et al.* [50], we take phase a to be a collection of ellipsoidal iron particles at 670 nm free–space wavelength, with phase b being free space (i.e., vacuum). The relative permittivity of iron at the chosen wavelength is $-4.34 + i\,20.5$. In order to examine the influence of covariance and correlation length on the percolation threshold anisotropy, we choose $U_x = 1$, $U_y = 1.5$ and $U_z = 0.1$ in the notation of (4.95). For such an inclusion topology, we anticipate the effective composite permittivity to exhibit a percolation threshold along the shortest principal axis — which corresponds to U_z — but not in the directions orthogonal to it, as per the Br formalism [50]. Values of σ were selected for the covariance functions (4.111) and (4.112) so that

$$\int_{\underline{R}} \Gamma_j(\underline{R})\, d^3\underline{R} = \frac{4\pi L^3}{3}, \qquad (j = 0, 1, 2), \tag{4.116}$$

where L is the correlation length. Hence, $\sigma = (\sqrt[3]{6})/L$ for Γ_1; and $\sigma = (\sqrt[3]{9\pi/16})/L^2$ for Γ_2.

Our SPFT calculations reveal that $\underline{\underline{\mathbf{K}}}_{Dy0}$ has the form

$$\underline{\underline{\mathbf{K}}}_{Dy0} = \begin{bmatrix} \epsilon_0\, \underline{\underline{\epsilon}}_{Dy0} & \underline{\underline{0}} \\ \underline{\underline{0}} & \mu_0\, \underline{\underline{I}} \end{bmatrix}, \tag{4.117}$$

where $\underline{\underline{\epsilon}}_{Dy0} = \text{diag}\,(\epsilon_x^{Dy0}, \epsilon_y^{Dy0}, \epsilon_z^{Dy0})$. Results are presented for $L = 0$ nm to $L = 70$ nm, in increments of 10 nm, with reference to the key given in Table 4.1.

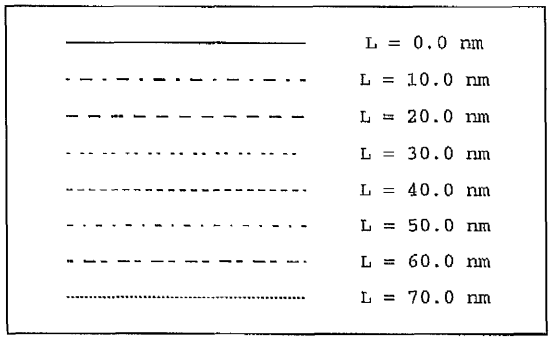

Table 4.1: Key for Figures 4.5–4.7.

The real and imaginary parts of the relative permittivity parameters ϵ_x^{Dy0}, ϵ_y^{Dy0} and ϵ_z^{Dy0}, calculated using covariance function Γ_0, are plotted as functions of f_a in Figure 4.5. The abrupt change in both the real and imaginary components of ϵ_z^{Dy0} in the vicinity of $f_a = 0.8$ indicates a percolation threshold. A corresponding threshold is not observed for the constitutive parameters ϵ_x^{Dy0} and ϵ_y^{Dy0}. As the correlation length increases, so the onset of percolation is seen to occur at higher values of f_a. At $L = 0$,

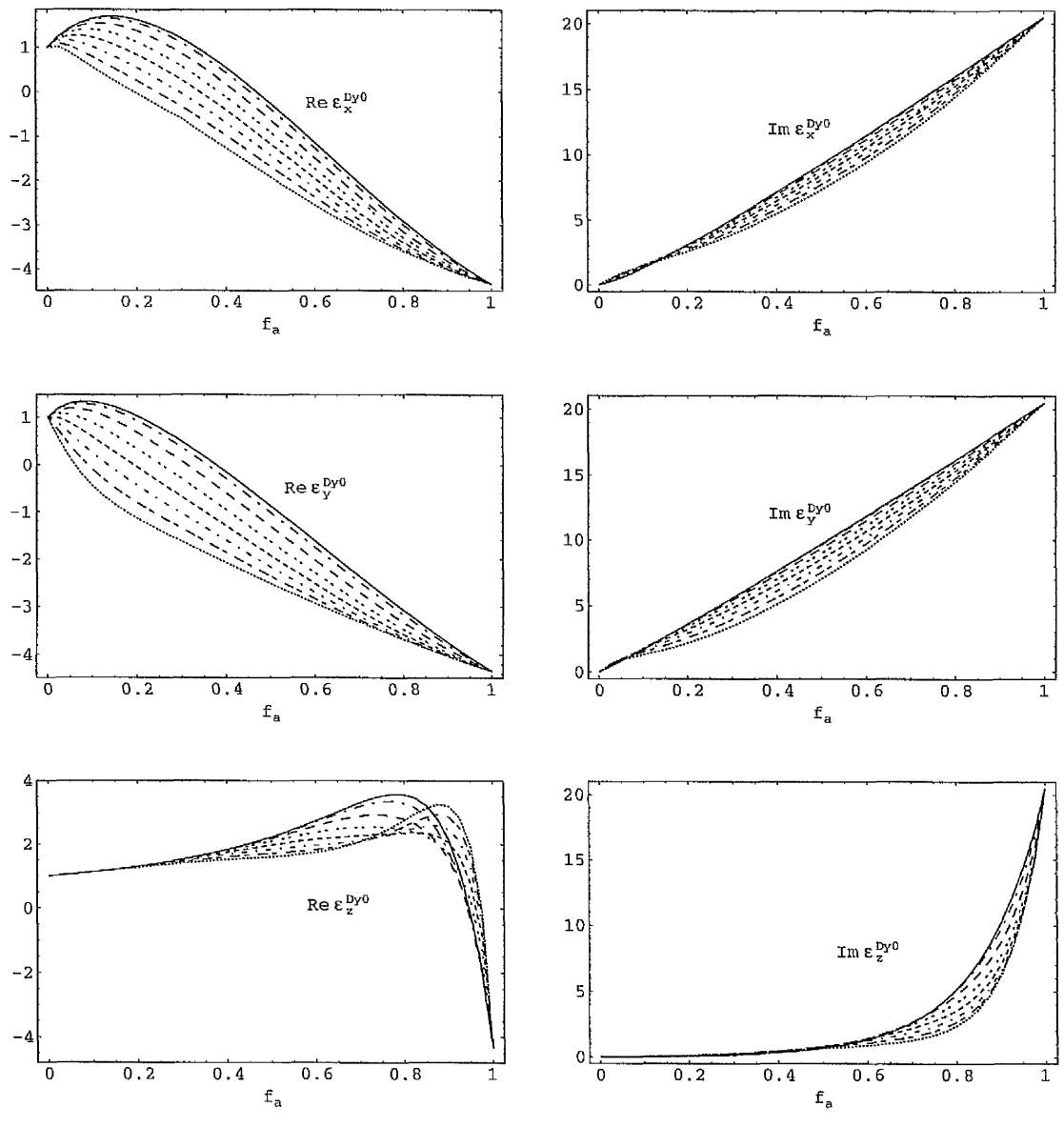

Figure 4.5: Real and imaginary components of the relative permittivity parameters ϵ_x^{Dy0}, ϵ_y^{Dy0} and ϵ_z^{Dy0} plotted against volume fraction f_a for covariance function Γ_0. See Table 4.1 for key.

the reverse effect may be achieved through increasing the magnitude of U_z relative to U_x and U_y [50].

The graphs for ϵ_x^{Dy0}, ϵ_y^{Dy0} and ϵ_z^{Dy0}, calculated using covariance functions Γ_1 and Γ_2 are presented in Figures 4.6 and 4.7, respectively. Comparing Figures 4.5, 4.6 and 4.7, we see that the influence of correlation length is least for the most slowly decreasing covariance function (namely, Γ_1), and greatest for the fastest decreasing covariance function (namely, Γ_0).

We infer from our numerical results that the correlated actions of neighbouring inclusions result in a considerable mitigation of the percolation threshold anisotropy

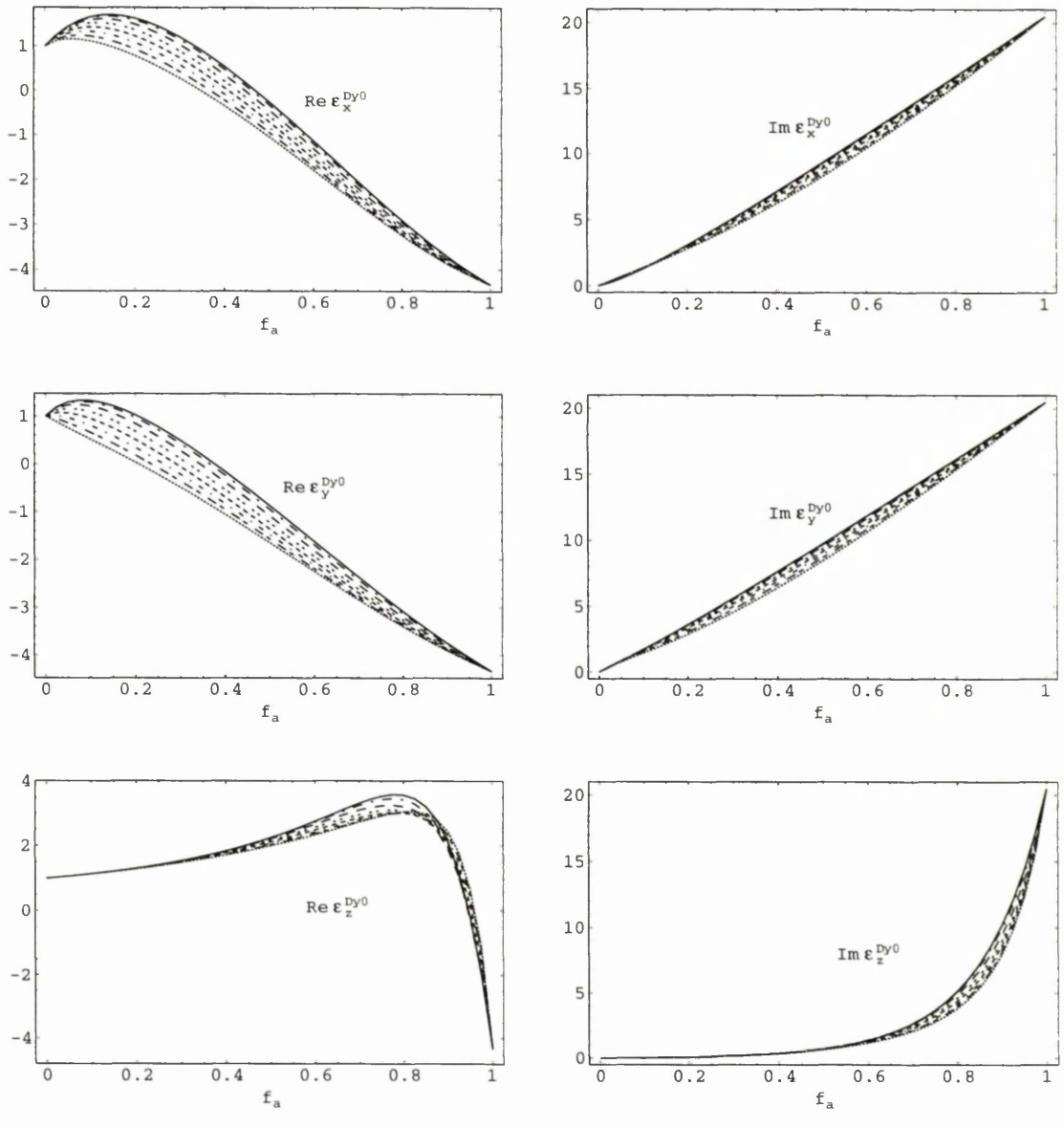

Figure 4.6: As for Figure 4.5 but with covariance function Γ_1. See Table 4.1 for key.

due to inclusion shape alone. Thus, the necessity of employing the SPFT, rather than the more simplistic Br formalism, is highlighted. We also conclude, from the presented numerical example, that the choice of covariance function may only have a secondary influence as compared with the effects of the correlation length.

4.5 Beyond the bilocal approximation

The SPFT has been widely applied, under the second–order approximation (also known as the bilocal approximation), to estimate the constitutive properties of HCMs [16], [53]–[55]. To our knowledge, higher–order approximations and the issue of convergence of the mass operator series have not hitherto been addressed. In this section, we

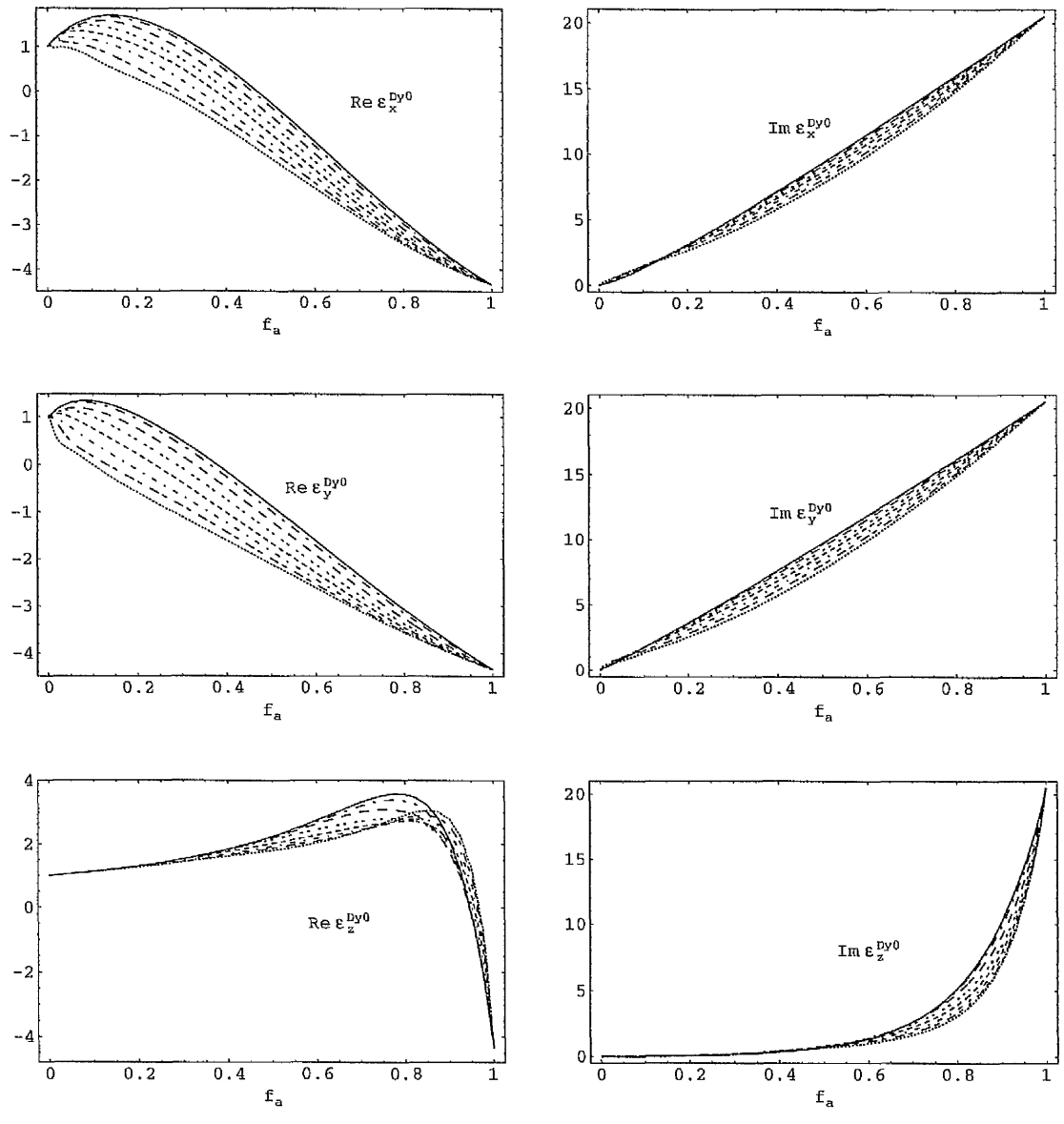

Figure 4.7: As for Figure 4.5 but with covariance function Γ_2. See Table 4.1 for key.

we develop a third–order approximation and investigate convergence of the mass operator series [19]. The analysis is presented for isotropic chiral composite mediums. Additionally, we conjecture that our conclusions hold for more general mediums; this conjecture is substantiated by our numerical results.

4.5.1 Third–order approximation

The second–order mass operator approximation $\underline{\underline{\Sigma}}(\underline{r}-\underline{r}') \approx \underline{\underline{\Sigma}}_2(\underline{r}-\underline{r}')$ was presented as (4.29) in Section 4.2.2. On retaining the next highest–order term (i.e., to third–order in $\underline{\underline{\chi}}$), the Born series expansion (4.23) yields the third–order mass operator

approximation as [6, 57]

$$\underline{\underline{\Sigma}}(\underline{r}-\underline{r}') \approx \underline{\underline{\Sigma}}_2(\underline{r}-\underline{r}') + \underline{\underline{\Sigma}}_3(\underline{r}-\underline{r}'), \tag{4.118}$$

where

$$\underline{\underline{\Sigma}}_3(\underline{r}-\underline{r}') = \int \langle\, \underline{\underline{\chi}}(\underline{r}) \cdot \mathcal{P}\underline{\underline{\mathbf{G}}}_{BCM}(\underline{r}-\underline{r}'') \cdot \underline{\underline{\chi}}(\underline{r}'') \cdot \mathcal{P}\underline{\underline{\mathbf{G}}}_{BCM}(\underline{r}''-\underline{r}') \cdot \underline{\underline{\chi}}(\underline{r}') \,\rangle\, d^3\underline{r}''. \tag{4.119}$$

Some algebraic manipulations utilising (4.30) and (4.27) lead to

$$\underline{\underline{\Sigma}}_3(\underline{r}-\underline{r}') = \left(\frac{1}{1-f_a}\right)^3 \underline{\underline{\chi}}_a \cdot \left[\underline{\underline{\mathbf{J}}} - f_a\left(\underline{\underline{\mathbf{M}}}_1 + \underline{\underline{\mathbf{M}}}_2 + \underline{\underline{\mathbf{N}}}\right)\right] \cdot \underline{\underline{\chi}}_a, \tag{4.120}$$

in which

$$\underline{\underline{\mathbf{J}}} = \int \langle\, \theta_a(\underline{r})\,\theta_a(\underline{r}')\,\theta_a(\underline{r}'')\,\rangle\, \mathcal{P}\underline{\underline{\mathbf{G}}}_{BCM}(\underline{r}-\underline{r}'') \cdot \underline{\underline{\chi}}_a \cdot \mathcal{P}\underline{\underline{\mathbf{G}}}_{BCM}(\underline{r}''-\underline{r}')\, d^3\underline{r}'', \tag{4.121}$$

$$\underline{\underline{\mathbf{M}}}_1 = \int \langle\, \theta_a(\underline{r})\,\theta_a(\underline{r}'')\,\rangle\, \mathcal{P}\underline{\underline{\mathbf{G}}}_{BCM}(\underline{r}-\underline{r}'') \cdot \underline{\underline{\chi}}_a \cdot \mathcal{P}\underline{\underline{\mathbf{G}}}_{BCM}(\underline{r}''-\underline{r}')\, d^3\underline{r}'', \tag{4.122}$$

$$\underline{\underline{\mathbf{M}}}_2 = \int \langle\, \theta_a(\underline{r}'')\,\theta_a(\underline{r}')\,\rangle\, \mathcal{P}\underline{\underline{\mathbf{G}}}_{BCM}(\underline{r}-\underline{r}'') \cdot \underline{\underline{\chi}}_a \cdot \mathcal{P}\underline{\underline{\mathbf{G}}}_{BCM}(\underline{r}''-\underline{r}')\, d^3\underline{r}'', \tag{4.123}$$

$$\underline{\underline{\mathbf{N}}} = \left(\langle\, \theta_a(\underline{r})\,\theta_a(\underline{r}')\,\rangle - 2f_a^2\right) \int \mathcal{P}\underline{\underline{\mathbf{G}}}_{BCM}(\underline{r}-\underline{r}'') \cdot \underline{\underline{\chi}}_a \cdot \mathcal{P}\underline{\underline{\mathbf{G}}}_{BCM}(\underline{r}''-\underline{r}')\, d^3\underline{r}'', \tag{4.124}$$

are all implicit functions of $\underline{R}$.

In order to estimate $\underline{\underline{\mathbf{K}}}_{Dy0}$ from (4.66), we need to evaluate the Fourier transform of the mass operator evaluated at zero spatial frequency; i.e.,

$$\tilde{\underline{\underline{\Sigma}}}(0) = \int \underline{\underline{\Sigma}}(\underline{R})\, d^3\underline{R}; \tag{4.125}$$

thus, we now consider the evaluation of $\int \underline{\underline{\mathbf{J}}}\, d^3\underline{R}$, $\int \underline{\underline{\mathbf{M}}}_{1,2}\, d^3\underline{R}$ and $\int \underline{\underline{\mathbf{N}}}\, d^3\underline{R}$: We must first specify the second and third moments of $\theta_a(\underline{r})$. Consistent with [16], we choose (4.61) along with

$$\langle\, \theta_a(\underline{r})\,\theta_a(\underline{r}')\,\theta_a(\underline{r}'')\,\rangle = \begin{cases} f_a^3 & \min\{L_{12}, L_{13}, L_{23}\} > L \\ f_a & \max\{L_{12}, L_{13}, L_{23}\} \le L \\ \frac{1}{3}\left(f_a + 2f_a^3\right) & \text{one of } L_{12}, L_{13}, L_{23} \le L \\ \frac{1}{3}\left(2f_a + f_a^3\right) & \text{two of } L_{12}, L_{13}, L_{23} \le L \end{cases}, \tag{4.126}$$

where

$$L_{12} = |\underline{r}-\underline{r}'|, \qquad L_{13} = |\underline{r}-\underline{r}''|, \qquad L_{23} = |\underline{r}'-\underline{r}''|. \tag{4.127}$$

From (4.126) we have

$$\int \langle\, \theta_a(\underline{r})\, \theta_a(\underline{r}')\, \theta_a(\underline{r}'')\, \rangle\, d^3\underline{r}'' = \int_{L_{13}\leq L} h\, d^3\underline{r}'' + \int_{L_{23}\leq L} h\, d^3\underline{r}'' + \int \left[\, f_a^3 + h\, w(\underline{r}-\underline{r}')\,\right]\, d^3\underline{r}'', \tag{4.128}$$

where

$$w(\underline{r}-\underline{r}') = \begin{cases} 1 & |\underline{r}-\underline{r}'| \leq L \\ \\ 0 & |\underline{r}-\underline{r}'| > L \end{cases}, \tag{4.129}$$

and $h = (f_a - f_a^3)/3$. Thus, selecting the origin of our coordinate system at $\underline{r}'$, we have

$$\underline{\underline{\mathbf{J}}} = \int \left\{\, f_a^3 + h\, [\, w(\underline{r}'') + w(\underline{R}-\underline{r}'') + w(\underline{R})\,]\,\right\} \times \mathcal{P}\underline{\underline{\mathbf{G}}}_{BCM}(\underline{R}-\underline{r}'') \cdot \underline{\underline{\boldsymbol{\chi}}}_a \cdot \mathcal{P}\underline{\underline{\mathbf{G}}}_{BCM}(\underline{r}'')\, d^3\underline{r}''\,. \tag{4.130}$$

Focussing on the term $w(\underline{R})\, \mathcal{P}\underline{\underline{\mathbf{G}}}_{BCM}(\underline{R}-\underline{r}'') \cdot \underline{\underline{\boldsymbol{\chi}}}_a \cdot \mathcal{P}\underline{\underline{\mathbf{G}}}_{BCM}(\underline{r}'')$ in (4.130), we assume that

$$w(\underline{R})\underline{\underline{\mathbf{G}}}_{BCM}(\underline{r}'') \cdot \underline{\underline{\mathbf{G}}}_{BCM}(\underline{r}''-\underline{R}) \approx \underline{\underline{\mathbf{0}}}, \tag{4.131}$$

for $|\,\underline{r}''\,| \gg L$. This simplification is justified in Appendix A for isotropic chiral mediums. It is highly probable that (4.131) is also valid for weakly anisotropic mediums with diagonally–dominant constitutive dyadics. However, in the absence of appropriate Green function representations for such general mediums, this remains a conjecture. Using (4.131), we make the approximation

$$\underline{\underline{\mathbf{J}}} \approx \int \left\{\, f_a^3 + h\, [\, w(\underline{r}'') + w(\underline{R}-\underline{r}'') + w(\underline{r}'')\, w(\underline{R}-\underline{r}'')\,]\,\right\} \times \mathcal{P}\underline{\underline{\mathbf{G}}}_{BCM}(\underline{R}-\underline{r}'') \cdot \underline{\underline{\boldsymbol{\chi}}}_a \cdot \mathcal{P}\underline{\underline{\mathbf{G}}}_{BCM}(\underline{r}'')\, d^3\underline{r}''\,. \tag{4.132}$$

Taking the spatial Fourier transform of (4.132) and applying the convolution theorem [60], we find

$$\int \underline{\underline{\mathbf{J}}}\, d^3\underline{R} = h\left(\underline{\underline{\mathbf{V}}} \cdot \underline{\underline{\boldsymbol{\chi}}}_a \cdot \underline{\underline{\mathbf{P}}}^{\Gamma_0} + \underline{\underline{\mathbf{P}}}^{\Gamma_0} \cdot \underline{\underline{\boldsymbol{\chi}}}_a \cdot \underline{\underline{\mathbf{V}}} + \underline{\underline{\mathbf{P}}}^{\Gamma_0} \cdot \underline{\underline{\boldsymbol{\chi}}}_a \cdot \underline{\underline{\mathbf{P}}}^{\Gamma_0}\right) + f_a^3\, \underline{\underline{\mathbf{V}}} \cdot \underline{\underline{\boldsymbol{\chi}}}_a \cdot \underline{\underline{\mathbf{V}}}, \tag{4.133}$$

where

$$\underline{\underline{\mathbf{V}}} = \int \mathcal{P}\underline{\underline{\mathbf{G}}}_{BCM}(\underline{R})\, d^3\underline{R} \tag{4.134}$$

$$= \frac{1}{i\omega}\underline{\underline{\mathbf{K}}}^{-1}_{BCM} - \underline{\underline{\mathbf{D}}}, \tag{4.135}$$

by (4.16), (4.54) and (4.55).

We consider now the integration of $\underline{\underline{\mathbf{M}}}_1$: Introducing

$$s(\underline{R}-\underline{r}'') = \begin{cases} f_a & |\underline{R}-\underline{r}''| \leq L \\ \\ f_a^2 & |\underline{R}-\underline{r}''| > L \end{cases}, \tag{4.136}$$

we have

$$\underline{\underline{\mathbf{M}}}_1 = \int s(\underline{R}-\underline{r}'')\,\mathcal{P}\underline{\underline{\mathbf{G}}}_{BCM}(\underline{R}-\underline{r}'')\cdot\underline{\underline{\chi}}_a\cdot\mathcal{P}\underline{\underline{\mathbf{G}}}_{BCM}(\underline{r}'')\,d^3\underline{r}'', \quad (4.137)$$

where, as previously for $\underline{\mathbf{J}}$, we have selected the origin of our coordinate system at $\underline{r}'$. By means of Fourier transformations and application of the convolution theorem again, the integral

$$\int \underline{\underline{\mathbf{M}}}_1\,d^3\underline{R} = (f_a - f_a^2)\,\underline{\underline{\mathbf{P}}}^{\Gamma_0}\cdot\underline{\underline{\chi}}_a\cdot\underline{\underline{\mathbf{V}}} + f_a^2\,\underline{\underline{\mathbf{V}}}\cdot\underline{\underline{\chi}}_a\cdot\underline{\underline{\mathbf{V}}}, \quad (4.138)$$

emerges. It follows similarly that

$$\int \underline{\underline{\mathbf{M}}}_2\,d^3\underline{R} = (f_a - f_a^2)\,\underline{\underline{\mathbf{V}}}\cdot\underline{\underline{\chi}}_a\cdot\underline{\underline{\mathbf{P}}}^{\Gamma_0} + f_a^2\,\underline{\underline{\mathbf{V}}}\cdot\underline{\underline{\chi}}_a\cdot\underline{\underline{\mathbf{V}}}. \quad (4.139)$$

For $\underline{\underline{\mathbf{N}}}$, we have

$$\begin{aligned}\underline{\underline{\mathbf{N}}} \;=\; & (f_a - f_a^2)\int w(\underline{R})\,\mathcal{P}\underline{\underline{\mathbf{G}}}_{BCM}(\underline{R}-\underline{r}''')\cdot\underline{\underline{\chi}}_a\cdot\mathcal{P}\underline{\underline{\mathbf{G}}}_{BCM}(\underline{r}''')\,d^3\underline{r}''' \\ & - f_a^2\int \mathcal{P}\underline{\underline{\mathbf{G}}}_{BCM}(\underline{R}-\underline{r}''')\cdot\underline{\underline{\chi}}_a\cdot\mathcal{P}\underline{\underline{\mathbf{G}}}_{BCM}(\underline{r}''')\,d^3\underline{r}'''. \end{aligned} \quad (4.140)$$

Utilising the approximation of (4.132) and repeating the procedure of Fourier transformations, we find

$$\int \underline{\underline{\mathbf{N}}}\,d^3\underline{R} \;=\; (f_a - f_a^2)\,\underline{\underline{\mathbf{P}}}^{\Gamma_0}\cdot\underline{\underline{\chi}}_a\cdot\underline{\underline{\mathbf{P}}}^{\Gamma_0} - f_a^2\,\underline{\underline{\mathbf{V}}}\cdot\underline{\underline{\chi}}_a\cdot\underline{\underline{\mathbf{V}}}. \quad (4.141)$$

Finally, combining (4.133), (4.138), (4.139) and (4.141) into (4.120) and integrating, we find

$$\begin{aligned}&\int \underline{\underline{\mathbf{\Sigma}}}_3(\underline{R})\,d^3\underline{R} = \\ &\frac{f_a(1-2f_a)}{3(1-f_a)^2}\,\underline{\underline{\chi}}_a\cdot\left(\underline{\underline{\mathbf{V}}}\cdot\underline{\underline{\chi}}_a\cdot\underline{\underline{\mathbf{P}}}^{\Gamma_0} + \underline{\underline{\mathbf{P}}}^{\Gamma_0}\cdot\underline{\underline{\chi}}_a\cdot\underline{\underline{\mathbf{V}}} + \underline{\underline{\mathbf{P}}}^{\Gamma_0}\cdot\underline{\underline{\chi}}_a\cdot\underline{\underline{\mathbf{P}}}^{\Gamma_0}\right)\cdot\underline{\underline{\chi}}_a. \end{aligned} \quad (4.142)$$

4.5.2 Numerical results

Using the zeroth–, second– and third–order–approximated SPFT in the long–wavelength regime, we investigate the constitutive properties of two examples of HCM. The volume fraction $f_a = 0.3$ and an angular frequency $\omega = 2\pi \times 10^{10}$ rad s^{-1} are selected for all numerical results presented in this section.

A. Isotropic chiral HCM

In the first example, component phase a was chosen to be an isotropic chiral material with constitutive relations

$$\underline{\underline{\epsilon}}^a = \epsilon_0\,\epsilon^a\,\underline{\underline{I}}, \qquad \underline{\underline{\xi}}^a = -\underline{\underline{\zeta}}^a = i\sqrt{\epsilon_0\mu_0}\,\xi^a\,\underline{\underline{I}}, \qquad \underline{\underline{\mu}}^a = \mu_0\,\mu^a\,\underline{\underline{I}}, \quad (4.143)$$

and parameter values

$$\epsilon^a = \delta\,(3 + i\,1.5)\,, \qquad \xi^a = \delta\,(1.5 + i\,)\,, \qquad \mu^a = \delta\,(2 + i\,0.8)\,, \tag{4.144}$$

where $\delta = 10$, 20 and 30. Component phase b was taken to be free space. The parameter δ provides the means to vary the constitutive contrast between the component phases. The relative permittivity ϵ^{HCM} of the resulting isotropic chiral HCM is plotted as a function of correlation length L in Figure 4.8. The values for the zeroth–order approximation—which are identical to those values calculated using the Br homogenisation formalism—are independent of correlation length. Furthermore, the calculated values for all orders of approximation coincide at $L = 0$. The HCM magnetoelectric parameter ξ^{HCM} and relative permeability μ^{HCM} behave in similar manner to the relative permittivity ϵ^{HCM} and are displayed in Figures 4.9 and 4.10, respectively.

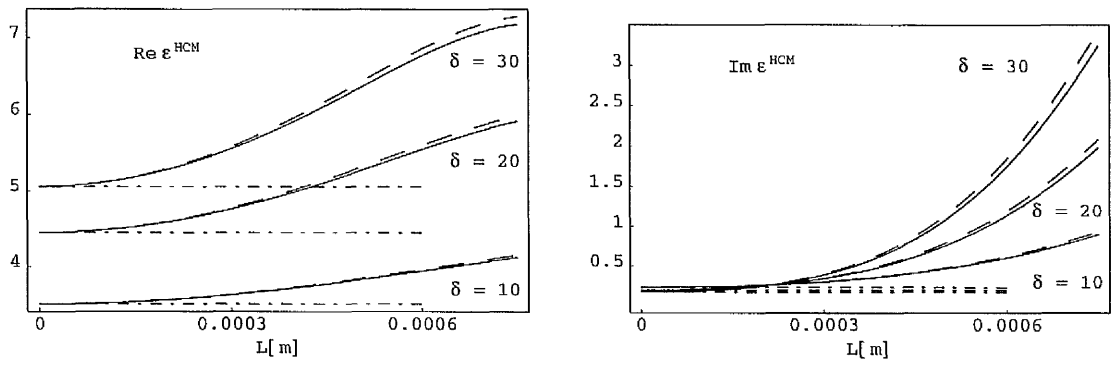

Figure 4.8: Real and imaginary parts of the HCM relative permittivity, calculated using the zeroth–, second– and third–order mass operator approximations, plotted against correlation length L for $\delta = 10$, 20, 30. At $L = 0$, the calculated values for all orders of approximation coincide. Key: broken dashed lines indicate zeroth–order values; solid lines indicate second–order values; dashed lines indicate third–order values.

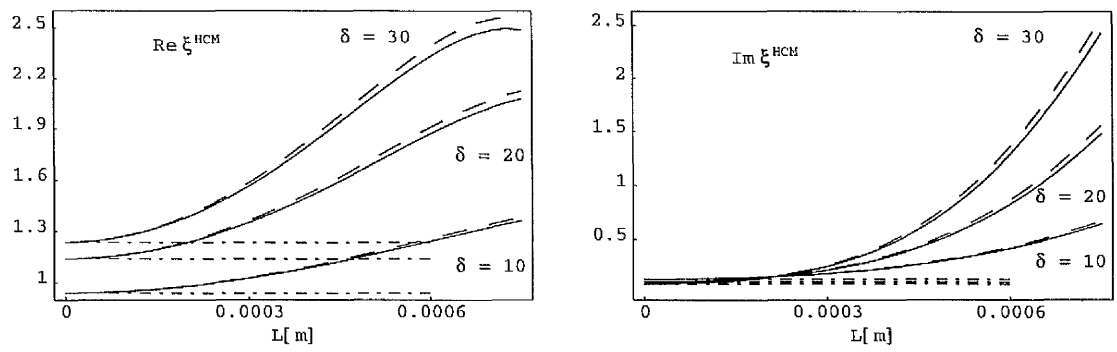

Figure 4.9: As for Figure 4.8, but the plotted values are of the HCM magnetoelectric parameter.

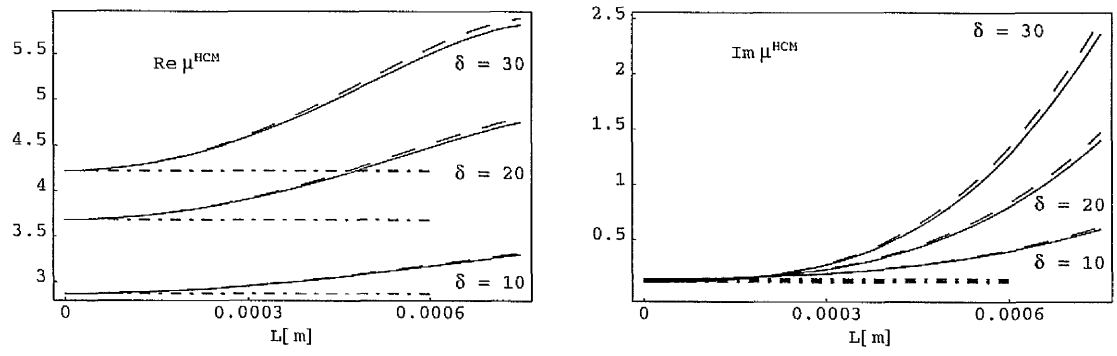

Figure 4.10: As for Figure 4.8, but the plotted values are of the HCM relative permeability.

Under the long–wavelength regime, we require $Q \ll 1$, where

$$Q = \frac{\max W_k}{2\pi} L \,. \tag{4.145}$$

For the present case in which the BCM is an *isotropic chiral* comparison medium,

$$W_k = \{ |\gamma^+|, |\gamma^-| \}, \tag{4.146}$$

where $\gamma^{\pm}$ denote the left– and right–handed wavenumbers in the BCM [33]. We find for the example illustrated in Figures 4.8 – 4.10, $Q = 0.1$ at $L = 5.1 \times 10^{-4}$ m for $\delta = 30$; at $L = 5.7 \times 10^{-4}$ m for $\delta = 20$; and at $L = 7.3 \times 10^{-4}$ m for $\delta = 10$. These limits establish the applicability ranges of the presented formalism.

B. Faraday chiral HCM

For our second example, we again selected the isotropic chiral medium of (4.143) and (4.144) as component phase a. A magnetically gyrotropic medium characterised by

$$\underline{\underline{\epsilon}}^b = \epsilon_0 \, \epsilon^b \, \underline{\underline{I}}, \qquad \underline{\underline{\xi}}^b = \underline{\underline{\zeta}}^b = \underline{\underline{0}}, \tag{4.147}$$

$$\underline{\underline{\mu}}^b = \mu_0 \left[\mu^b \, \underline{\underline{I}} - i\mu_g^b \, \underline{\hat{u}}_z \times \underline{\underline{I}} + (\mu_u^b - \mu^b) \, \underline{\hat{u}}_z \, \underline{\hat{u}}_z \right], \tag{4.148}$$

was chosen as component phase b, along with the parameter values $\epsilon^b = 1.2 + i0.4$, $\mu^b = 2.5 + i0.5$, $\mu_u^b = 2.1 + i0.4$ and $\mu_g^b = 0.2 + i0.1$.

The resulting HCM, with the constitutive relations

$$\underline{\underline{\epsilon}}^{HCM} = \epsilon_0 \left[\epsilon^{HCM} \, \underline{\underline{I}} - i\epsilon_g^{HCM} \, \underline{\hat{u}}_z \times \underline{\underline{I}} + (\epsilon_u^{HCM} - \epsilon^{HCM}) \, \underline{\hat{u}}_z \, \underline{\hat{u}}_z \right], \tag{4.149}$$

$$\underline{\underline{\xi}}^{HCM} = i\sqrt{\epsilon_0 \mu_0} \left[\xi^{HCM} \, \underline{\underline{I}} - i\xi_g^{HCM} \, \underline{\hat{u}}_z \times \underline{\underline{I}} + (\xi_u^{HCM} - \xi^{HCM}) \, \underline{\hat{u}}_z \, \underline{\hat{u}}_z \right], \tag{4.150}$$

$$\underline{\underline{\zeta}}^{HCM} = -\underline{\underline{\xi}}^{HCM}, \tag{4.151}$$

$$\underline{\underline{\mu}}^{HCM} = \mu_0 \left[\mu^{HCM} \, \underline{\underline{I}} - i\mu_g^{HCM} \, \underline{\hat{u}}_z \times \underline{\underline{I}} + (\mu_u^{HCM} - \mu^{HCM}) \, \underline{\hat{u}}_z \, \underline{\hat{u}}_z \right], \tag{4.152}$$

belongs to the general class of *Faraday chiral mediums* [12, 34]. Such HCMs have been comprehensively studied using both the MG and Br formalism [35, 11] (see Chapter 2),

as well as the bilocally–approximated SPFT [17] (see Section 4.3.3). The calculated HCM relative permittivity parameters ϵ^{HCM}, ϵ_u^{HCM} and ϵ_g^{HCM}; magnetoelectric parameters ξ^{HCM}, ξ_u^{HCM} and ξ_g^{HCM}; and relative permeability parameters μ^{HCM}, μ_u^{HCM} and μ_g^{HCM}, are graphed as functions of correlation length L in Figures 4.11, 4.12 and 4.13, respectively. For clarity, the zeroth–order approximation values—which are constant with respect to L and are equal to the second– and third–order values in the limit $L \to 0$—are not displayed. The BCM lies in the category of weakly anisotropic mediums with diagonally–dominant constitutive dyadics, for which we anticipate that the simplification (4.131) is valid.

Since the Faraday chiral HCM is a Lorentz–nonreciprocal medium [73], the corresponding dispersion equation yields four distinct wavenumbers: γ_1, γ_2, γ_3 and γ_4. Accordingly, here we have

$$W_k = \{ |\gamma_1|, |\gamma_2||\gamma_3|, |\gamma_4| \}, \tag{4.153}$$

and we find $Q = 0.1$ at $L = 3.6 \times 10^{-4}\,\mathrm{m}$ for $\delta = 30$; at $L = 4.3 \times 10^{-4}\,\mathrm{m}$ for $\delta = 20$; and at $L = 5.5 \times 10^{-4}\,\mathrm{m}$ for $\delta = 10$.

4.5.3 Conclusion

It is clear from Figures 4.8 – 4.13 that the third–order–approximated SPFT yields significantly different results from the bilocally–approximated SPFT only as either (i) the correlation length L becomes electrically larger and/or (ii) the constitutive contrast between the component phases a and b increases. However, in case (i), the long–wavelength approximation begins to lose validity; while in case (ii), spatial fluctuations in the generalised polarisability $\underline{\underline{\chi}}(\underline{r})$ are likely to become strong. Thus, in either instance the addition of the third–order term $\underline{\underline{\Sigma}}_3(\underline{R})$ to the mass operator is not significant, provided the basic assumptions underlying the long–wavelength SPFT remain valid. We therefore conclude that the SPFT converges at the level of the bilocal approximation for isotropic chiral mediums, as well as for chiroferrite mediums which are both weakly uniaxial and weakly gyrotropic.

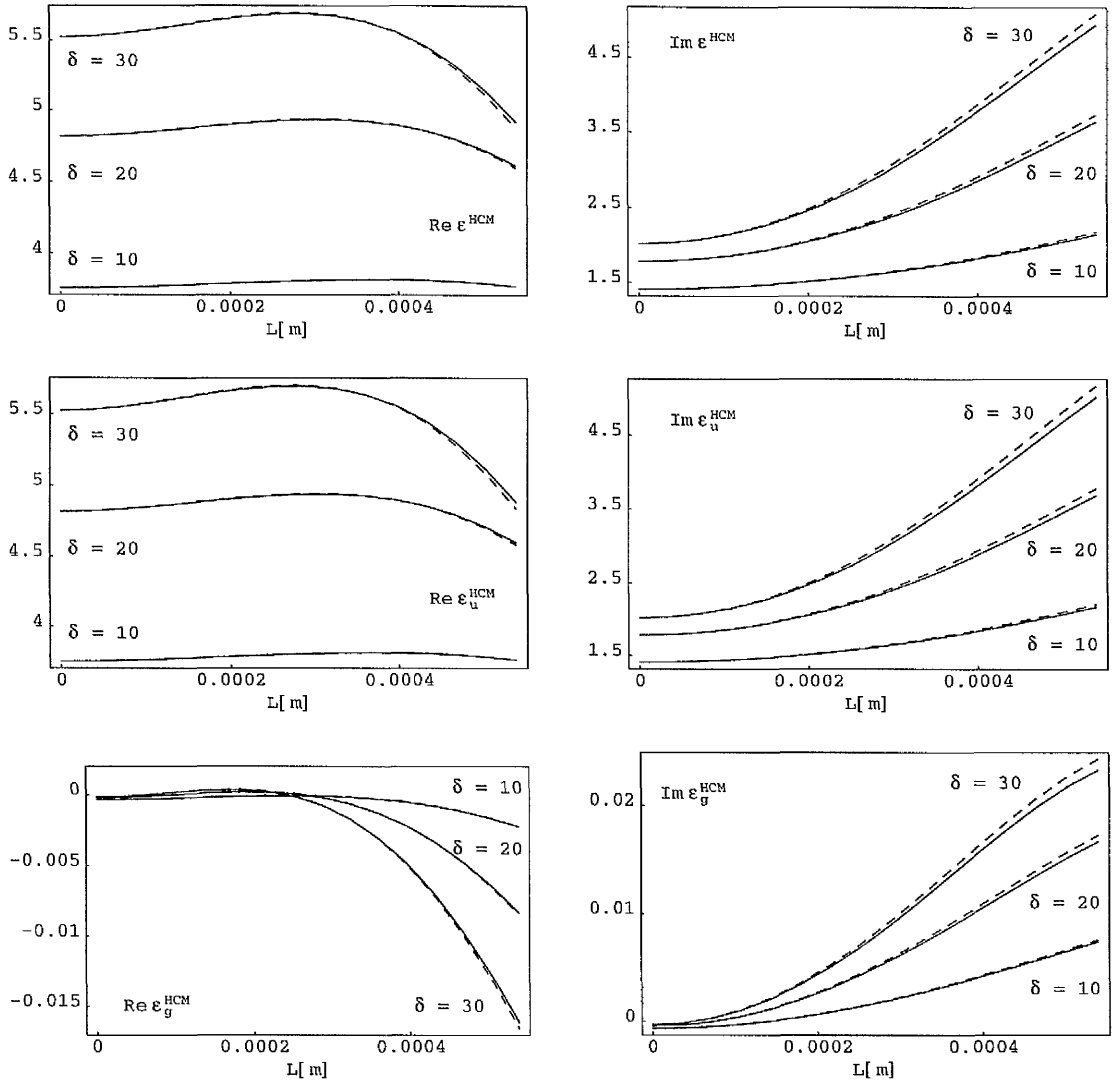

Figure 4.11: Real and imaginary parts of the HCM relative permittivity parameters ϵ^{HCM}, ϵ_u^{HCM} and ϵ_g^{HCM}, calculated using the second– and third–order mass operator approximations, plotted against correlation length L for $\delta = 10, 20, 30$. Key: solid lines indicate second–order values; dashed lines indicate third–order values.

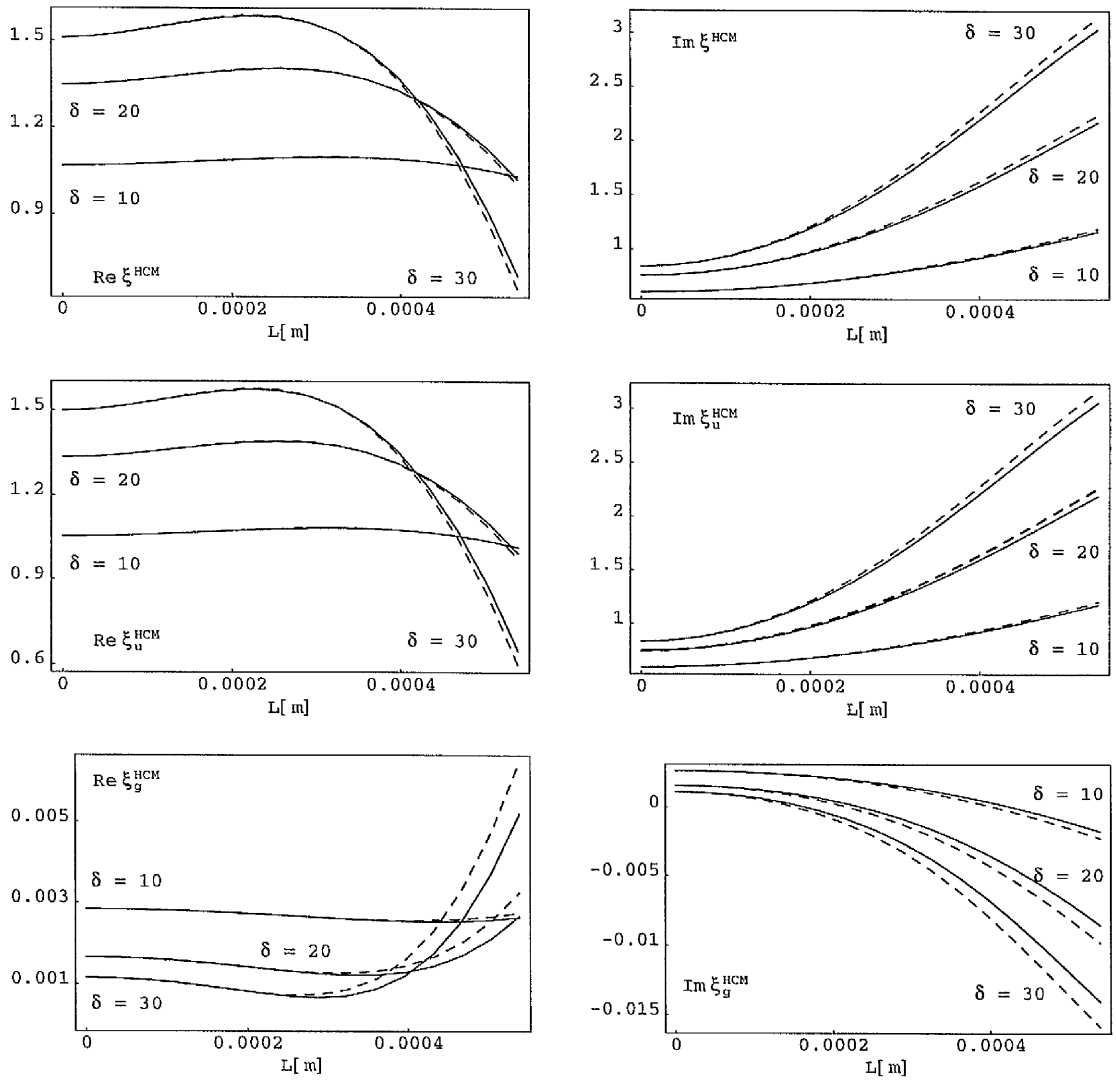

Figure 4.12: As for Figure 4.11, but the plotted values are of the HCM magnetoelectric parameters ξ^{HCM}, ξ_u^{HCM} and ξ_g^{HCM}.

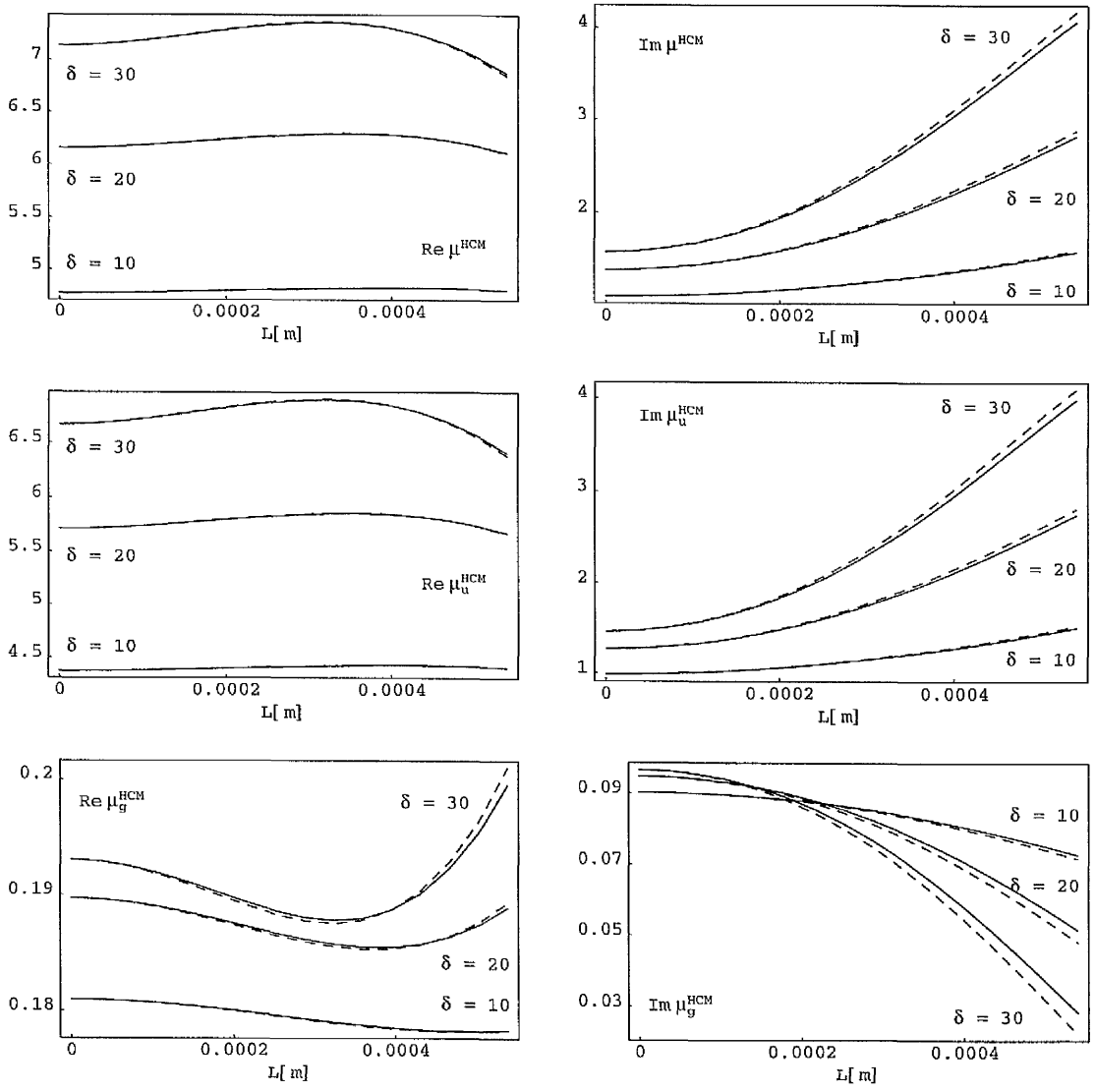

Figure 4.13: As for Figure 4.11, but the plotted values are of the HCM permeability parameters μ^{HCM}, μ_u^{HCM} and μ_g^{HCM}.

Chapter 5

Discussion

5.1 General remarks

In the consideration of electromagnetic properties of materials, the concept of *homogenisation* — combining multiple (simple) components into an effectively single complex structure — is extremely important, both scientifically and technologically. This is particularly so in the case of the most general linear HCMs, namely bianisotropic HCMs. While the occurrence of fully bianisotropic materials in nature is rare, they may be readily synthesised through the homogenisation of relatively simple materials.

Through the work of this thesis, the theory of linear HCMs has been advanced on two fronts:

(i) By utilising the well–established MG and Br homogenisation formalisms, along with the recently–developed IMG and DMG formalisms, the constitutive properties of complex HCM structures were revealed and related to the properties of their constituents. Specifically, in Chapter 2, a detailed parametric study of a chiroplasma HCM revealed a composite structure more general than that of the Faraday chiral mediums [11]. This general structure — which has not hitherto been described in the scientific literature — arises when the component phases possess non–spherical topology. The issue of biaxiality in HCMs was fully explored in Chapter 3. Biaxial HCMs were shown to arise when the component phases present two noncollinear distinguished axes; both electromagnetic and topological distinguished axes were considered for nondissipative dielectric [13], dissipative dielectric–magnetic [14] and bianisotropic [15] HCMs. Generalised biaxial HCM structures in which the principal axes of the real and imaginary parts of the constitutive dyadics do not coincide were described. Furthermore, for HCMs arising from component phases with non–orthogonal distinguished axes, methods of achieving orthorhombic biaxiality were presented.

(ii) The bilocally–approximated SPFT was developed for bianisotropic HCMs [16] in Chapter 4. The SPFT represents a significant advance over the MG and

Br homogenisation formalisms, through accommodating a more comprehensive description of the distributional statistics of the component phases. In particular, the SPFT predicts scattering losses (unlike the MG and Br formalisms) and in its simplest implementations (i.e. either as the correlation length $L \to 0$ or utilising the zero–order mass operator), the SPFT reduces to the Br formalism. Detailed numerical studies highlighted the particular influence of the correlation length, as compared to that of the topology and orientation of the component phases [17]. Additionally, the choice of covariance function was shown to have only a secondary influence as compared with the effects of the correlation length [18]. Finally, through calculating the third–order mass operator approximation [19], the convergence of the bilocally–approximated SPFT was demonstrated for isotropic chiral HCMs, as well as for chiroferrite HCMs which are both weakly uniaxial and weakly gyrotropic.

5.2 Further studies

The work of this thesis pertains exclusively to the linear electromagnetic properties of HCMs. Within the linear regime, an area which requires further work is the convergence of the mass operator series in the SPFT for anisotropic and bianisotropic mediums. Convergence at the level of the bilocal approximation was demonstrated in Section 4.5 for isotropic chiral HCMs. Verification of the mass operator convergence for more general mediums may require explicit expressions for the corresponding dyadic Green functions; however, such explicit Green function representations are not available [24]. Another area of future development for the linear SPFT lies in the establishment of a homogenisation formalism appropriate to component phases with needle–shaped or pillbox–shaped topologies. Earlier, Lakhtakia *et al.* [74] implemented the Br formalism for such a homogenisation scenario in uniaxial dielectric materials. We remark that the depolarisation dyadics corresponding to cylindrical exclusion volumes, derived recently for anisotropic dielectric mediums [30], may well facilitate such a study.

Considerably greater scope for extending the studies described herein lies within the realm of nonlinear materials. The MG formalism has been developed for weakly nonlinear bianisotropic HCMs [75]. However, as in the linear regime, the nonlinear MG is applicable only to dilute composites—a nonlinear IMG or DMG formalism, applicable to arbitrary concentrations of inclusion particles, has yet to emerge. The Br formalism has recently been implemented for weakly nonlinear anisotropic dielectric composites [76]; more general Br implementations have not been reported as yet. As regards the nonlinear bilocally–approximated SPFT, only the simplest homogenisation scenario, namely that relating to cubically–nonlinear isotropic dielectric HCMs, has been developed to date [77]. Thus, there is clearly considerable scope for the advancement of the SPFT in the nonlinear regime. Furthermore, such extensions to the SPFT

are not restricted to only electromagnetic properties. The SPFT has previously been implemented for acoustic wave propagation [78] and elastodynamic wave propagation [79] in linear composite materials. The prospect of developing a comprehensive non-linear SPFT, capable of describing the electromagnetic, acoustic and elastodynamic constitutive properties of composite materials, is highly desirable, and may well lead to interesting applications in biological environments, for example.

Appendix A

The assumption that $w(\underline{R})\,\underline{\underline{\mathbf{G}}}_{BCM}(\underline{r}) \cdot \underline{\underline{\mathbf{G}}}_{BCM}(\underline{R}-\underline{r})$ for $|\,\underline{r}\,| \gg L$ is negligible in comparison with its evaluation for $|\,\underline{r}\,| < L$, where $w(\underline{R})$ is defined as the step function (4.129), is made in Section 4.5.1, equation (4.131). Here we justify this assumption for isotropic chiral BCMs. To do so, we express the 6×6 dyadic Green function $\underline{\underline{\mathbf{G}}}_{BCM}(\underline{R})$ in terms of 3×3 dyadics as

$$\underline{\underline{\mathbf{G}}}_{BCM}(\underline{R}) = \left(\begin{array}{cc} \underline{\underline{G}}^{ee}_{BCM}(\underline{R}) & \underline{\underline{G}}^{em}_{BCM}(\underline{R}) \\ \underline{\underline{G}}^{me}_{BCM}(\underline{R}) & \underline{\underline{G}}^{mm}_{BCM}(\underline{R}) \end{array} \right) . \tag{1}$$

We begin by considering the isotropic dielectric–magnetic case: the 3×3 constitutive dyadics are

$$\underline{\underline{\epsilon}}_{BCM} = \epsilon\,\underline{\underline{I}}, \qquad \underline{\underline{\mu}}_{BCM} = \mu\,\underline{\underline{I}}, \qquad \underline{\underline{\xi}}_{BCM} = \underline{\underline{\zeta}}_{BCM} = \underline{\underline{0}}, \tag{2}$$

and the wavenumber $k = \omega\sqrt{\epsilon\mu}$. An explicit representation of $\underline{\underline{G}}^{ee}_{BCM}(\underline{R})$ is available as [80]

$$\begin{aligned} \underline{\underline{G}}^{ee}_{BCM}(\underline{R}) \;=\; & \frac{1}{i\omega\epsilon}\Big[\frac{1}{3}\,\delta(\underline{R})\,\underline{\underline{I}} - \frac{1}{4\pi}\,(-1+ikR+k^2R^2)\,\frac{\exp(ikR)}{R^3}\,\underline{\underline{I}} \\ & -\frac{1}{4\pi}\,(3-3ikR-k^2R^2)\,\frac{\exp(ikR)}{R^3}\,\underline{\hat{R}}\,\underline{\hat{R}}\Big]. \end{aligned} \tag{3}$$

For $r \gg L$, and introducing constants α, β and γ of order unity, we have

$$\begin{aligned} \frac{\Big|\Big[\underline{\underline{G}}^{ee}_{BCM}(\underline{r})\Big]_{jj}\Big|}{\Big|\Big[\underline{\underline{G}}^{ee}_{BCM}(L\,\underline{\hat{r}})\Big]_{jj}\Big|} \;&\approx\; \frac{\dfrac{\alpha+\beta kr+\gamma k^2r^2}{r^3}}{\dfrac{\alpha+\beta kL+\gamma k^2L^2}{L^3}} \qquad (j=1,2,3) \\ &\approx\; \left(\frac{L^3}{r^3}\right)\frac{\alpha+\beta kr+\gamma k^2r^2}{\alpha} \\ &=\; \frac{L^3}{r^3}+\beta(kL)\frac{L^2}{r^2}+\gamma(kL)^2\frac{L}{r} \\ &\approx\; 0\,, \end{aligned} \tag{4}$$

since $|\,kL\,| \ll 1$ in the long–wavelength regime.

For the case of the $\underline{\underline{G}}^{ee}_{BCM}(\underline{R}-\underline{r})$ term, we need only consider $R \le L$ (since $w(\underline{R}) = 0$ for $R > L$). Again, for $r \gg L$ and with constants α, β and γ of order unity,

we have

$$\frac{\left|\left[\underline{\underline{G}}^{ee}_{BCM}(\underline{R}-\underline{r})\right]_{jj}\right|}{\left|\left[\underline{\underline{G}}^{ee}_{BCM}(\underline{R}-L\hat{\underline{r}})\right]_{jj}\right|} \approx \frac{\dfrac{\alpha+\beta k(R-r)+\gamma k^2(R-r)^2}{(R-r)^3}}{\dfrac{\alpha+\beta k(R-L)+\gamma k^2(R-L)^2}{(R-L)^3}} \qquad (j=1,2,3)$$

$$\approx \left(\frac{(R-L)^3}{(R-r)^3}\right)\frac{\alpha+\beta k(R-r)+\gamma k^2(R-r)^2}{\alpha}$$

$$= \frac{(R-L)^3}{(R-r)^3} + \beta\left[k(R-L)\right]\frac{(R-L)^2}{(R-r)^2} + \gamma\left[k(R-L)\right]^2\frac{R-L}{R-r}$$

$$\approx 0\,, \qquad (5)$$

since $(L-R) \ll (r-R)$. For the isotropic dielectric–magnetic case, the corresponding terms for $\underline{\underline{G}}^{mm}_{BCM}(\underline{R})$ behave similarly to $\underline{\underline{G}}^{ee}_{BCM}(\underline{R})$; the corresponding terms for $\underline{\underline{G}}^{em}_{BCM}(\underline{R})$ and $\underline{\underline{G}}^{me}_{BCM}(\underline{R})$ do not contribute to the analysis of Section 4.5 as they disappear upon integration.

For an isotropic chiral medium, the diagonal terms of $\underline{\underline{G}}^{ee}_{BCM}(\underline{R})$, $\underline{\underline{G}}^{em}_{BCM}(\underline{R})$, $\underline{\underline{G}}^{me}_{BCM}(\underline{R})$ and $\underline{\underline{G}}^{mm}_{BCM}(\underline{R})$ are all of the same form as those in (3) [33], while the integrals of the off–diagonal terms are null–valued. Therefore, we have that $w(\underline{R})\underline{\mathbf{G}}_{BCM}(\underline{r}) \cdot \underline{\mathbf{G}}_{BCM}(\underline{R}-\underline{r})$ for $|\underline{r}| \gg L$ is negligible in comparison with its evaluation for $|\underline{r}| < L$, for an isotropic chiral medium.

Bibliography

[1] A. Lakhtakia (ed.), *Selected Papers on Linear Optical Composite Materials*. SPIE Optical Engineering Press, Bellingham, WA, USA, 1996.

[2] A. Sihvola, *Electromagnetic Mixing Formulas and Applications*. IEE, Stevenage, UK, 1999.

[3] A. Lakhtakia, "On direct and indirect scattering approaches for the homogenization of particulate composites", *Microw. Opt. Technol. Lett.* **25**, 53–56 (2000).

[4] O.N. Singh and A. Lakhtakia (eds.), *Electromagnetic Fields in Unconventional Materials and Structures*. Wiley, New York, USA, 2000.

[5] L. Ward, *The Optical Constants of Bulk Materials and Films*. Adam Hilger, Bristol, UK, 1988.

[6] L. Tsang, J.A. Kong and R.T. Shin, *Theory of Microwave Remote Sensing*. Wiley, New York, USA, 1985.

[7] C.F. Bohren and D.R. Huffman, *Absorption and Scattering of Light by Small Particles*. Wiley, New York, USA, 1983.

[8] A. Lakhtakia, "Incremental Maxwell Garnett formalism for homogenizing particulate composite media", *Microw. Opt. Technol. Lett.* **17**, 276–279 (1998).

[9] B. Michel, A. Lakhtakia, W.S. Weiglhofer and T.G. Mackay, "Incremental and differential Maxwell Garnett formalisms for bi–anisotropic composites", *Compos. Sci. Technol.* **61**, 13–18 (2001).

[10] B. Michel, "Recent developments in the homogenization of linear bianisotropic composite materials", in: O.N. Singh and A. Lakhtakia (eds.), *Electromagnetic Fields in Unconventional Materials and Structures*. Wiley, New York, USA, 2000, pp39–82.

[11] W.S. Weiglhofer and T.G. Mackay, "Numerical studies on the constitutive parameters of a chiroplasma composite medium", *Arch. Elektron. Übertr.* **54**, 259–265 (2000).

[12] N. Engheta, D.L. Jaggard and M.W. Kowarz, "Electromagnetic waves in Faraday chiral media", *IEEE Trans. Antennas Propagat.* **40**, 367–374 (1992).

[13] T.G. Mackay and W.S. Weiglhofer, "Homogenization of biaxial composite materials: nondissipative dielectric properties", *Electromagnetics* **21**, 15–26 (2001).

[14] T.G. Mackay and W.S. Weiglhofer, "Homogenization of biaxial composite materials: dissipative anisotropic properties", *J. Opt. A: Pure Appl. Opt.* **2**, 426–432 (2000).

[15] T.G. Mackay and W.S. Weiglhofer, "Homogenization of biaxial composite materials: bianisotropic properties", *J. Opt. A: Pure Appl. Opt.* **3**, 45–52 (2001).

[16] T.G. Mackay, A. Lakhtakia and W.S. Weiglhofer, "Strong–property–fluctuation theory for homogenization of bianisotropic composites: formulation", *Phys. Rev. E* **62**, 6052–6064 (2000); erratum **63**, 049901(E) (2001).

[17] T.G. Mackay, A. Lakhtakia and W.S. Weiglhofer, "Ellipsoidal topology, orientation diversity and correlation length in bianisotropic composite mediums", *Arch. Elektron. Übertr.* **55**, 243–251 (2001).

[18] T.G. Mackay, A. Lakhtakia and W.S. Weiglhofer, "Homogenisation of similarly oriented, metallic, ellipsoidal inclusions using the bilocal–approximated strong–property–fluctuation theory", *Opt. Comm.* **197**, 89–95, (2001).

[19] T.G. Mackay, A. Lakhtakia and W.S. Weiglhofer, "Third–order implementation and convergence of the strong–property–fluctuation theory in electromagnetic homogenisation", Department of Mathematics, University of Glasgow, preprint 2001/11 (2001).

[20] J.D. Jackson, *Classical Electrodynamics.* 2nd Ed., Wiley, New York, USA, 1975.

[21] A. Lakhtakia,"Frequency–dependent continuum electromagnetic properties of a gas of scattering centers", in: M. Evans and S. Kielich (eds.), *Modern Nonlinear Optics, Part 2.* Advances in Chemical Physics Series, Vol. LXXXV, Wiley, New York, USA, 1993, pp311–359.

[22] W.S. Weiglhofer, "A perspective on bianisotropy and Bianisotropics '97", *Int. J. Appl. Electromagn. Mech.* **9**, 93–101 (1998).

[23] W.S. Weiglhofer, "Frequency–dependent dyadic Green functions for bianisotropic media", in: T.W. Barrett and D.M. Grimes (eds.), *Advanced Electromagnetism: Foundations, Theory, Applications.* World Scientific, Singapore, 1995, pp376–389.

[24] W.S. Weiglhofer, "Analytic methods and free–space dyadic Green's functions", *Radio Sci.* **28**, 847–857 (1993).

[25] W.S. Weiglhofer and A. Lakhtakia, "Uniformity constraint on recently conceptualized linear uniaxial bianisotropic media", *Electron. Lett.* **30**, 1656–1657 (1994).

[26] A. Lakhtakia and W.S. Weiglhofer, "Lorentz covariance, Occam's razor, and a constraint on linear constitutive relations", *Phys. Lett.* **213**, 107–111 (1996); erratum **222**, 459 (1996).

[27] W.S. Weiglhofer and A. Lakhtakia, "The Post constraint revisited", *Arch. Elektron. Übertr.* **52**, 276–279 (1998).

[28] H.C. Chen, *Theory of Electromagnetic Waves.* TechBooks, Fairfax, VA, USA, 1993.

[29] B. Michel and W.S. Weiglhofer, "Pointwise singularity of dyadic Green function in a general bianisotropic medium", *Arch. Elektron. Übertrag.* **51**, 219–223 (1997); erratum **52**, 31 (1998).

[30] W.S. Weiglhofer and T.G. Mackay, "Needles and pillboxes in anisotropic mediums", *IEEE–Trans. Antennas Propagat.* **49**, (2001) (in press).

[31] W.S. Weiglhofer, A. Lakhtakia and B. Michel, "Maxwell Garnett and Bruggeman formalisms for a particulate composite with bianisotropic host medium", *Microw. Opt. Technol. Lett.* **15**, 263–266 (1997); erratum **22**, 221 (1999).

[32] B. Michel, A. Lakhtakia and W.S. Weiglhofer, "Homogenization of linear bianisotropic particulate composite media — Numerical studies", *Int. J. Appl. Electromag. Mech.* **9**, 167–178 (1998); erratum **10**, 537–538 (1999).

[33] A. Lakhtakia, *Beltrami Fields in Chiral Media.* World Scientific, Singapore, 1994.

[34] W.S. Weiglhofer and A. Lakhtakia, "The correct constitutive relations of chiroplasmas and chiroferrites", *Microw. Opt. Technol. Lett.* **17**, 405–408 (1998).

[35] W.S. Weiglhofer, A. Lakhtakia and B. Michel, "On the constitutive parameters of a chiroferrite composite medium", *Microw. Opt. Technol. Lett.* **18**, 342–345 (1998).

[36] L.B. Felsen and N. Marcuvitz, *Radiation and Scattering of Waves.* IEEE Press, Piscataway, NJ, USA, 1994.

[37] A. Lakhtakia and W.S. Weiglhofer, "On electromagnetic fields in a linear medium with gyrotropic–like magnetoelectric properties", *Microw. Opt. Technol. Lett.* **15**, 168–170 (1997).

[38] M. Born M and E. Wolf, *Principles of Optics.* 7th Ed., Cambridge University Press, Cambridge, UK, 1999.

[39] J.F. Nye, *Physical Properties of Crystals.* Oxford University Press, London, UK, 1957.

[40] D.I. Kaklamani and N.K. Uzunoglu, "Radiation properties of a biaxially anisotropic dielectric sphere excited by a dipole", *Electromagnetics* **15**, 631–647 (1995).

[41] W.S. Weiglhofer and A. Lakhtakia, "On singularities of dyadic Green functions and long–wavelength scattering", *Electromagnetics* **15**, 209–222 (1995).

[42] P.G. Cottis, C.N. Vazouras and C. Spyrou, "Green's function for an unbounded biaxial medium in cylindrical coordinates", *IEEE Trans. Antennas Propagat.* **47**, 195–199 (1999).

[43] W.S. Weiglhofer, "Electromagnetic depolarization dyadics and elliptic integrals", *J. Phys. A: Math. Gen.* **31**, 7191–7196 (1998).

[44] M.A. Dreger, "Optical beam propagation in biaxial crystals", *J. Opt. A.: Pure Appl. Opt.* **1**, 601–616 (1999).

[45] I. Abdulhalim, "2×2 matrix summation method for multiple reflections and transmissions in a biaxial slab between two anisotropic media", *Opt. Comm.* **163**, 9–14 (1999).

[46] I. Abdulhalim, "Analytic propagation matrix method for linear optics of arbitrary biaxial layered media", *J. Opt. A.: Pure Appl. Opt.* **1**, 646–653 (1999).

[47] I. Abdulhalim, "Exact 2×2 matrix method for the transmission and reflection at the interface between two arbitrarily oriented biaxial crystals", *J. Opt. A.: Pure Appl. Opt.* **1**, 655–661 (1999).

[48] W.S. Weiglhofer and A. Lakhtakia, "On electromagnetic waves in biaxial bianisotropic media", *Electromagnetics* **19**, 351–362 (1999).

[49] O. Wiener, "Die Theorie des Mischkörpers für das Feld der Stationären Strömung", *Abh. Math.–Phys. Kl. Sächs.* **32**, 507–604 (1912).

[50] J.A. Sherwin, A. Lakhtakia and B. Michel, "Homogenization of similarly oriented, metallic, ellipsoidal inclusions using the Bruggeman formalism", *Opt. Comm.* **178**, 267–273 (2000).

[51] J.A. Kong, *Electromagnetic Wave Theory*. Wiley, New York, USA, 1986.

[52] N.W. Ashcoft and N.D. Mermin, *Solid State Physics*. Saunders College, Philadelphia, Pa, USA, 1986.

[53] L. Tsang and J.A. Kong, "Scattering of electromagnetic waves from random media with strong permittivity fluctuations", *Radio Sci.* **16**, 303–320 (1981).

[54] N.P. Zhuck, "Strong–fluctuation theory for a mean electromagnetic field in a statistically homogeneous random medium with arbitrary anisotropy of electrical and statistical properties", *Phys. Rev. B* **50**, 15636–15645 (1994).

[55] B. Michel and A. Lakhtakia, "Strong–property–fluctuation theory for homogenizing chiral particulate composites", *Phys. Rev. E* **51**, 5701–5707 (1995).

[56] H. Hochstadt, *Integral Equations*. Wiley, New York, USA, 1973.

[57] U. Frisch, "Wave propagation in random media." in: A.T. Bharucha–Reid (ed.), *Probabilistic Methods in Applied Mathematics, Vol. 1*. Academic Press, London, UK, 1970, pp75–198.

[58] V.V. Tamoikin, "The average field in a medium having strong anisotropic inhomogeneities", *Radiophys. Quantum Electron.* **14**, 228–233 (1971).

[59] A. Stogryn, "The bilocal approximation for the electric field in the strong fluctuation theory", *IEEE Trans. Antennas Propagat.* **31**, 985–986 (1983).

[60] G.B. Arfken and H.J. Weber, *Mathematical Methods for Physicists*. 4th Ed., Academic Press, London, UK, 1995.

[61] L. Tsang, J.A. Kong and R.W. Newton, "Application of strong fluctuation random medium theory to scattering of electromagnetic waves from a half–space of dielectric mixture", *IEEE Trans. Antennas Propagat.* **30**, 292–302 (1982).

[62] B. Michel, "A Fourier space approach to the pointwise singularity of an anisotropic dielectric medium", *Int. J. Appl. Electromagn. Mech.* **8**, 219–227 (1997).

[63] N.P. Zhuck and A.S. Omar, "Radiation and low–frequency scattering of EM waves in a general anisotropic homogeneous medium", *IEEE Trans. Antennas Propagat.* **47**, 1364–1373 (1999).

[64] B. Michel and A. Lakhtakia, "On the application of the strong property fluctuation theory for homogenizing chiral–in–chiral composites", *J Phys. D: Appl. Phys.* **29**, 1431–1440 (1996).

[65] B. Michel and A. Lakhtakia, "The covariance function, bilocal approximation and homogenization of chiral–in–chiral composite materials", *J. Phys. D: Appl. Phys.* **32**, 404–406 (1999).

[66] P.G. Cottis and G.D. Kondylis, "Properties of the dyadic Green's function for an unbounded anisotropic medium", *IEEE Trans. Antennas Propagat.* **43**, 154–161 (1995).

[67] W.T. Doyle, "Optical properties of a suspension of metal spheres", *Phys. Rev. B* **39**, 9852–9858 (1989).

[68] B. Shanker and A. Lakhtakia, "Extended Maxwell Garnett model for chiral–in–chiral composites", *J. Phys. D: Appl. Phys.* **26**, 1746–1758 (1993).

[69] B. Shanker,"The extended Bruggeman approach for chiral particulate composites", *J. Phys. D: Appl. Phys.* **29**, 281–288 (1996).

[70] R. Ruppin, "Evaluation of extended Maxwell–Garnett theories", *Opt. Comm.* **182**, 273–279 (2000).

[71] E.J. Garboczi, K.A. Snyder, J.F. Douglas and M.F. Thorpe, "Geometric percolation theshold of overlapping ellipsoids", *Phys. Rev. E* **52**, 819–828 (1995).

[72] I.S. Gradshteyn and I.M. Ryzhik, *Table of Integrals, Series, and Products.* Academic Press, London, UK, 1980.

[73] C.M. Krowne, "Electromagnetic theorems for complex anisotropic media", *IEEE Trans. Antennas Propagat.* **32**, 1224–1230 (1984).

[74] A. Lakhtakia, B. Michel and W.S. Weiglhofer, "Bruggeman formalism for two models of unixial composite media: dielectric properties", *Compos. Sci. Technol.* **57**, 185–196 (1997).

[75] A. Lakhtakia and W.S. Weiglhofer, "Maxwell Garnett formalism for weakly nonlinear, bianisotropic, dilute, particulate composite media", *Int. J. Electronics* **87**, 1401–1408 (2000).

[76] M.N. Lakhtakia and A. Lakhtakia, "Anisotropic composite materials with intensity–dependent permittivity tensor: the Bruggeman approach", *Electromagnetics* **21**, 129–138 (2001).

[77] A. Lakhtakia, "Application of strong permittivity fluctuation theory for isotropic, cubically nonlinear, composite mediums", *Opt. Comm.* **192**, 145–151 (2001).

[78] N.P. Zhuck, "Effective parameters of a statistically homogeneous fluid with strong density and compressibility fluctuations", *Phys. Rev. B* **52**, 919–926 (1995).

[79] N.P. Zhuck and A. Lakhtakia, "Effective constitutive properties of a disordered elastic solid medium via the strong–fluctuation approach", *Proc. R. Soc. Lond. A* **455**, 543–566 (1999).

[80] W.S. Weiglhofer, "Delta–function identities and electromagnetic field singularities", *Am. J. Phys.* **57**, 455–456 (1989).